THESIS

HOPBA1, A PATHOGEN VIRULENCE FACTOR, REVEALS TISSUE-SPECIFIC IMMUNE RESPONSES WITHIN THE *PSEUDOMONAS SYRINGAE* PV. *TOMATO*–*NICOTIANA BENTHAMIANA* PATHOSYSTEM

Submitted by

Tyler Scott Todd

Graduate Degree Program in Cell and Molecular Biology

In partial fulfilment of the requirements

For the degree of Master of Science

Colorado State University

Fort Collins, Colorado

Summer 2024

Master's Committee:

Advisor: Marc Nishimura

Dan Sloan
Robyn Roberts

ABSTRACT

HOPBA1, A PATHOGEN VIRULENCE FACTOR, REVEALS TISSUE-SPECIFIC IMMUNE RESPONSES WITHIN THE *PSEUDOMONAS SYRINGAE* PV. *TOMATO–NICOTIANA BENTHAMIANA* PATHOSYSTEM

Plant pathogens represent a major threat to food security as they dramatically reduce crop yield, impact the expression of desirable traits, and reduce post-harvest longevity. To infect host plants, bacteria like *Pseudomonas syringae* pv. *tomato* DC3000 (*Pst* DC3000) utilize a type III secretion system to deliver virulence proteins (also known as effectors) into the host cytoplasm to suppress immunity. In response, plants have evolved intracellular immune receptors that perceive immunosuppression and reactivate immunity. Thus, a given pathogen effector can both suppress and activate immunity depending on the host genome. Dissecting the molecular mechanisms of plant pathogen effectors helps inform our understanding of both disease and resistance.

The present work reveals an uncharacterized role for *Pst* DC3000 as an aggressive vascular pathogen, causing systemic infection in the model plant *Nicotiana benthamiana* (*Nb*). Further, it establishes that the bacterial effector HopBA1 inhibits movement through the vascular system, despite increasing pathogen persistence within the primary infection site in leaves. Simultaneously, HopBA1 was found to induce irreversible upward vertical bending (i.e., hyponasty) in the petioles of infiltrated leaves, a novel phenotype for a bacterial effector. LC-MS/MS and RNA-Seq revealed phytohormone alteration (notably, a reduction in auxin and jasmonic acid-related metabolites) and transcriptional reprogramming of both developmental and defense genes. HopBA1-dependent growth restriction was suppressed in *Nb eds1* (*ENHANCED DISEASE SUSCEPTIBILITY 1*)

mutant plants, which still undergo HopBA1-induced hyponasty. Together, these results suggest that (1) HopBA1 triggers tissue-specific immune responses and (2) hyponasty is due to HopBA1's virulence activity, rather than host immune activation. Thus, HopBA1 in combination with the model pathogen *Pst* DC3000 becomes an important tool to dissect the poorly understood area of vascular-specific immunity. Vascular pathogens are particularly devastating and difficult to manage in crop species owing to the pathogen's internal location and systemic route of infection, making this research useful in crop improvement.

ACKNOWLEDGMENTS

I would like to express my appreciation to everyone in the Nishimura Lab (Samuel Ogden III, Dr. Adam Bayless, Caio Mendes, and Eliza Walthers) for their time, as well as thoughtful feedback and discussion on my research over the years. I would like to thank Jaden Eisenach, Gus Contreras, Maci Schaub, and Gabe Dattilo for their assistance in supporting my research. Finally, I would like to thank Dr. Marc Nishimura for the opportunity to do meaningful research in a relatively low stress and supportive environment. He has been a helpful mentor, particularly in his willingness to discuss ideas and experiments, as well as generously giving his time to do so. I am very grateful to have had partial funding for graduate school from the National Science Foundation (IOS-1758400) and from the Biology Department as a GTA.

I would like to thank my remaining committee members, Dr. Dan Sloan and Dr. Robyn Roberts, for their patience and understanding with short notice scheduling and wordy presentations, as well as for their thoughtful feedback on my project and encouragement over time. I would like to thank those who have provided critical feedback on my work during our bi-weekly NLR meetings: Dr. Nak Hyun, Dr. Farid El Kasmi, Dr. Sarah Grant, and Dr. Pierre Jacob. I would also like to express my gratitude to Dr. Jeff Dangl, not only for ideas and feedback on my research, but for his positivity toward and encouragement of my scientific career/development.

Finally, I would like to thank my family for their encouragement over many years and through the many situations of life. Thank you to my parents Chuck and Debbie Todd for their unconditional love, support, and belief in me, especially at times when I couldn't do the same for myself. Thank you all.

TABLE OF CONTENTS

1 Chapter 1: Introduction

1.1 Constitutive & inducible defenses: physiochemical barriers to entry

Plants are sessile and nutrient-rich organisms, making them attractive targets for colonization and exploitation by microorganisms. Plants, however, are not defenseless against microbes as they possess constitutive defenses or structural barriers, as well as inducible defenses which are further activated upon the perception of pathogens. For plants, the primary pre-formed structural barrier to invasion comes in the form of a diverse and complex cell wall structure, consisting of cellulose, hemicellulose, pectin, and often lignin. The composition of these cell wall components is critical to prevent entry into or access to cells for an extremely wide range of pathogens (Vorwerk *et al.*, 2004). These rigid, but molecularly porous, structures gain additional fortification through the deposition of cutin and waxes (Jarvis, 1984). Further, plants readily perceive modification of these structures (Vorwerk *et al.*, 2004). Perception of pathogen activity can lead to increased deposition of these existing polymers and substances, as well as the synthesis and deposition of distinct compounds (e.g., callose) and reactive oxygen species (ROS) in and around the cell wall (Wan *et al.*, 2021).

Within extracellular spaces (i.e., the apoplast), pre-existing antimicrobial compounds (i.e., phytoanticipins) preemptively inhibit establishment and proliferation of invading organisms (Kaur *et al.*, 2022). Likewise, plants generate a diversity of functionally similar compounds or secondary metabolites (e.g., phytoalexins, peroxidases, and phenolic compounds) in response to pathogens (Kaur *et al.*, 2022). It is also important to note that the production of many of these compounds occurs more generally in relation to stress (of specific interest here is the accumulation of

anthocyanins, flavonoids, and lignin, as well as modulation of numerous phytohormones during abiotic stress e.g., light intensity) (Saijo and Loo, 2020).

Once pathogens bypass the plant's initial line of exterior physical defenses, there are additional barriers that act to prevent systemic infection (i.e., access to and colonization of the vascular system, as well as distant extracellular spaces). Pre-existing barriers to vascular entry are similar to the plant cell wall itself (e.g., helical and annular lining of xylem by lignin) and there are relatively limited points of natural entry or access to pathogens (e.g., hydathodes present a possible, but also sparse and guarded route of entry into xylem), without the employment of cell wall degrading enzymes (CWDEs) or other forms of specialization (Yadeta and Thomma, 2013). The plant vascular system (collectively, the xylem and phloem), spans the entirety of the plant and provides material transport both shootward and rootward, making pathogen entry a critical threat to plant health.

Accordingly, the internal environment (and external structures) of the vascular system is subject to numerous specialized inducible defense mechanisms. Plants can occlude xylem vessels with bladder-like cell protrusions (tyloses) and produce vascular coatings (gels and gums) to impede pathogen movement and attachment (Kashyap *et al.*, 2021). Further, excessive pathogen growth and development (e.g., biofilm formation) within xylem can itself become self-limiting, resulting in embolism formation, which can impede bacterial movement through the vascular system (De La Fuente *et al.*, 2022). In addition to the xylem, which is "dead" at functional maturity, the phloem presents a much more dynamic and complex component of plant vasculature. Unlike xylem, phloem is directly linked to the symplast by plasmodesmata, which are targets for callose deposition upon pathogen perception (Lee and Lu, 2011). The phloem, through its living companion cells is inherently more responsive to pathogen activity, as well as through sieve element-based

defenses which facilitate localized closure/removal from the overall transport system of the phloem with little or no consequence to the health and function of the plant (Lewis *et al.*, 2022). The phloem is nutrient-rich relative to xylem, representing an attractive niche for pathogen growth; however, in both instances (i.e., within the vascular system) a substantial level of pathogen adaptation/specialization has been demonstrated or in some cases, presumed for successful colonization (De La Fuente *et al.*, 2022).

1.2 Historical context: rediscovery of Mendel, Gene-for-Gene & beyond

Although disease resistance of plants to pathogens has been the object of selection and manipulation since the emergence of agriculture, it wasn't until the mid-19th century that a means of systematically and predictably generating resistant plants began to take form with the introduction of Mendel's Laws. Following the rediscovery of Mendel's work, R.H. Biffen explored the general applicability of the Law of Inheritance to selective wheat breeding to improve various traits of existing British wheat varieties (Biffen, 1905). Through his breeding efforts, Biffen generated a yellow rust resistant wheat variety and in doing so, revealed that disease resistance conformed to Mendelian inheritance (Biffen, 1907). This milestone is generally regarded as the first demonstration of a genetic basis for disease resistance in plants.

The next major advancement to our understanding of plant disease resistance came approximately 40 years later with Flor's conceptualization of the gene-for-gene model (Flor, 1947; Flor, 1971). The critical novelty and genius of this model, which was informed by studies of Flax Rust, was that it recognized that the outcome of a plant-pathogen interaction (i.e., resistance or susceptibility) was defined equally by a specific host (plant) gene and a specific pathogen gene, so the genetic interaction or relationship between both organisms. The gene-for-gene model (Figure 1.1) proposed that if a pathogen carried an avirulence (*avr*) gene and interacted with a host with a

dominant resistance gene, then the outcome would be a resistant interaction (i.e., the pathogen would be avirulent on that particular host genotype, and not cause disease/virulence symptoms). However, a susceptible interaction would result in disease if either the host lacked the resistance gene, or the pathogen lacked the corresponding avirulence gene.

		Plant host	
		R/R or R/r	r/r
Pathogen	*avr*	resistant	susceptible
	no *avr*	susceptible	susceptible

Figure 1.1. Summary model of the gene-for-gene hypothesis.

The genetic underpinnings of the gene-for-gene model were first revealed at the end of the 20th century. The first avirulence gene, *avrA,* was cloned from *Pseudomonas syringae* pv. *glycinea* (*Psg*), demonstrating the validity of the gene-for-gene model, but revealing little insight into mechanism (Staskawicz *et al.,* 1984). The first resistance or "*R* gene" recognizing a biotrophic pathogen wouldn't be cloned for another 9 years, when the serine-threonine kinase, Pto, was cloned from tomato (Martin *et al.*, 1993). In both cases, it would take extensive further studies to understand how these types of proteins contributed to susceptibility and resistance. Much of this work would be done using the model pathogen *Pseudomonas syringae* pv. *tomato* DC3000.

1.3 *Pseudomonas syringae* & the Type III Secretion System

Pseudomonas syringae pv. *tomato* DC3000 (*Pst* DC3000, hereafter DC3000) is a gram-negative bacterium and plant pathogen. DC3000 can infect a range of plant species, including its species of isolation, *Solanum lycopersicum* (tomato), in which it causes bacterial speck (Okabe, 1933; note this is *Pst* generally, rather than DC3000 specifically), and the model plant *Arabidopsis thaliana* (Arabidopsis) (Cuppels, 1986; Whalen *et al.*, 1991). The coincidence of this finding with

advancements in molecular biology, and the subsequent sequencing of the genomes for both Arabidopsis (The Arabidopsis Genome Initiative, 2000) and *Pst* DC3000 (Buell *et al.*, 2003) positioned the Arabidopsis-DC3000 pathosystem as a powerful model system for understanding plant-pathogen interactions and the basis of *avr-R* gene interactions at a molecular level.

DC3000 is present within the phyllosphere of plants where it can thrive both as an epiphyte or as an endophyte, though greatest proliferation occurs in the latter lifestyle (Xin and He, 2013). In either instance, DC3000 can persist without causing obvious disease symptoms in the host. During initial colonization and infection, DC3000 typically utilizes natural openings (i.e., stomata) to access the apoplast, but can also gain entry through wounds generated by wind, hail, herbivory, frost damage, etc. (Chen *et al.*, 2022). Once inside the apoplast, DC3000 can manipulate an array of physiological processes to generate a favorable environment for growth and infection of adjacent tissue (Xin and He, 2013).

How *Pseudomonas syringae* regulates stomata, manipulates host physiology and ultimately causes disease was revealed by studies of its type III secretion (T3SS) system (reviewed in Kvitko and Collmer, 2023). Originally identified as a cluster of genes required for *h*ypersensitive *r*esponse and *p*athogenesis (*hrp)*, the type III secretion system encodes a molecular syringe that delivers a set of virulence proteins directly into the host cytoplasm to enable pathogenesis. In a confusing twist of nomenclature, these virulence proteins are encoded by the *avirulence* genes of the gene-for-gene model. The outcome of their activities within the host cell, either disease or resistance, are dependent on the genotype of the host and its repertoire of cytoplasmic receptors encoded by R-genes (discussed below). Delivered virulence proteins have been alternatively referred to as: “avr proteins,” “type III effector (T3E) proteins,” “hrp outer proteins (Hops),” or

simply “effectors” (Lindeberg *et al.*, 2005). The study of numerous Avr and Hop proteins at a molecular level has been critical to revealing fundamental mechanisms of plant biology.

1.4 The plant immune system: PTI, ETI & coevolution

In parallel to studies of the T3SS and virulence effectors, the molecular cloning of plant R genes revealed the mechanism of the other half of the gene-for-gene model. While the first R gene, was a cytoplasmic kinase (Pto, discussed above), it has become clear that the vast majority of R genes encode a class of multi-domain cytoplasmic receptors historically called NBS-LRR, or NLR, proteins (for nucleotide-binding site domain, leucine-rich repeat) (Kourelis and van der Hoorn, 2018). NLR proteins detect the presence, or activity, of pathogen virulence proteins in the cytoplasm and reactivate immunity. Direct recognition is typically conferred by effector binding to the C-terminal LRR, or post-LRR, region of the receptor. Indirect recognition is conferred by similar binding to a pathogen-modified host protein (Jones *et al.*, 2016). For example, the Pto kinase R gene is now considered a “decoy” protein that is “unintentionally” modified by a pathogen effector that seeks to modify other structurally related kinases that are necessary for host defense signal transduction downstream of plasma membrane receptors (“PRRs,” discussed below). This indirect recognition is often referred to as the “guard hypothesis” (Van der Biezen and Jones, 1998; Dangl and Jones, 2001).

The zig-zag model (Jones and Dangl, 2006), provides a comprehensive framework to explain the dynamic and complex evolutionary interplay between pathogen effectors and plant immune receptors. The model (provided in Figure 1.2) begins with initial perception of pathogen-associated molecular patterns (PAMPs), utilizing cell surface receptors known as pattern recognition receptors (PRRs). This recognition, based upon the binding of a recognized ligand (e.g., flg22 of bacterial flagella) then triggers a cascade of signaling events, known as PAMP-triggered

immunity (PTI), to restrict colonization and infection by a pathogen. PTI employs a range of responses, including the activation of mitogen-activated protein kinase (MAPK) cascades, generation of reactive oxygen species (ROS), calcium influx, and transcriptional reprogramming of plant defenses. It is this PTI, or "basal resistance" that pathogens seek to suppress with cytoplasmic virulence proteins. NLRs are the evolutionary response to PTI-suppression. Immunity triggered by NLR recognition of an effector, or "effector-triggered immunity" (ETI), often results in localized cell death, this has been classically referred to as the "hypersensitive response" (Klement, 1963; Greenberg, 1997).

Other forms of ETI include systemic acquired resistance (SAR), a broad-spectrum, plant-wide form of defense that protects against subsequent pathogen challenge for a period of time. The zig-zag model emphasizes the dynamic state of plant-pathogen interactions and casts this relationship as a co-evolutionary "arms race," where pathogens are under selective pressure to gain or perhaps lose effectors to effectively suppress PTI and plants are similarly under a selective pressure to evolve new NLRs or other means of effector recognition. Importantly, with this synthesis we clearly understand why pathogens would maintain "avirulence genes" within their genome, a question that was baffling at their discovery. This two-tiered PTI/ETI view of the plant immune system has been useful to frame hypotheses, but recently it has become clear that these pathways are interdependent, functioning and evolving together to appropriately recognize and respond to pathogens (Ngou *et al.*, 2021; Yuan *et al.*, 2021).

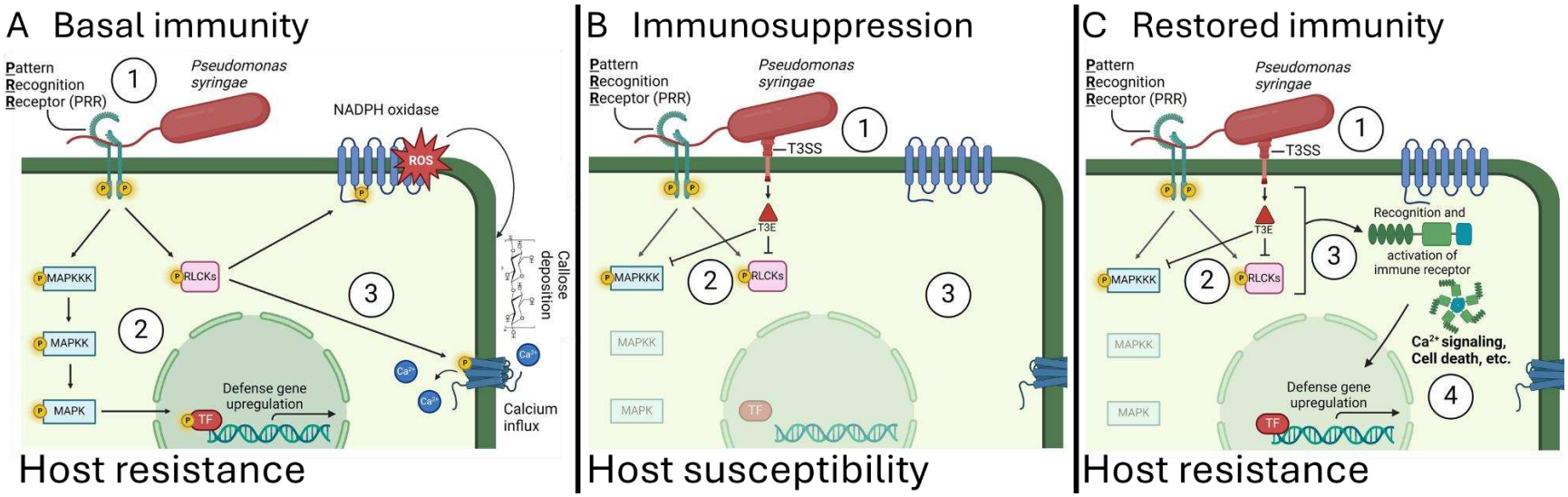

Figure 1.2. A simplified model of the dynamic process of plant resistance, induced susceptibility, and restoration of host resistance or immunity. (A) A depiction of basal immunity in plants, which relies on pathogen/microbe/damage associated molecular pattern (P/M/DAMP) detection via cell-surface receptors (Pattern Recognition Receptors, PRRs, or more accurately PRR complexes, involving co-receptors) (1), which transmit cellular signals upon (extracellular) ligand binding via MAP Kinase cascades and signaling/activation of Receptor-like cytoplasmic Kinases (RLCKs) (2), ultimately leading to up-regulation of defense gene expression, generation of reactive oxy- gen species (ROS), callose deposition, and calcium influx (non-exhaustive) to facilitate resistance (3). (B) An example of how adapted pathogens deactivate basal immunity or recognition (1) by utilizing the type three secretion system (TTSS) to deliver virulence proteins (or effectors) into the cytoplasm, which target defense signaling and immune processes (2) to deactivate these responses and cause disease susceptibility within the host plant (3). (C) Provides an example of adapted plants, which have evolved intracellular means of effector perception (3), namely nucleotide-binding leucine-rich repeat receptors (NLRs), which facilitate immunity or disease resistance either by direct or indirect recognition of effectors/effector activities via calcium signaling, small molecule signaling, programmed cell death, and up-regulation of defense gene expression upon activation (4).

1.5 The Type III effector HopBA1

HopBA1 is a type III secreted effector of an unknown function produced by the plant pathogen *Pseudomonas syringae*. HopBA1 is not present in DC3000 and falls outside of the core "effectorome" (Baltrus et al., 2011). HopBA1 was first identified in two *Pseudomonas syringae* pathovars: *Pseudomonas syringae* pv. *aptata* (*Ptt*), and pv. *japonica* (*Pja*) (Baltrus *et al.*, 2011). *Ptt* is a pathogen of *Beta vulgaris* (sugarbeet) (Maraite and Weyns, 1997), while *Pja* is a pathogen of *Triticum aestivum* (wheat) (Baltrus *et al.*, 2011). Following the initial identification of HopBA1, a subsequent study found that its deletion from *Psy* SM-R, resulted in a marginal decrease in virulence during the colonization of wheat leaves (Dudnik and Dudler, 2014). Aside from this, very little was known about HopBA1 until 2017, when HopBA1 was found to result in macroscopic cell death in two Arabidopsis accessions (Ag-0 and Ws-2), while eliciting no visible response in all other screened accessions (Nishimura *et al.*, 2017). Ultimately, this led to the identification and characterization of the Toll/interleukin1 receptor (TIR) domain protein Response to HopBA1 (RBA1). RBA1 is required for full HopBA1-triggered cell death in Ag-0. RBA1, the first identified receptor of its class, is considered a "truncated" TIR-NLR, or a "TIR-only" protein as it lacks the canonical NBS-LRR domains. Like other characterized plant TIR proteins, RBA1 has a conserved NADase enzymatic activity which generates small molecule signals perceived by the Enhanced Disease Susceptibility 1 (EDS1) pathway (Wan *et al.*, 2019; Huang *et al*., 2022; Jia *et al*., 2022).

TIR-only receptors are common in most plant genomes, but how RBA1 functions without canonical NBS-LRR domains is mysterious. This provides a rationale for understanding how effectors, such as HopBA1, can activate TIR-only receptors. HopBA1 is structurally similar to diverse bacterial proteins including a heme-binding protein (ChaN), an esterase (EreA), and an

uncharacterized domain of the *Pasturella multocida* toxin (PMT), but none of these similarities have revealed a function for HopBA1. (Nishimura *et al.*, 2017).

Subsequent work revealed that an additional, non-TIR, immune receptor was responsible for the recognition of HopBA1 in the Arabidopsis accession Col-0 (Laflamme *et al.*, 2020). This receptor, HopZ-Activated Resistance 1 (ZAR1) is a canonical intracellular immune receptor with an N-terminal coiled-coil (CC) domain, a nucleotide-binding site (NBS), and a C-terminal leucine-rich repeat (LRR) domain (CC-NLR or CNL) (Lewis *et al.*, 2010). In contrast to TIR receptors, ZAR1-mediated immunity has been characterized as EDS1-independent (Lewis *et al.*, 2010). *ZAR1* is present in both the Col-0 and Ag-0 genomes, while *RBA1* is only expressed in Ag-0. ZAR1 likely explains a late residual cell death phenotype found in Ag-0 *rba1* mutants, however in Col-0 ZAR1 ETI restricts DC3000 HopBA1 growth in the absence of cell death (Laflamme *et al*., 2020). It is unknown if RBA1 and ZAR1 are functioning independently or interact in some way to trigger strong cell death in Ag-0.

In addition to HopBA1, four sequence-unrelated *P. syringae* effector proteins are perceived by ZAR1 in Arabidopsis*:* HopZ1, HopF1, HopO1, and HopX1 (Lewis *et al.*, 2010; Huard-Chauveau *et al.*, 2013; Seto *et al.*, 2017; Laflamme *et al*., 2020). ZAR1 also confers immunity to two *Xanthomonas spp*. by recognizing the effectors AvrAC and XopJ4 in Arabidopsis and *Nicotiana benthamiana* (*Nb*), respectively (Bi *et al.*, 2021; Schultink *et al.*, 2019). Among characterized NLRs, this ability to recognize a broad range of effectors is unusual. At the same time, ZAR1 is remarkably well conserved within flowering land plants, a rare occurrence among plant immune receptors (Gong *et al.*, 2022).

The basis for ZAR1's broad effector recognition and conservation across plant species became more apparent following the discovery that ZAR1 functions with a co-receptor pseudokinase

called HOPZ-ETI DEFICIENT 1 (ZED1) to recognize HopZ1 (Lewis *et al.*, 2013). In Arabidopsis, ZED1 is a member of an expanded sub-family of 13 ZED1-related kinases and pseudokinases (ZRKs, or RECEPTOR-LIKE CYTOPLASMIC KINASE (RLCK) family XII-2) found in a 13-gene cluster. There are seven bacterial effectors known to be recognized by ZAR1, each requiring a specific ZRK co-receptor (four in Arabidopsi*s* and one in *Nb*). This NLR-adapter system, with "off-shoring" of effector/receptor interaction surfaces, presumably explains both the broad recognition specificity of ZAR1 and its relatively slow evolution. Of interest to this work is the ZAR1 co-receptor, ZED1-related kinase 2 (ZRK2), which is required for HopBA1-triggered immunity in Arabidopsis (Martel *et al.*, 2020). To date, HopBA1 is the only known effector recognized through ZRK2.

While ZAR1/ZRK receptors recognize diverse effectors, the known host proteins that they guard are all contained within the RLCK VII family of receptor-like cytoplasmic kinases. Numerous RLCK VIIs are well-characterized immune signaling intermediates involved in pattern-triggered immunity (PTI) (Lu *et al.*, 2010; Singh *et al.*, 2022), while others function in diverse aspects of plant development (Fujita *et al.*, 2020), or in some cases, even both defense and development (Rao *et al.*, 2018; Luo *et al.*, 2020, Wang *et al.*, 2022, and Wang *et al.*, 2023). In the context of PTI, RLCK VIIs relay phosphorylation signals from plasma membrane-resident pattern recognition receptors (PRRs) upon extracellular ligand recognition. Accordingly, RLCK VIIs are known to facilitate a range of downstream defensive responses (e.g., ROS generation, callose deposition, and calcium influx) upon recognition of flg22 (flagella, bacteria) and chitin (cell wall, fungi), among many other elicitors (Lu *et al.*, 2010; Rao *et al.*, 2018; Singh *et al.*, 2022).

Given their critical role in PTI signal transduction, it is not surprising that RLCK VII family members are common targets of diverse pathogen effectors. Accordingly, the plant immune system

has evolved multiple NLR systems to monitor RLCK VIIs for pathogen immunosuppression. In addition to ZAR1, Arabidopsis genomes contain *Resistance to P. syringae 5* (*RPS5*), a CNL that monitors AvrPphB-susceptible 1 (PBS1) for cleavage by the *Pseudomonas syringae* effector AvrPphB (Swiderski and Innes, 2001; Qi *et al.*, 2014). In light of this complexity, it remains an open possibility that any given RLCK VII could function in PTI and be targeted for suppression by a pathogen effector as a true virulence function or it could be a decoy that is monitored by the host immune system, resulting in ETI.

We have a relatively complete understanding of the recognition of AvrAC by ZAR1. In this system, uridylation of the RLCK VII protein PBL2 by Xanthomonas campestris effector, AvrAC, leads to interaction with RKS1-ZAR1 (Bi *et al.*, 2021). The formation of the heterotrimeric complex induces conformational change in the ZAR1 NBS domain and then a pentameric $PBL2^{UMP}$-RKS1-ZAR1 'resistosome' (Bi *et al.*, 2021). In other ZAR1/ZRK systems, the exact activation events remain less clear, although effector targeting of RLCK VIIs is partially defined in some cases (Lewis *et al.*, 2013; Liu *et al.*, 2019; Seto *et al.*, 2021). The remaining ZAR1-recognized effectors have a variety of putative or demonstrated biochemical functions: HopO1 have ADP-ribosyltransferase activity, HopBA1 has similarity to heme-binding proteins and esterase, and XopJ4 is a member of the YopJ acetyletransferase family (Aung *et al.*, 2020; Nishimura *et al.*, 2017; Jayaraman *et al.*, 2017). The actual targets of these remaining effectors (HopO1, HopBA1, and XopJ4) are unknown. However, given the existing precedence for RLCK VII targets within ZAR1-mediated ETI, this family is speculated to be the target of these remaining effectors. Figure 1.3 provides a visual summation of what is presently known and unknown for this system.

This knowledge gap, for HopBA1 specifically, was the basis of this project's initial research inquiry (provided within Appendix A). We hypothesized that HopBA1 targets an RLCK

VII for modification, an activity which is monitored or recognized by the ZRK2-ZAR1 system in Arabidopsis. To provide an alternative approach to ongoing studies in Arabidopsis, we developed a transient reconstruction assay in *Nicotiana benthamiana*. This system used *Agrobacterium*-mediated transient expression to co-express HopBA1 and *At* ZRK2 to activate *Nb* ZAR1-dependent cell death (Appendix A, Figure A1). In this reconstruction, the expression of *At* ZRK2 is necessary for HopBA1 immune recognition, likely because of the relatively simple ZRK repertoire in *Nb* (Figure 1.3). The reconstructed HopBA1-recognition system allowed for a high-throughput screening of candidate *Nb* RLCK VIIs using gene silencing (Appendix A, Figures A3 – A4). Silencing of HopBA1-targeted *Nb* RLCK VIIs, if relevant to immune recognition, should result in loss of ZKR2/ZAR1-depenent cell death. Putative HopBA1-targets are being verified in *Nb* with CAS9-derived deletion polymutants (Appendix A, Figures A5 – A6).

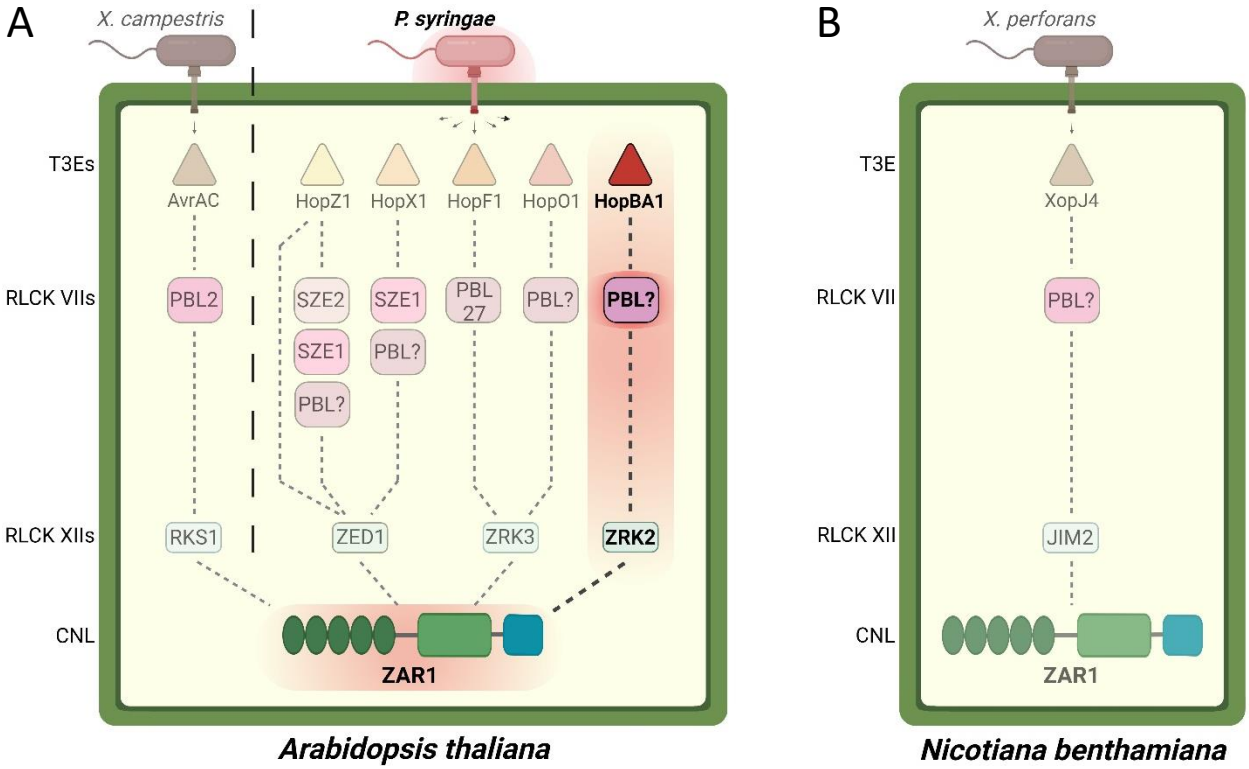

Figure 1.3. Summary model of ZAR1 effector recognition in Arabidopsis in contrast with Nicotiana benthamiana. (A) Arabidopsis ZAR1 recognizes numerous *Pseudomonas* and *Xanthomonas* effectors through their modification of both known and unknown RLCK VII targets. HopBA1 is hypothesized to

1.6 Research Overview

Appendix A provides results for the initial research that lead to the project described in subsequent chapters (i.e., Ch. 2 and Ch. 3). The objectives for this portion of the research can be summarized as follows: (i) the transient reconstruction of a plant immune pathway in *N. benthamiana* (*Nb*) utilizing *Agrobacterium* for protein expression (specifically, HopBA1 and *At* ZRK2), (ii) the silencing of *Nb* RLCK VIIs to identify possible genes that are required for the reconstructed immune response (i.e., cell death), and (iii) use of these results to inform the generation of *Nb* RLCK VII polymutants.

The remainder of the research presented here was conducted with the following objectives in mind: (i) the characterization of *Pseudomonas syringae* DC3000 Δ*hopQ* disease in *Nb* and the impact of HopBA1 delivery in this pathosystem, (ii) the description of a novel effector-induced phenotype (specifically, petiole hyponasty which is induced by HopBA1), (iii) the characterization of *Pseudomonas syringae* DC3000 Δ*hopQ* as a vascular pathogen, and (iv) the identification of phytohormone and transcriptional changes brought about by HopBA1 delivery.

Figure 1.3 (Continued). modify an unknown RLCK VII, which is monitored by ZRK2, and triggers activation of the ZAR1 resistosome. (B) To date, only a single RLCK XII has been characterized for its role in mediating ZAR1 effector recognition in *N. benthamiana*. In this instance, XopJ4's target is unknown, but requires JIM2 and ZAR1 for immune activation in *N. benthamiana*. Although ZAR1 is conserved in both plant species, pseudokinases like ZRK2 in Arabidopsis are not.

1.7 References

Aung K, Kim P, Li Z, Joe A, Kvitko B, Alfano JR, He SY. 2020. Pathogenic Bacteria Target Plant Plasmodesmata to Colonize and Invade Surrounding Tissues. *Plant Cell*. **32**, 595—611.

Baltrus DA, Nishimura MT, Romanchuk A, Chang JH, Mukhtar MS, Cherkis K, Roach J, Grant SR, Jones CD, Dangl JL. 2011. Dynamic evolution of pathogenicity revealed by sequencing and comparative genomics of 19 Pseudomonas syringae isolates. *PLoS Pathog*. **7**, e1002132.

Bi G, Su M, Li N, Liang Y, Dang S, Xu J, Hu M, Wang J, Zou M, Deng Y, Li Q, Huang S, Li J, Chai J, He K, Chen YH, Zhou JM. 2021. The ZAR1 resistosome is a calcium-permeable channel triggering plant immune signaling. *Cell*. **184**, 3528—3541.e12.

Biffen RH. 1905. Mendel's laws of inheritance and wheat breeding. *J Agric Sci.* **1**, 4—48.

Biffen RH. 1907. Studies in the inheritance of Disease-Resistance. *J Agric Sci.* **2**, 109—128.

Buell CR, Joardar V, Lindeberg M, Selengut J, Paulsen IT, Gwinn ML, Dodson RJ, Deboy RT, Durkin AS, Kolonay JF, Madupu R, *et al*. 2003. The complete genome sequence of the *Arabidopsis* and tomato pathogen *Pseudomonas syringae* pv. *tomato* DC3000. *Proc Natl Acad Sci USA.* **100**, 10181—10186.

Chen H, Chen J, Zhao Y, Liu F, Fu ZQ. 2022. Pseudomonas syringae pathovars. *Trends Microbiol.* **30**, 912—912.

Cuppels DA. 1986. Generation and characterization of Tn5 insertion mutations in *Pseudomonas syringae* pv. *tomato*. *Appl Environ Microbiol.* **51**, 323—327.

Dangl JL and Jones JDG. 2001. Plant pathogens and integrated defense responses to infection. *Nature*. **411**, 826–833.

De La Fuente L, Merfa MV, Cobine PA, Coleman JJ. 2022. Pathogen adaptation to the xylem environment. *Annu Rev Phytopathol.* **60**, 163—186.

Dudnik A, Dudler R. 2014. Virulence determinants of *Pseudomonas syringae* strains isolated from grasses in the context of a small type III effector repertoire. *BMC Microbiology.* **14**, 1—9.

Flor HH. 1947. Inheritance of reaction to rust in flax. *J Agric Res.* **74**, 241—262.

Flor HH. 1971. Current Status of the Gene-For-Gene Concept. *Annu Rev Phytopathol.* **9**, 275—296.

Fujita S, De Bellis D, Edel KH, Köster P, Andersen TG, Schmid-Siegert E, Tendon VD, Pfister A, Marhavý P, Ursache R, Doblas VG, Barberon M, Daraspe J, Creff A, Ingram G, Kudla J,

Geldner N. 2020. SCHENGEN receptor module drives localized ROS production and lignification in plant roots. *EMBO J.* **39**, e103894.

Gong Z, Qi J, Hu M, Bi G, Zhou J, Han G. 2022. The origin and evolution of a plant resistosome, *Plant Cell*. **34**, 1600—1620.

Greenberg JT. 1997. Programmed cell death in plant–pathogen interactions. *Annu Rev Plant Physiol Plant Mol Biol.* **48**, 525—545.

Huang S, Jia A, Song W, Hessler G, Meng Y, Sun Y, Xu L, Laessle H, Jirschitzka J, Ma S, Xiao Y, Yu D, Hou J, Liu R, Sun H, Liu X, Han Z, Chang J, Parker JE, Chai J. 2022. Identification and receptor mechanism of TIR-catalyzed small molecules in plant immunity. *Science*. **377**, eabq3297.

Huard-Chauveau C, Perchepied L, Debieu M, Rivas S, Kroj T, Kars I, Bergelson J, Roux F, Roby D. 2013. An atypical kinase under balancing selection confers broad-spectrum disease resistance in Arabidopsis. *PLoS Genet*. **9**, e1003766.

Jarvis MC. 1984. Structure and properties of pectin gels in plant-cell walls. *Plant Cell Environ*. **7**, 153–164.

Jayaraman J, Choi S, Prokchorchik M, Choi DS, Spiandore A, Rikkerink EH, Templeton MD, Segonzac C, Sohn KH. 2017. A bacterial acetyltransferase triggers immunity in Arabidopsis thaliana independent of hypersensitive response. *Sci Rep*. **7**, 3557.

Jia A, Huang S, Song W, Wang J, Meng Y, Sun Y, Xu L, Laessle H, Jirschitzka J, Hou J, Zhang T, Yu W, Hessler G, Li E, Ma S, Yu D, Gebauer J, Baumann U, Liu X, Han Z, Chang J, Parker JE, Chai J. 2022. TIR-catalyzed ADP-ribosylation reactions produce signaling molecules for plant immunity. *Science*. **377**, eabq8180.

Jones JDG, Dangl JL. 2006. The plant immune system. *Nature*. **444**, 323–329.

Jones JD, Vance RE, Dangl JL. 2016. Intracellular innate immune surveillance devices in plants and animals. *Science*. **354**, aaf6395.

Kashyap A, Planas-Marquès M, Capellades M, Valls M, Coll NS. 2021. Blocking intruders: inducible physico-chemical barriers against plant vascular wilt pathogens. *J Exp Bot.* **72**, 184—198.

Kaur S, Samota MK, Choudhary M, Choudhary M, Pandey AK, Sharma A, Thakur J. 2022. How do plants defend themselves against pathogens-Biochemical mechanisms and genetic interventions. *Physiol Mol Biol Plants*. **28**, 485–504.

Klement Z. 1963. Rapid detection of pathogenicity of phytopathogenic pseudomonads. *Nature*. **199**, 299–300.

Kourelis J, van der Hoorn RAL. 2018. Defended to the Nines: 25 Years of Resistance Gene Cloning Identifies Nine Mechanisms for R Protein Function. *Plant Cell*. **30**, 285—299.

Kvitko BH, Collmer A. 2023. Discovery of the Hrp Type III secretion system in phytopathogenic bacteria: how investigation of hypersensitive cell death in plants led to a novel protein injector system and a world of inter-organismal molecular interactions within plant cells. *Phytopathology*. **113**, 626—636.

Laflamme B, Dillon MM, Martel A, Almeida RND, Desveaux D, Guttman DS. 2020. The pan-genome effector-triggered immunity landscape of a host-pathogen interaction. *Science*. **367**, 763—768.

Lee JY, Lu H. 2011. Plasmodesmata: the battleground against intruders. *Trends Plant Sci.* **16**, 201—210.

Lewis JD, Knoblauch M, Turgeon R. 2022. The Phloem as an Arena for Plant Pathogens. *Annu Rev Phytopathol*. **60**, 77—96.

Lewis JD, Lee AH, Hassan JA, Wan J, Hurley B, Jhingree JR, Wang PW, Lo T, Youn JY, Guttman DS, Desveaux D. 2013. The Arabidopsis ZED1 pseudokinase is required for ZAR1-mediated immunity induced by the Pseudomonas syringae type III effector HopZ1a. *Proc Natl Acad Sci USA*. **110**, 18722—18727.

Lewis JD, Wu R, Guttman DS, Desveaux D. 2010. Allele-specific virulence attenuation of the *Pseudomonas syringae* HopZ1a type III effector via the Arabidopsis ZAR1 resistance protein. *PLoS Genet*. **6**, e1000894.

Lindeberg M, Stavrinides J, Chang JH, Alfano JR, Collmer A, Dangl JL, Greenberg JT, Mansfield JW, Guttman DS. 2005. Proposed guidelines for a unified nomenclature and phylogenetic analysis of type III Hop effector proteins in the plant pathogen Pseudomonas syringae. *Mol Plant Microbe Interact.* **18**, 275—282.

Liu C, Cui D, Zhao J, Liu N, Wang B, Liu J, Xu E, Hu Z, Ren D, Tang D, Hu Y. 2019. Two Arabidopsis Receptor-like Cytoplasmic Kinases SZE1 and SZE2 Associate with the ZAR1-ZED1 Complex and Are Required for Effector-Triggered Immunity. *Mol Plant.* **12**, 967—983.

Lowe-Power TM, Khokhani D, Allen C. 2018. How *Ralstonia solanacearum* exploits and thrives in the flowing plant xylem environment. *Trends in Microbiology*. **26**, 1—14.

Lu D, Wu S, Gao X, Zhang Y, Shan L, He P. 2010. A receptor-like cytoplasmic kinase, BIK1, associates with a flagellin receptor complex to initiate plant innate immunity. *Proc Natl Acad Sci USA*. **107**, 496—501.

Luo X, Wu W, Liang Y, Xu N, Wang Z, Zou H, Liu J. 2020. Tyrosine phosphorylation of the lectin receptor-like kinase LORE regulates plant immunity. *EMBO J.* **39**, 1—16.

Maraite H, Weyns J. 1997. *Pseudomonas syringae* pv. *Aptata* and pv. *Atrofaciens*, specific pathovars or members of pv. *syringae*? *Unite de Phytopathologie*, 515—520.

Martel A, Laflamme B, Seto D, Bastedo DP, Dillon MM, Almeida RND, Guttman DS, Desveaux D. 2020. Immunodiversity of the *Arabidopsis* ZAR1 NLR Is Conveyed by Receptor-Like Cytoplasmic Kinase Sensors. *Front Plant Sci*. doi: 10.3389/fpls.2020.01290.

Martin GB, Brommonschenkel SH, Chunwongse J, Frary A, Ganal MW, Spivey R, Wu T, Earle ED, Tanksley SD. 1993. Map-based cloning of a protein kinase gene conferring disease resistance in tomato. *Science*. **262**, 1432—1436.

Ngou BPM, Ahn HK, Ding P, Jones JDG. 2021. Mutual potentiation of plant immunity by cell-surface and intracellular receptors. *Nature*. **592**, 1—22.

Nishimura MT, Anderson RG, Cherkis KA, Law TF, Liu QL, Machius M, Nimchuk ZL, Yang L, Chung E, El Kasmi F, Hyunh M, Nishimura EO, Sondek JE, Dangl JL. 2017. TIR-only protein RBA1 recognizes a pathogen effector to regulate cell death in *Arabidopsis*. *Proc Natl Acad Sci USA.* **114**, 2053—2062.

Okabe N. 1933. Bacterial diseases of plants occurring in Formosa. *J Trop Agric.* **5**, 26—36.

Qi D, Dubiella U, Kim SH, Sloss DI, Dowen RH, Dixon JE, Innes RW. 2014. Recognition of the protein kinase AVRPPHB SUSCEPTIBLE1 by the disease resistance protein RESISTANCE TO PSEUDOMONAS SYRINGAE5 is dependent on s-acylation and an exposed loop in AVRPPHB SUSCEPTIBLE1. *Plant Physiol*. **164**, 340—351.

Rao S, Zhou Z, Miao P, Bi G, Hu M, Yu Y, Feng F, Zhang X, Zhou JM. 2018. Roles of receptor-like cytoplasmic kinase VII members in pattern-triggered immune signaling. *Plant Physiol*. **177**, 1679—1690.

Saijo Y, Loo EP. 2020. Plant immunity in signal integration between biotic and abiotic stress responses. *New Phytol.* **225**, 87—104.

Seto D, Khan M, Bastedo DP, Martel A, Vo T, Guttman D, Subramaniam R, Desveaux D. 2021. The small molecule Zaractin activates ZAR1-mediated immunity in *Arabidopsis*. *Proc. Natl Acad Sci USA*. **118**, e2116570118.

Seto D, Koulena N, Lo T, Menna A, Guttman DS, Desveaux D. 2017. Expanded type III effector recognition by the ZAR1 NLR protein using ZED1-related kinases. *Nat Plants.* **3**, 17027.

Singh P, Mishra V, Tripathi DK, Corpas FJ, Singh VP. 2022. RIPK: a crucial ROS signaling component in plants. *Trends Plant Sci*. **27**, 214—216.

Staskawicz BJ, Dahlbeck D, Keen NT. 1984. Cloned avirulence gene of *Pseudomonas syringae* pv. *glycinea* determines race-specific incompatibility on *Glycine max* (L.) Merr. *Proc Natl Acad Sci USA*. **81**, 6024—6028.

Swiderski MR, Innes RW. 2001. The Arabidopsis PBS1 resistance gene encodes a member of a novel protein kinase subfamily. *Plant J*. **26**,101—112.

The Arabidopsis Genome Initiative. 2000. Analysis of the genome sequence of the flowering plant Arabidopsis thaliana. *Nature.* **408**, 796—815.

Van der Biezen EA, Jones JDG. (1998). Plant disease-resistance proteins and the gene-for-gene concept. *Trends Plant Sci.* **23**, 454—456.

Vorwerk S, Somerville S, Somerville C. 2004. The role of plant cell wall polysaccharide composition in disease resistance. *Trends Plant Sci.* 9, 203–209.

Wan J, He M, Hou Q, Zou L, Yang Y, Wei Y, Chen X. 2021. Cell wall associated immunity in plants. *Stress Biol.* **1**. 10.1007/s44154-021-00003-4.

Wan L, Essuman K, Anderson RG, Sasaki Y, Monteiro F, Chung EH, Nishimura EO, DiAntonio A, Milbrandt J, Dangl JL, Nishimura MT. 2019. TIR domains of plant immune receptors are NAD+-cleaving enzymes that promote cell death. *Science.* **365**, 799–803.

Wang Q, Aliaga Fandino AC, Graeff M, DeFalco TA, Zipfel C, Hardtke CS. 2023. A phosphoinositide hub connects CLE peptide signaling and polar auxin efflux regulation. *Nat Commun*. **14**, 423.

Wang W, Hu C, Li X, Zhu Y, Tao L, Cui Y, Deng D, Fan X, Zhang H, Li J, Gou X, Yi J. 2022. Receptor-like cytoplasmic kinases PBL34/35/36 are required for CLE peptide-mediated signaling to maintain shoot apical meristem and root apical meristem homeostasis in Arabidopsis. *Plant Cell.* **34**, 1289—1307.

Whalen MC, Innes RW, Bent AF, Staskawicz BJ. 1991. Identification of *Pseudomonas syringae* pathogens of *Arabidopsis* and a bacterial locus determining avirulence on both *Arabidopsis* and soybean. *Plant Cell*. **3**, 49—59.

Xin XF, He SY. 2013. *Pseudomonas syringae* pv. *tomato* DC3000: A model pathogen for probing disease susceptibility and hormone signaling in plants. *Annu Rev Phytopathol*. **51**, 473—498.

Xin XF, Kvitko B, He SY. 2018. *Pseudomonas syringae*: what it takes to be a pathogen. *Nat Rev Microbiol.* **16**, 316—328.

Yadeta KA, Thomma BPHJ. 2013. The xylem as battleground for plant hosts and vascular wilt pathogens. *Front Plant Sci.* **4**, 1—12.

Yuan M, Jiang Z, Bi G, Nomura K, Liu M, Wang Y, Cai B, Zhou JM, He SY, Xin XF. 2021. Pattern-recognition receptors are required for NLR-mediated plant immunity. *Nature*. **592**, 105—109.

2 Chapter 2: Characterization of *Pseudomonas syringae* DC3000 Δ*hopQ* disease in *Nicotiana benthamiana* & the impact of HopBA1 delivery

2.1 Results

HopBA1 enhances bacterial persistence within the primary infection site of leaves

To date, studies of HopBA1 in Arabidopsis have not revealed its presumed function as a virulence factor to promote pathogen success. Since HopBA1 only appeared to be recognized by *N. benthamiana* (*Nb*) when transiently expressed with *At* ZRK2 (Appendix A), we hypothesized that *Nb* would be a good system to investigate potential HopBA1 virulence functions in the absence of immune activation. To investigate this, we delivered HopBA1 from the virulent pathogen *Pseudomonas syringae* pv. *tomato* DC3000 Δ*hopQ*, (hereinafter DC3000 Δ*hopQ*). This deletion mutant is used to avoid recognition of the effector HopQ1 by the TIR-NLR ROQ1 (Schultink *et al.*, 2017). Growth curve assays in this background revealed that the addition of HopBA1 led to a sustained high bacterial population within infiltrated leaves relative to both the virulent strain (DC3000 Δ*hopQ* + empty vector (EV)) strain and the avirulent strain (DC3000 Δ*hopQ* + *hopQ1*) (Figure 2.1).

The addition of HopBA1 had no apparent effect on bacterial growth at early time points (days 0 to 6) when compared to DC3000 Δ*hopQ* + EV (Figure 2.1). However, sampling leaf tissue at later time points revealed that DC3000 Δ*hopQ* + *hopBA1* grew to significantly greater levels than DC3000 Δ*hopQ* + EV (6-fold greater growth at 9 dpi and ~31,000-fold greater growth at 12 dpi) (Figure 2.1). In contrast, DC3000 Δ*hopQ* + *hopBA1* resulted in significantly greater growth than the avirulent DC3000 Δ*hopQ* + *hopQ1* at all time points except 0 dpi when all strains should be equal (Figure 2.1). DC3000 Δ*hopQ* + *hopBA1* had 14-fold (3 dpi), 476-fold (6 dpi), ~1,600-fold (9 dpi), and 1,400-fold greater growth than DC3000 Δ*hopQ* + *hopQ1* (Figure 2.1).

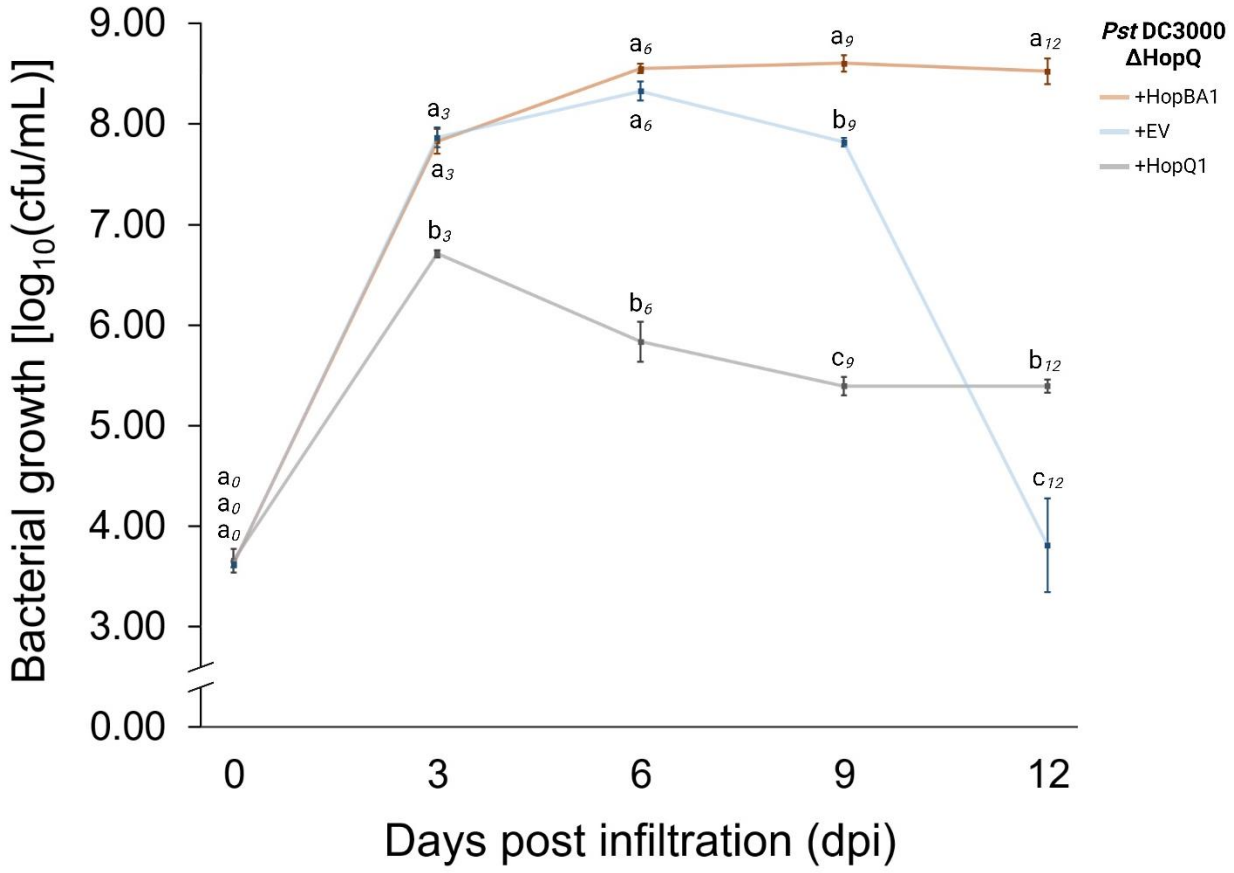

Figure 2.1. HopBA1 enhances bacterial persistence and stabilizes a high bacterial population within the primary infection of leaves. DC3000 Δ*hopQ* + *hopBA1* extends the localized persistence of bacteria within leaf tissue over time. + *hopBA1* leads to 6-fold to ~31,000-fold greater bacterial growth than + EV at 9 and 12 dpi, respectively. + EV leads to a local bacterial population crash starting at 6 dpi. + *hopBA1* growth is equal to + EV at 0 – 6 dpi. + *hopQ1* results in bacterial growth restriction within leaves and has significantly less growth than + EV and + *hopBA1* at 3, 6, and 9 dpi (as well as at 12 dpi for + *hopBA1*). The assay was repeated four times with similar results. Strains were infiltrated at OD_{600} = 0.0002 ($1x10^5$ cfu) into 4 – 5 leaves per plant. Each plant was infiltrated with a single strain. Error bars indicate SD. Samples consist of 3 biological replicates and 3 technical replicates per strain at each time point. Significance groups are assigned within a given time point using one-way ANOVA and Tukey's HSD.

Similar to previously published DC3000 experiments in tomato (Pérez-Mendoza *et al.*, 2019), DC3000 Δ*hopQ* + EV (the virulent strain in these experiments) undergoes a substantial population crash within infiltrated leaves, which appears to begin at ~6 dpi (Figure 2.1). Unexpectedly, the addition of HopBA1 to DC3000 prevents this population crash, resulting in sustained high density bacterial population. Notably, DC3000 Δ*hopQ* + *hopBA1* leads to a reduced rate and spatial distribution of necrosis within leaves compared to DC3000 Δ*hopQ* + EV (Figure 2.2 A and

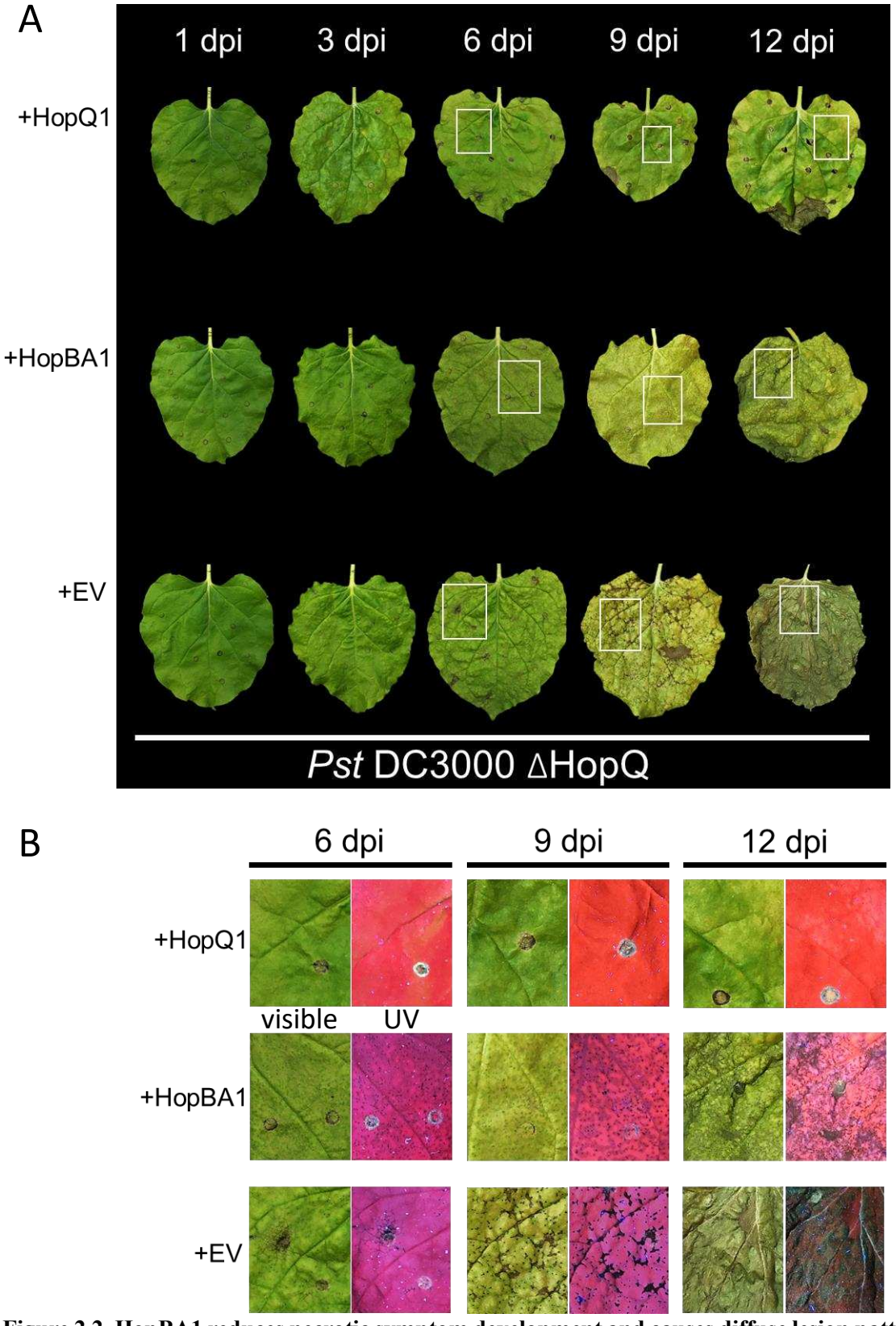

Figure 2.2. HopBA1 reduces necrotic symptom development and causes diffuse lesion patterns within infected leaves. (A) A representative overview of leaf disease symptoms and/or general phenotypes that develop following whole leaf infiltration with DC3000 Δ*hopQ* + *hopQ1* (top), + *hopBA1* (middle), and +

B). Differential disease symptoms for DC3000 Δ*hopQ* + EV and DC3000 Δ*hopQ* + *hopBA1* became apparent by 6 dpi and continued to diverge over the remaining timepoints (i.e., 9 and 12 dpi) (Figure 2.2 A and B).

DC3000 Δ*hopQ* + *hopBA1* resulted in a distinctly diffuse and speckled lesion pattern and was accompanied by mottled pigmentation in leaf tissue (6 and 9 dpi), which becomes more apparent under UV light (Figure 2.2 B). DC3000 Δ*hopQ* + EV resulted in strong necrotic symptoms, which were generally observed as clustered or dense interconnected patches that were spatially biased along leaf venation (6 and 9 dpi), prior to total collapse and desiccation of leaf tissue (12 dpi) (Figure 2.2 B). Both DC3000 Δ*hopQ* + *hopBA1* and DC3000 Δ*hopQ* + EV undergo similar levels of chlorosis within the infiltrated leaf tissue starting around 5 to 7 dpi. Leaves infiltrated with DC3000 Δ*hopQ* + *hopQ1* showed chlorosis earlier than the other two strains at 3 dpi and often became waxier in appearance than leaves infiltrated with either of the other strains (Figure 2.2 B). This phenotype persisted and/or resulted in chlorosis intermixed with cell death (distinct from necrosis i.e., relating to host recognition).

Relative conductivity was then utilized as a quantitative metric of the observed difference in cell death and/or necrosis progression between DC3000 Δ*hopQ* + EV and + *hopBA1* (Figure 2.3). We hypothesized that spot infiltrations of DC3000 Δ*hopQ* + EV would result in greater relative conductivity than DC3000 Δ*hopQ* + *hopBA1*. This assay confirmed that ion leakage, a cell death-associated metric, was greater at 3 and 6 dpi following spot infiltration with DC3000 Δ*hopQ* + EV than DC3000 Δ*hopQ* + *hopBA1* (Figure 2.3 A), which fits the overall phenotypic appearance

Figure 2.2 (Continued). EV (bottom). All plants were *Nb* WT and were infiltrated with a bacterial cell suspension of $1x10^5$ cfu. dpi: days post infiltration. (B) Closeups of selected leaf areas from (A) presented under visible and ultraviolet (UV) light at 6, 9, and 12 dpi for improved visualization. The detailed areas are denoted by the white rectangular frames in (A).

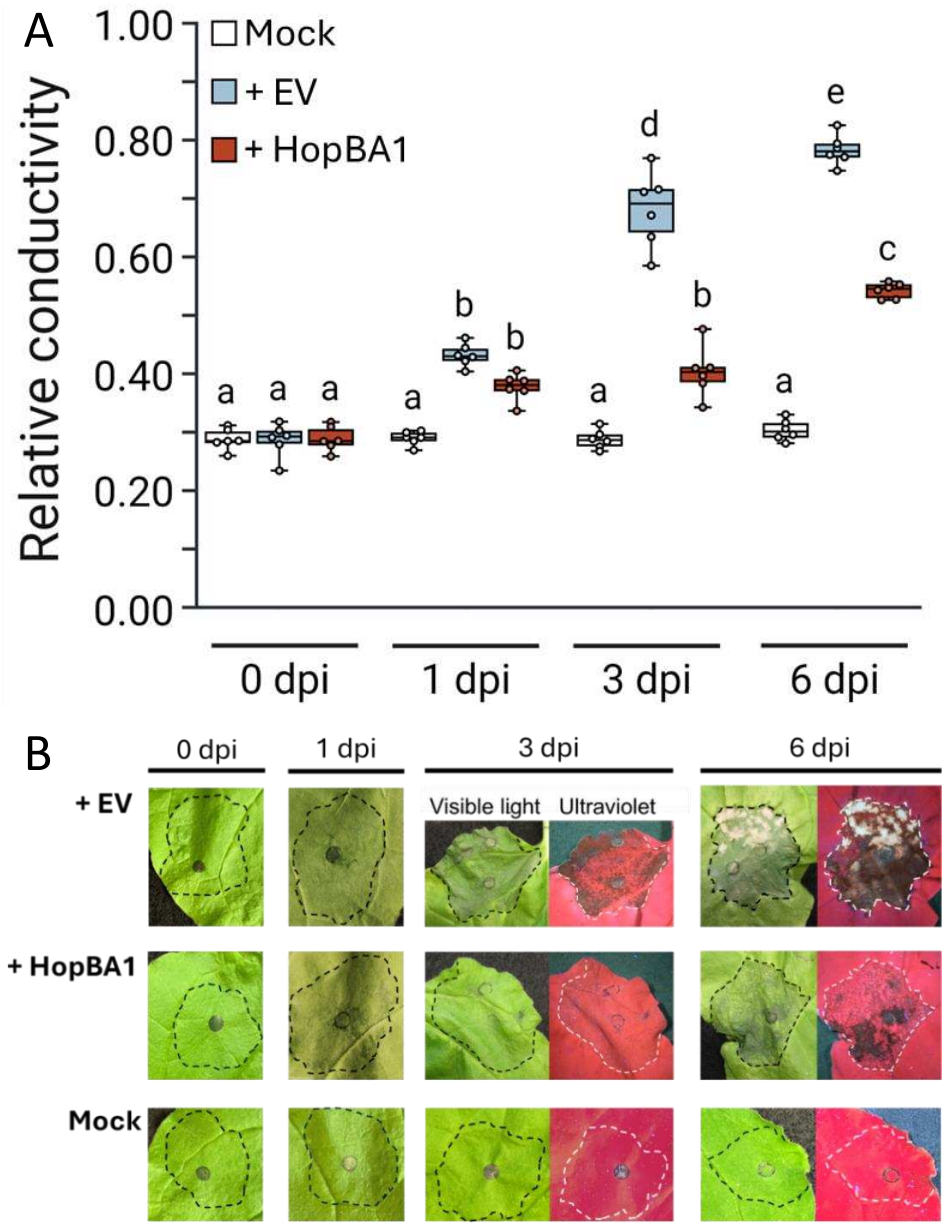

Figure 2.3. HopBA1 slows the rate of cell death in DC3000 Δ*hopQ* spot infiltrations. (A) Measured relative conductivity over time for DC3000 Δ*hopQ* + EV, DC3000 Δ*hopQ* + *hopBA1*, and mock infiltrations relative conductivity comparison. Relative conductivity was measured at 0, 1, 3, and 6 dpi. Ion leakage for mock infiltrations is stable, DC3000 Δ*hopQ* + *hopBA1* slowly increases, and DC3000 Δ*hopQ* + EV rapidly increases over time, reaching ~80% (relative conductivity = 0.80) total ion content loss at 6 dpi. Significance groups are assigned with two-way ANOVA and Tukey's HSD. (B) Representative images of infiltrated areas at measured time points. Cell death phenotype differences are more apparent under UV light.

for cell death following spot infiltration (Figure 2.3 B). Mock infiltration was included in the assay to demonstrate relative conductivity in the absence of cell death, which was significantly lower than either DC3000 Δ*hopQ* strain at all time points (Figure 2.3 A).

HopBA1 induces hyponasty of petioles in *N. benthamiana* when delivered by *Pst* DC3000 Δ*hopQ*

During bacterial growth assay infiltrations, we observed an atypical and undescribed morphological phenotype that only occurred in the petioles of leaves infiltrated with DC3000 Δ*hopQ* + *hopBA1*. We found that the petioles associated with DC3000 Δ*hopQ* + *hopBA1* whole leaf infiltrations became rigidly and permanently hyponastic in a process that, at least phenotypically, begins to become apparent at 3 dpi. The hallmark of this HopBA1-induced phenotype is the upward bending of the petiole, which features a prominent abaxial arc (Figure 2.4 A and C). In terms of petiole form, this ranges from a sigmoidal to parabolic curve (i.e., the petiole is bent backward toward the stem and the leaf is fully overturned/inverted), while the typical petiole form following infiltration with DC3000 Δ*hopQ* + EV is approximately linear, or slightly downward bending (Figure 2.4 C). In addition to petiole hyponasty, DC3000 Δ*hopQ* + *hopBA1* also induces changes to floral phyllotaxy and petal morphology in mature plants (Appendix B, Figure S5).

Most change in petiole form was reached by 6 dpi, so this point was selected for terminal petiole angle measurements to quantify the differences between DC3000 Δ*hopQ* + *hopBA1* infiltrations and all other bacterial infiltrations or treatments. In terms of petiole angle, HopBA1-induced hyponasty is characterized by its positive degree, while other strains (e.g., DC3000 Δ*hopQ* + EV and + *hopQ1*), as well as mock infiltration (10 mM $MgCl_2$) all result in negative petiole angles (Figure 2.4 B). Across many independent experiments, *Nb* WT inoculated with DC3000 Δ*hopQ* + *hopBA1* had a mean petiole angle of 54°, while DC3000 Δ*hopQ* + EV had a mean petiole angle of -38° (Appendix B, Figure S4; Supplemental Table 1).

We next sought to better understand the genetic requirements for hyponasty. First, we tested HopBA1 mutants that were previously shown to lose recognition by the immune receptor RBA1

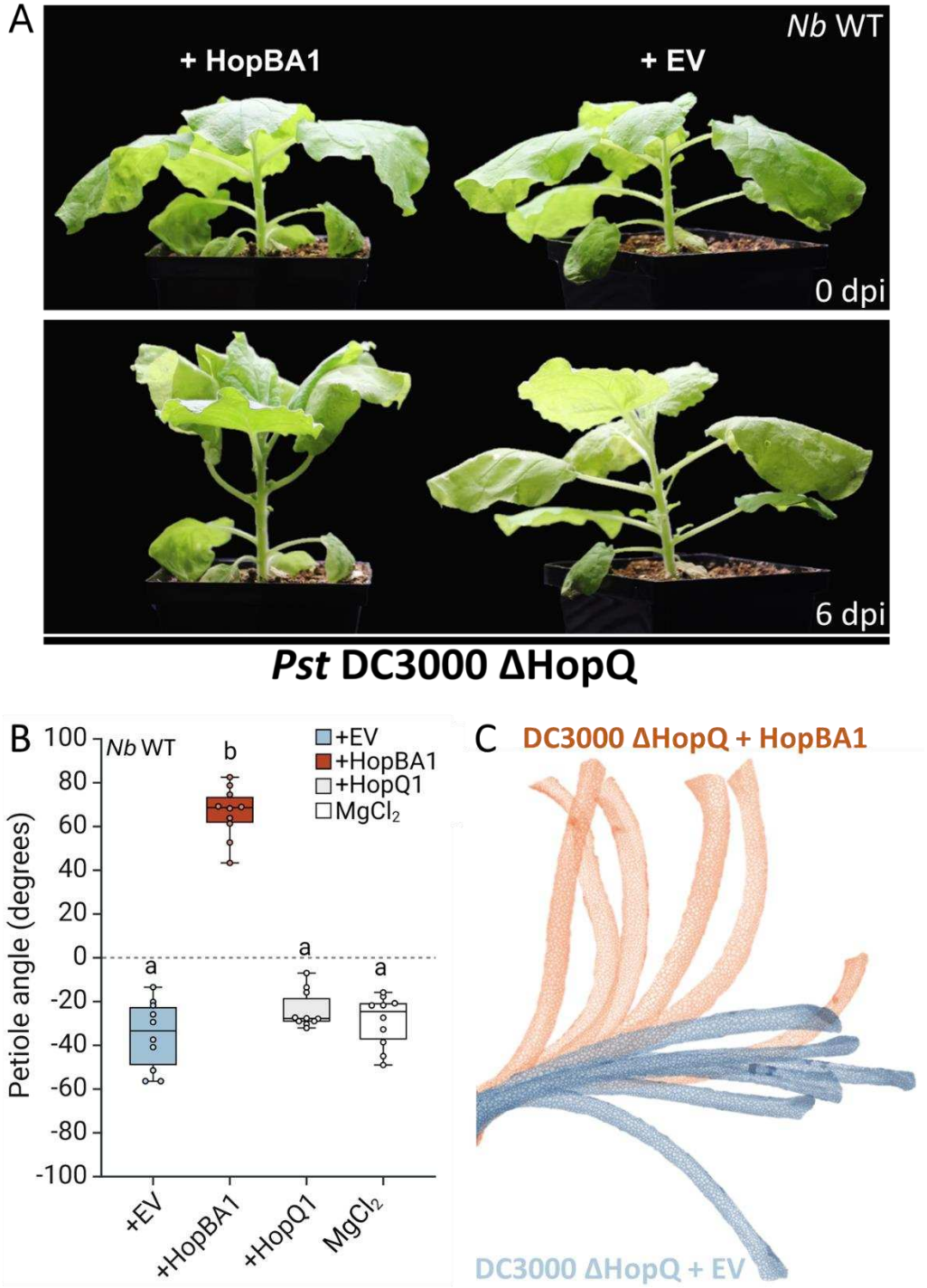

Figure 2.4. HopBA1 induces hyponasty in the petioles of infiltrated leaves. (A) Plants showing the morphological change that occurs after bacterial infiltration, where + *hopBA1* induces hyponasty (left) and + EV is hyponasty negative (right). (B) Whole leaf infiltration with DC3000 Δ*hopQ* + *hopBA1* leads to a positive petiole angle (degrees) by 6 dpi. All other treatments (+ EV, + *hopQ1*, and 10mM $MgCl_2$) result in negative petiole angles at 6 dpi. 5 biological replicates used over multiple experiments. One-way ANOVA and Tukey's HSD were used to assign significance groups. (C) Stylized petioles showing the morphology associated with + *hopBA1* (orange, upward bend) vs. + EV (blue, downward bend) at 6 dpi. Leaf and stem tissue excised to improve petiole visibility.

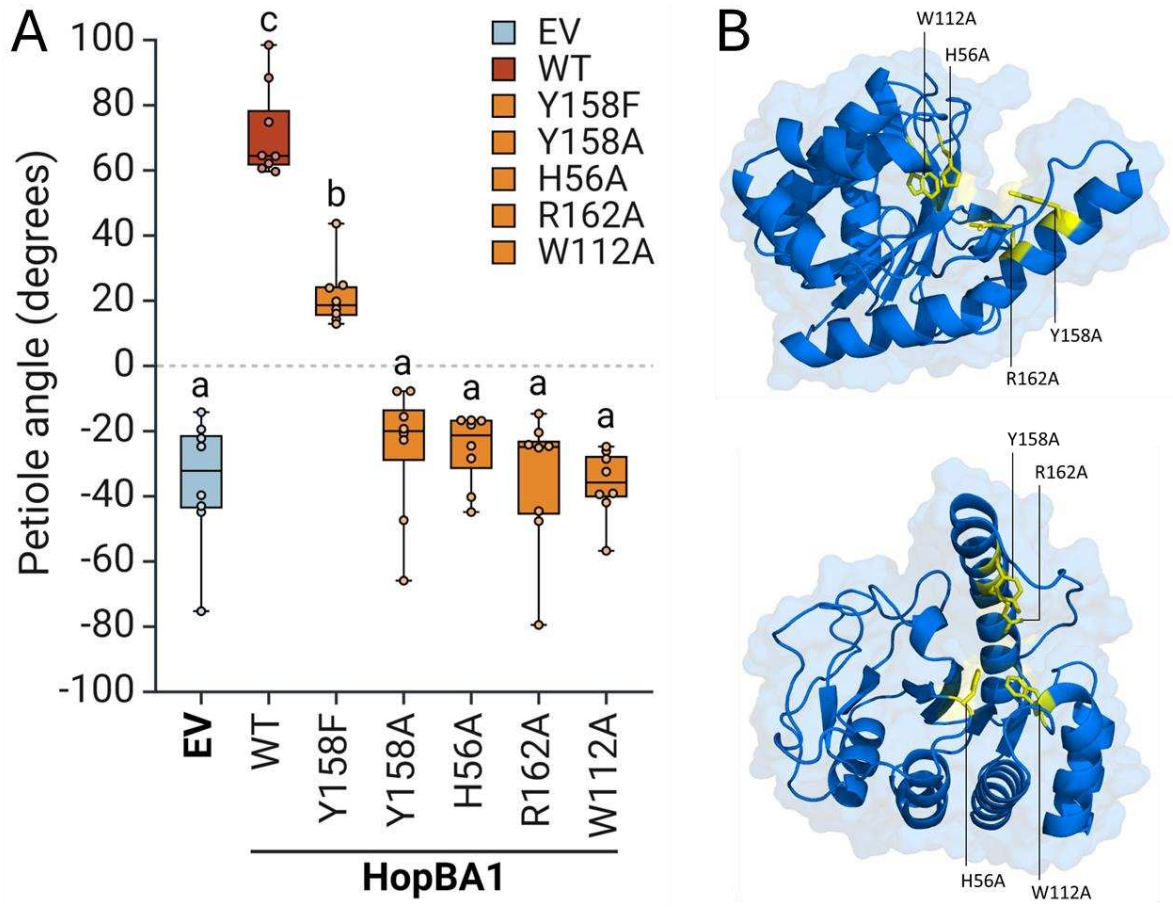

Figure 2.5. A subset of HopBA1 mutants lose the ability to induce petiole hyponasty. (A) Petiole angle measurements for DC3000 Δ*hopQ* + HopBA1^{Y158F}, ^{Y158A}, ^{H56A}, ^{R162A}, and ^{W112A}, as well as + EV and + HopBA1 (WT) controls. All X residue-to-A mutants result in loss of HopBA1's functional ability to induce hyponasty. +HopBA1^{Y158F}, presumed to not be a full LOF mutation, retains a dampened capacity to cause hyponasty (statistically greater petiole angle than +EV, but also a significantly lower angle than +HopBA1). 8 biological replicates (plants) were used, and petiole angles were measured at 6 dpi. All plants were *Nb* WT. One-way ANOVA and Tukey's HSD were used to assign significance groups. (B) HopBA1 protein structure (PDB ID code 5T09) showing the locations of mutated residues (yellow with sidechains shown and individual residue callouts).

in Arabidopsis (Nishimura *et al.*, 2017) to see if these mutations also resulted in a loss of hyponasty. DC3000 Δ*hopQ* + *hopBA1*^{Y158A}, *hopBA1*^{H56A}, *hopBA1*^{R162A}, and *hopBA1*^{W112A} were all found to lose hyponasty, resulting in negative petiole angles (means ~ -26°, -26°, -35°, and -36°, respectively), which were not statistically different than DC3000 Δ*hopQ* + EV (mean ~ -35°) (Figure 2.5 A). One of the tested mutants, HopBA1^{Y158F}, appeared to retain partial function based on a positive petiole angle (mean ~22°) that was significantly lower than DC3000 Δ*hopQ* + *hopBA1*

(WT) (mean ~72°), but significantly higher than DC3000 Δ*hopQ* + EV and all other HopBA1 mutants (Figure 2.5 A).

Next, we sought to test HopBA1's ability to induce hyponasty when delivered by *Pst* mutants lacking key virulence factors. A putative motility mutant with defects in flagella and Type IV pili (DC3000 Δ*hopQ* Δ*fliC* Δ*pilA*) was generated and tested (Figure 2.6 A), a coronatine-deficient strain (DC3118) was tested in *Nb roq1* plants (Figure 2.6 B), and finally, a strain lacking all 36 effectors (DC3000 D36E) was tested (Figure 2.6 C). In all three cases, strains delivering HopBA1 were found to induce hyponasty, albeit to differing extents.

DC3000 Δ*hopQ* Δ*fliC* Δ*pilA* + *hopBA1* resulted in petiole angles (mean ~ 41°), which were not significantly different from DC3000 Δ*hopQ* + *hopBA1* (mean ~ 44°) (Figure 2.6 A). Likewise, we observed no significant difference in petiole angles for DC3000 Δ*hopQ* Δ*fliC* Δ*pilA* + EV (mean ~ -30°) and DC3000 Δ*hopQ* + EV (mean ~ -33°) (Figure 2.6 A). DC3118 is derived from DC3000 but lacks the ability to synthesize coronatine (Ma *et al.*, 1991), a key phytotoxin enhancing the strain's pathogenic capacity. Since DC3118 contains *hopQ1*, hyponasty experiments were necessarily conducted in *Nb roq1* plants rather than *Nb* WT. In this experiment DC3118 + *hopBA1* resulted in petiole angles that were not statistically different than DC3000 Δ*hopQ* + *hopBA1* (mean ~ 24° and ~ 29°, respectively) (Figure 2.6 B). Although a positive petiole angle is observed for both strains, it is worth noting that all strains delivering HopBA1 that were tested in *Nb roq1* consistently yielded lower mean petiole angles than in *Nb* WT and other *Nb* mutants that were tested (FIG 2.16 E; Supplemental Table 1). Interestingly, DC3118 + EV resulted in a significantly greater petiole angle (mean ~ -14°) than DC3000 Δ*hopQ* + EV (mean ~ -67°) (Figure 2.6 B).

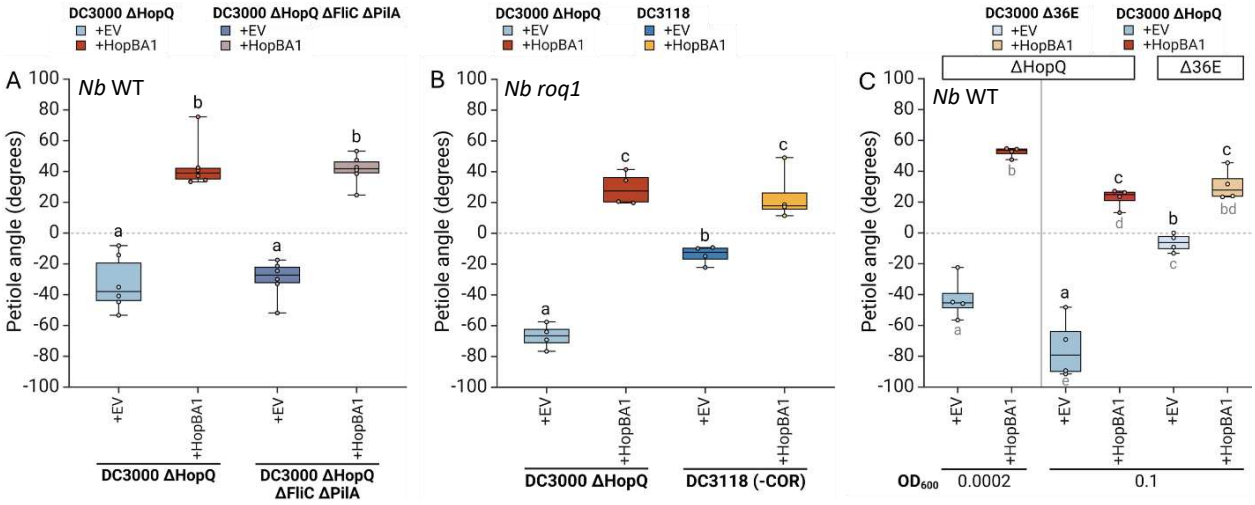

Figure 2.6. HopBA1 induces hyponasty in a subset of *Pst* virulence-defective mutants. (A) HopBA1 petiole angle isn't impacted by in the generated double-motility mutant, DC3000 Δ*hopQ* Δ*fliC* Δ*pilA* (predicted -gliding and -twitch motility). Six biological replicates were utilized. (B) Production of the phytotoxin coronatine isn't required for HopBA1-induced hyponasty. Four biological replicates were utilized. (C) HopBA1 induces hyponasty in absence of all other DC3000 effectors at high OD (OD_{600} = 0.1). Further, higher bacterial concentration reduces petiole angle in a strain-independent manner. Four biological replicates were used. One-way ANOVA and Tukey's HSD were used in A, B, and C (only black significance groups). Two-way ANOVA (strain by concentration) and Tukey's HSD were additionally applied in C (gray significance groups). All petiole angles (A – C) were measured at 6 dpi.

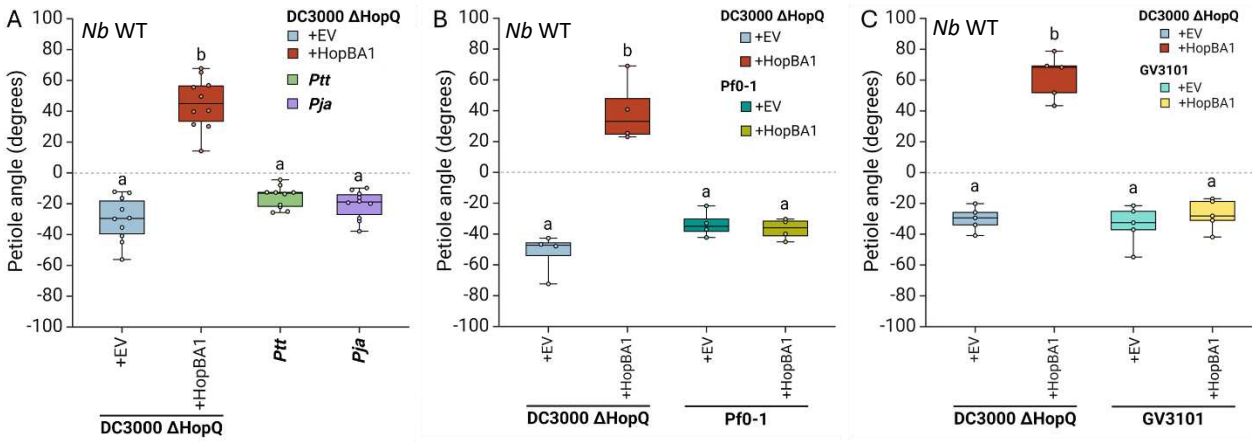

Figure 2.7. HopBA1 fails to induce hyponasty in other *Pst* pathovars, *Pf0-1*, and *Agrobacterium*. (A) HopBA1 origin strains, *Pseudomonas syringae* pv. *aptata* (*Ptt*) and pv. *japonica* (*Pja*) are hyponasty negative. Petiole angles were measured at 6 dpi with 10 biological replicates over multiple experiments. (B) *Pseudomonas fluorescens* expressing a TTSS (*Pf0-1*) delivering HopBA1 fails to induce hyponasty. 5 biological replicates were used. (C) Delivery of HopBA1 by *Agrobacterium* (GV3101) likewise does not induce hyponasty in *Nb* WT. 5 biological replicates were used. Petiole angles were measured at 9 dpi (B and C). One-way ANOVA and Tukey HSD were used to assign statistical groups (A – C).

DC3000 D36E is dramatically less virulent than DC3000 Δ*hopQ* (Bao *et al.*, 2014; Wei *et al.*, 2018) and is essentially a non-pathogen. To compensate for D36E's lack of growth after infiltration, we used a higher bacterial inoculum (i.e., OD_{600} = 0.1 vs. OD_{600} = 0.0002) to ensure bacterial density would be similar to experiments using DC3000 Δ*hopQ*. When DC3000 D36E + *hopBA1* and DC3000 Δ*hopQ* + *hopBA1* were infiltrated at the same high OD, petiole angles were statistically equal (Figure 2.6 C). However, use of such a high OD seems to be a confounding factor in the assay for DC3000 Δ*hopQ* strains because high OD results in significantly lower petiole angles for both DC3000 Δ*hopQ* + EV and + *hopBA1* when compared to their OD_{600} = 0.0002 counterparts (Figure 2.6, gray significance groups below boxplots). Notably, regardless of OD and strain that HopBA1 was added to, petiole angles maintain a positive value and thus are hyponastic (Figure 2.6). As a final observation, DC3000 D36E + EV appears to result in the opposite effect, where petiole angle is significantly increased relative to DC3000 Δ*hopQ* + EV at any concentration (Figure 2.6).

Since hyponasty was still induced by HopBA1 in impaired DC3000/*Pst* strains, we wondered if HopBA1 could induce hyponasty when delivered by (1) *Pseudomonas syringae* pathovars that natively contain HopBA1, (2) non-pathogenic *Pseudomonas fluorescens*e engineered to deliver single effectors , and (3) *Agrobacterium* transient expression. *Pseudomonas syringae* pv. *aptata* (*Ptt*) and *Pseudomonas syringae* pv. *japonica* (*Pja*) both natively contain alleles of HopBA1. Surprisingly, neither strain induced hyponasty in *N. benthamiana*, resulting in negative petiole angles equal to DC3000 Δ*hopQ* + EV (Figure 2.7 A). This phenotypic difference was not due to differences at the level of coding sequence as the $HopBA1_{Ptt}$ allele is 100% nucleotide-identical to the HopBA1 allele used in DC3000-based experiments ($HopBA1_{Pja}$ is polymorphic at 2/239 amino acids). Next, we tested non-pathogenic *Pseudomonas fluorescens*, engineered to deliver effectors

with a TTSS (*Pf0-1* EtHAn, "*Pf0-1*" hereafter) (Thomas *et al.*, 2009). Similar to native strains, *Pf0-1* + *hopBA1* failed to induce hyponasty (Figure 2.7 B). Finally, *Agrobacterium* (GV3101) was used to transiently express HopBA1 (Figure 2.7 C). Previous work (Appendix A), although not using whole leaf infiltration, suggested that *Agrobacterium*-delivered HopBA1 would lead to no observable phenotypes. As anticipated, transient expression of HopBA1 from GV3101 did not induce hyponasty. Next, DC3000 Δ*hopQ* + *hopBA1* was assessed for its ability to induce hyponasty in WT and *EDS1*-silenced *Nicotiana tabacum*, as well as numerous immunocompromised Arabidopsis mutants, none of which displayed hyponasty (Supplemental Table 1).

HopBA1 alters host phytohormones in leaves and petioles

After finding that HopBA1 causes petiole hyponasty, we were interested in identifying phytohormone changes within infiltrated leaves and within the associated petioles. Since many phytohormones are implicated in both development and immunity (Berens *et al.*, 2017), we also hoped to gain additional data that might be informative to defense and/or pathogenesis differences dependent on HopBA1. To do this we employed targeted LC-MS/MS with internal standards to determine the relative abundances (normalized peak area) of abscisic acid (ABA), gibberellic acid (GA), indole-3-acetic acid (IAA), Indole-3-acetyl-aspartic acid (IA-Asp), jasmonic acid (JA), jasmonoyl isoleucine (JA-Ile), 12-oxo-phytodienoic acid (ODPA), salicylic acid (SA), and trans-zeatin (tZ). For all detectable phytohormones, except for ABA, infiltrations of DC3000 Δ*hopQ* + *hopBA1* resulted in no significant change or a decrease in hormone abundance relative to DC3000 Δ*hopQ* + EV (Figure 2.8; Appendix B, Figure S7 A). The most significant reduction to phytohormones paired with DC3000 Δ*hopQ* + *hopBA1* infiltration was to JA-related compounds (Figure 2.8 B) and auxin (IAA) (Figure 2.8 A). In leaves, JA-Ile mean normalized peak area was reduced from ~5.059 in DC3000 Δ*hopQ* + EV infiltrations to ~1.285 in DC3000 Δ*hopQ* + *hopBA1*

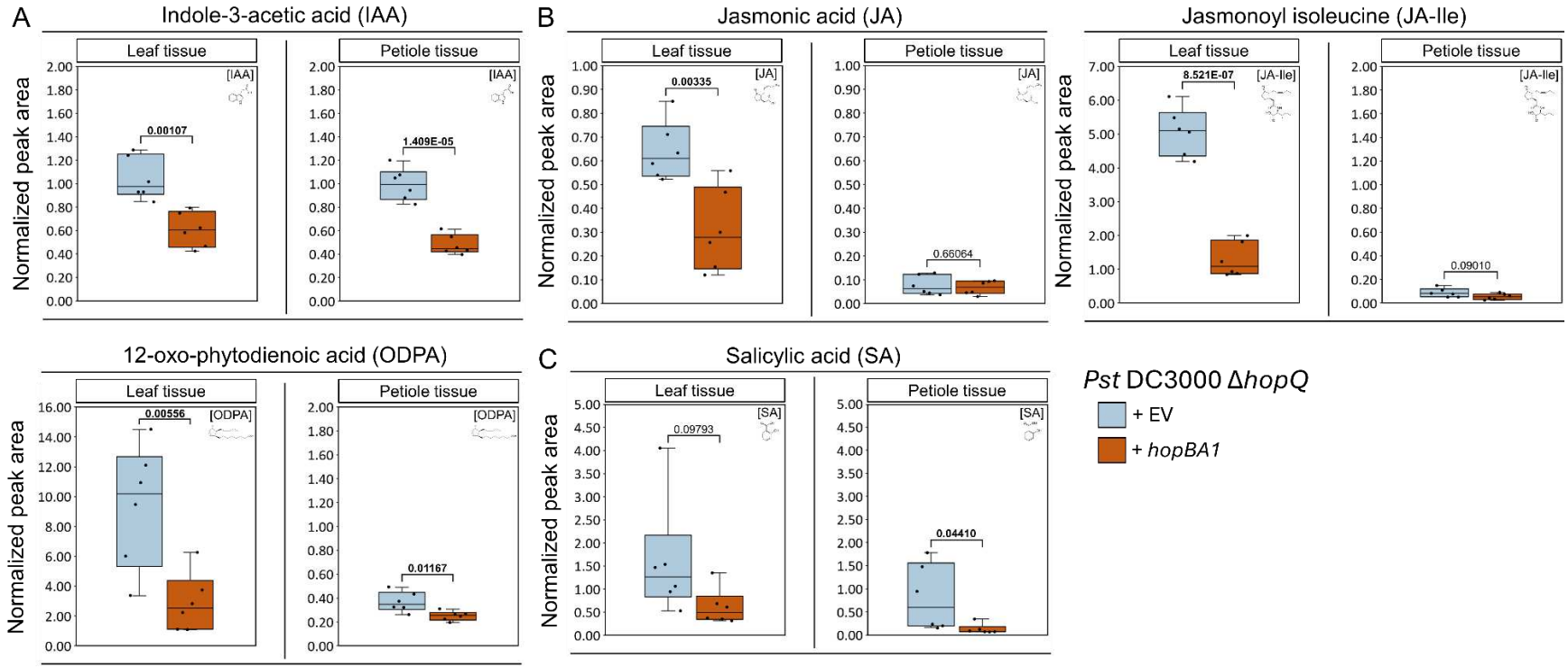

Figure 2.8. A phytohormone panel reveals an association between HopBA1 and reduced abundance of several key hormones involved in defense and development. (A) **IAA**-related results with significantly different normalized peak area between strains. Leaf + EV ~1.043, leaf + HopBA1 ~0.608 ($P \approx 0.011$). Petiole + EV ~0.993, petiole + HopBA1 ~0.480 ($P \approx 1.41E-05$). (B) JA-related hormones with at least one tissue type result with significantly different normalized peak area between strains. **JA**: Leaf + EV ~0.641, leaf + HopBA1 ~0.309 ($P \approx 3.35E-03$). Petiole + EV ~0.076, petiole + HopBA1 ~0.067 ($P \approx 0.660$). **JA-Ile**: Leaf + EV ~5.059, leaf + HopBA1 ~1.285 ($P \approx 8.52E-07$). Petiole + EV ~0.087, petiole + HopBA1 ~0.053 ($P \approx 0.090$). **ODPA**: Leaf + EV ~9.380, leaf + HopBA1 ~2.879 ($P \approx 0.006$). Petiole + EV ~0.367, petiole + HopBA1 ~0.251 ($P \approx 0.012$). (C) **SA**: results with at least one tissue type result with significantly different normalized peak area between strains. Leaf + EV ~1.595, leaf + HopBA1 ~0.613 ($P \approx 0.098$). Petiole + EV ~0.807, petiole + HopBA1 ~0.131 ($P \approx 0.044$). Tissue sampled at 3 dpi. 6 biological replicates. Strain used: DC3000 ΔHopQ + EV (blue) or + HopBA1 (orange). One-way ANOVA.

infiltrations (Figure 2.8 B). JA and ODPA followed a similar trend in leaves (Figure 2.8 B). IAA was notably reduced strongly in both petioles and leaves following infiltration with DC3000 Δ*hopQ* + *hopBA1* (Figure 2.8 A). SA content was reduced in petioles following infiltration with DC3000 Δ*hopQ* + *hopBA1* (Figure 2.8 C). Although ABA was not significantly different when comparing DC3000 Δ*hopQ* + EV and + *hopBA1*in either tissue type, this was the only elevated hormone observed in + *hopBA1*infiltrations (Appendix B, Figure S7 A). For leaves, mean peak area for DC3000 Δ*hopQ* + EV was ~0.693 and this was increased to ~1.004 for DC3000 Δ*hopQ* + *hopBA1* infiltrations at a marginal $P = 0.070$ (Appendix B, Figure S7 A). GA and tZ were not detectable in the panel.

RNA-Seq results reveal that HopBA1 perturbs host development and defense in a tissue-specific fashion

Next, we sought to better understand and complement phytohormone data, by characterizing HopBA1-dependent transcriptional responses using RNA-Sequencing (RNA-Seq). Parallel to the approach taken with the phytohormone panel, processing and analysis was conducted by tissue type (leaf or petiole) 3 days after bacterial infiltration. Preliminary assessment of RNA-Seq data (DESeq2) supported differential expression of genes between DC3000 Δ*hopQ* + EV infiltration and DC3000 Δ*hopQ* + *hopBA1*infiltration. Principal component analysis supports distinct transcriptional profiles that separate or cluster by strain and tissue type (Figure 2.9 A). We found that 1,154 genes were differentially up-regulated in leaves infiltrated with DC3000 Δ*hopQ* + *hopBA1*, while 904 were differentially up-regulated in petioles with 638 of these genes being shared between leaves and petioles (Figure 2.9 B). 806 genes were differentially down-regulated in leaves, while 588 were down-regulated in petioles with 169 of these genes being shared between leaves and petioles (Figure 2.9 B). Finally, 22 genes were found to have an inverse regulation between leaves (down-regulated) and petioles (up-regulated), and 12 genes were inverted in the opposite

direction (up-regulated in leaves and down-regulated in petioles) when infiltrated with DC3000 Δ*hopQ* + *hopBA1* (Figure 2.9 B).

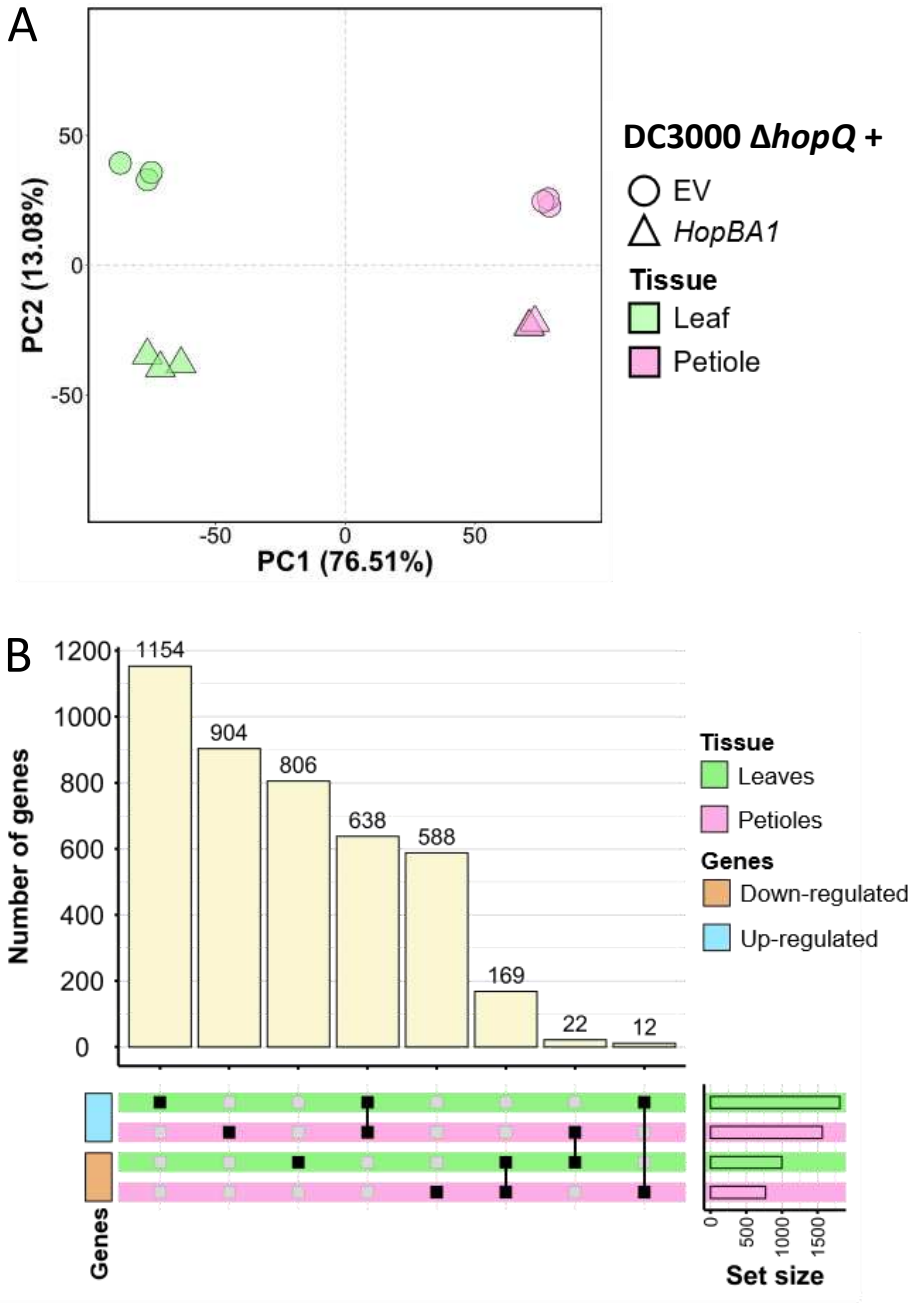

Figure 2.9. RNA-Seq summary data for leaf and petiole tissues infiltrated with *Pst* DC3000 ΔHopQ1 + EV vs. + HopBA1. (A) Principal Component Analysis (PCA) of the four datasets compared (+ EV leaf tissue, + EV petiole tissue, + *hopBA1* leaf tissue, and + HopBA1 petiole tissue). (B) An upset plot showing the distribution of differentially expressed genes (DEGs). An FDR of 0.05 was used with a shrunken LFC and $\log_2$ of 1. Three biological replicates (i.e., plants) were used for libraries and total RNA was extracted from tissue from four distinct leaves/petioles within each biological replicate.

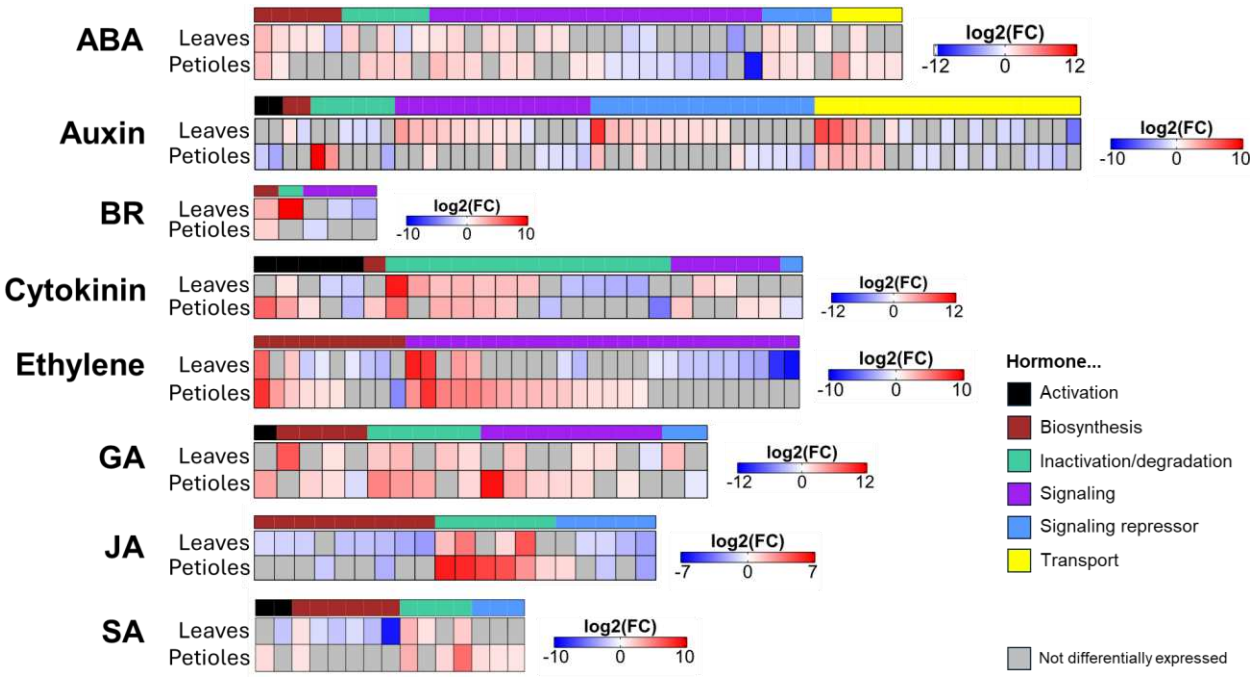

Figure 2.10. Transcriptional differences for genes responsible for activation, biosynthesis, inactivation/degradation, signaling (general and repressing), and transport of all major phytohormones. Heatmaps indicate the range of $\log_2$(fold change) in expression. Red indicates up-regulation, blue indicates down-regulation, and gray indicates that the gene is not differentially expressed. Gene activity is color-coded (bar immediately above heatmap) and expression is separated by leaf and petiole identities.

We then used the draft *N. benthamiana* genome, NbLab360 (Ranawaka *et al.*, 2023) and EggNog mapper to generate a functionally annotated proteome grouped by differential regulation (up and down) within each tissue type (leaf and petiole) for DC3000 Δ*hopQ* + *hopBA1* relative to DC3000 Δ*hopQ* + EV expression. Functional annotations and Gene Ontology (GO) term assignment of differentially expressed genes identified genes involved in the synthesis, signaling, and transport of phytohormones (Figure 2.10). In terms of sheer number, auxin, ethylene, and ABA-related genes are broadly the most involved/differentially regulated as a response to infiltration with DC3000 Δ*hopQ* + *hopBA1* (Figure 2.10). ABA-related genes had the general trend of up-regulation in both tissue types, with the exception of the signaling class which contained both up- and down-regulated genes (Figure 2.10). Auxin signaling and repression appeared to be up-regulated in leaves, while transport of auxin was both up- and down-regulated in leaves and petioles

(Figure 2.10). Ethylene related gene regulation was perhaps the most interesting within this grouping as there is a heavy bias toward up-regulation of ethylene related genes in petioles (with a few exceptions for signaling within leaf tissue), while the general trend in leaves is either down-regulation or no differential regulation relative to + EV (Figure 2.10).

GO terms were further assessed for enrichment utilizing the BiNGO feature in Cytoscape to gain insight into large-scale categorized process and responses that occurred following infiltration with DC3000 Δ*hopQ* + *hopBA1* in leaves and petioles. This analysis suggested that cell wall (CW) remodeling and biosynthesis of CW components were under the greatest level of change (and these genes were exclusively up-regulated) in petioles following infiltration with DC3000 Δ*hopQ* + *hopBA1*, with some commonality found in leaves as well (Figure 2.11-A). Of these terms, cell wall macromolecule catabolic process, galacturonate and glucan biosynthetic processes were the only three that appear to have a larger role within leaves than in petioles (Figure 2.11-A). We were also interested in how DC3000 Δ*hopQ* + *hopBA1* might be affecting developmental processes more broadly (Figure 2.11-B), immune responses (Figure 2.11-C), induced defenses (Figure 2.11-D), phytohormone biosynthesis and perception (Figure 2.11-E), as well as stress responses (Appendix B, Figure S8-A) and transport (Appendix B, Figure S8-B) in leaves and petioles following infiltration with DC3000 Δ*hopQ* + *hopBA1*.

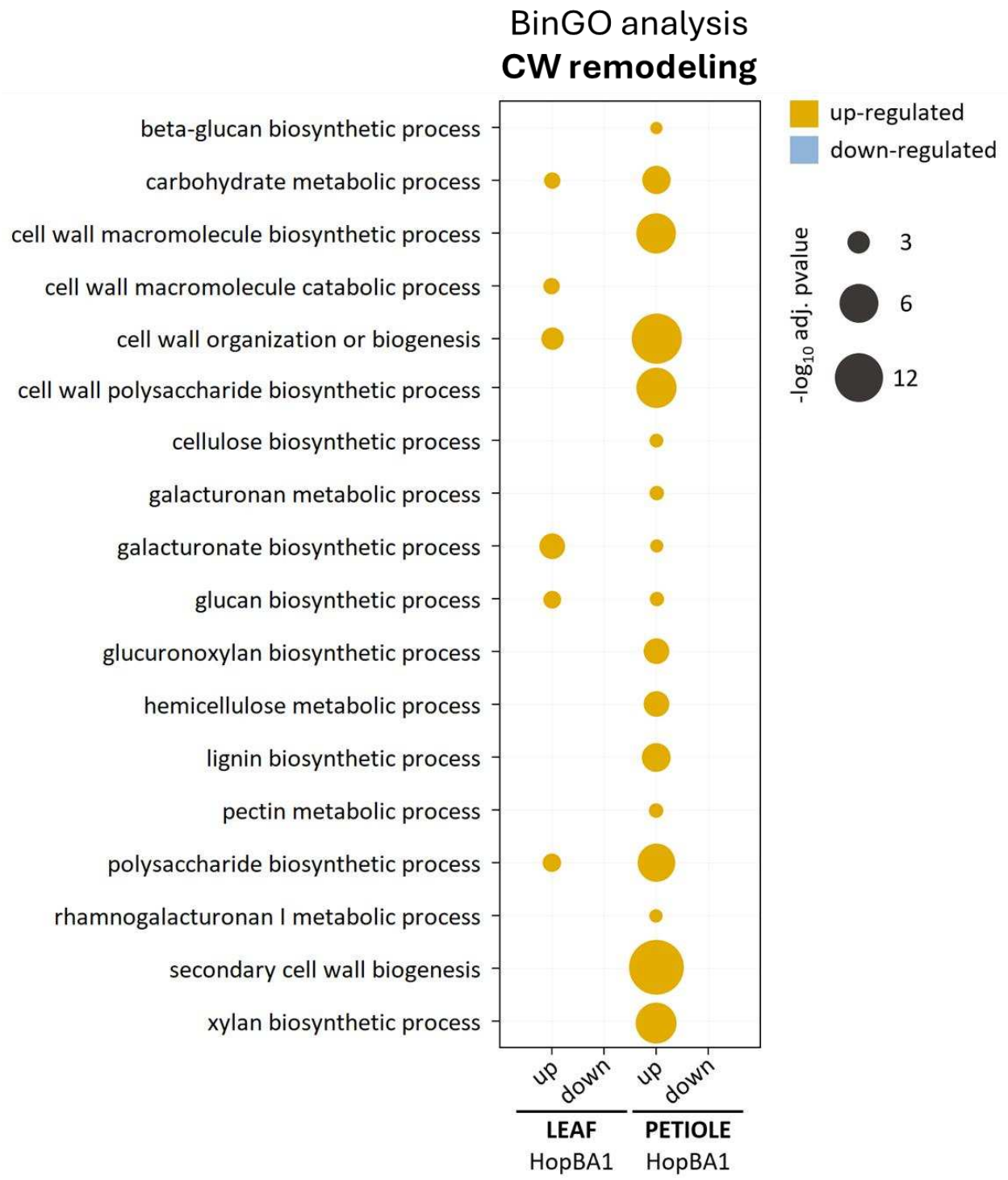

Figure 2.11-A. Enriched GO terms relating to cell wall (CW) structural components, biogenesis, and modification, which were up-regulated in petioles following DC3000 Δ*hopQ* + *hopBA1* infiltration.

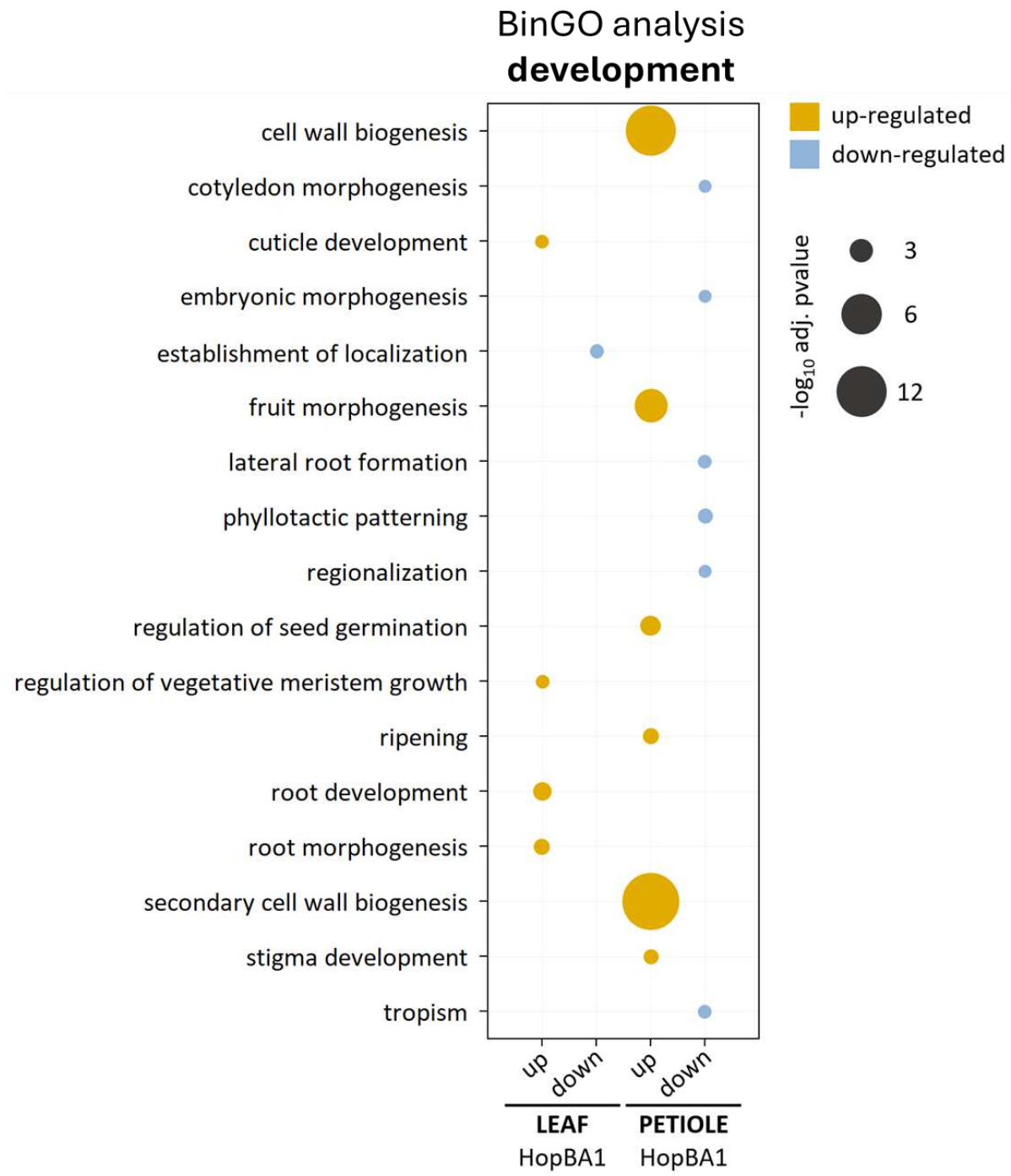

Figure 2.11-B. Enriched GO term analysis suggests that HopBA1 leads to diverse developmental changes, both relating to and independent from cell wall-related processes.

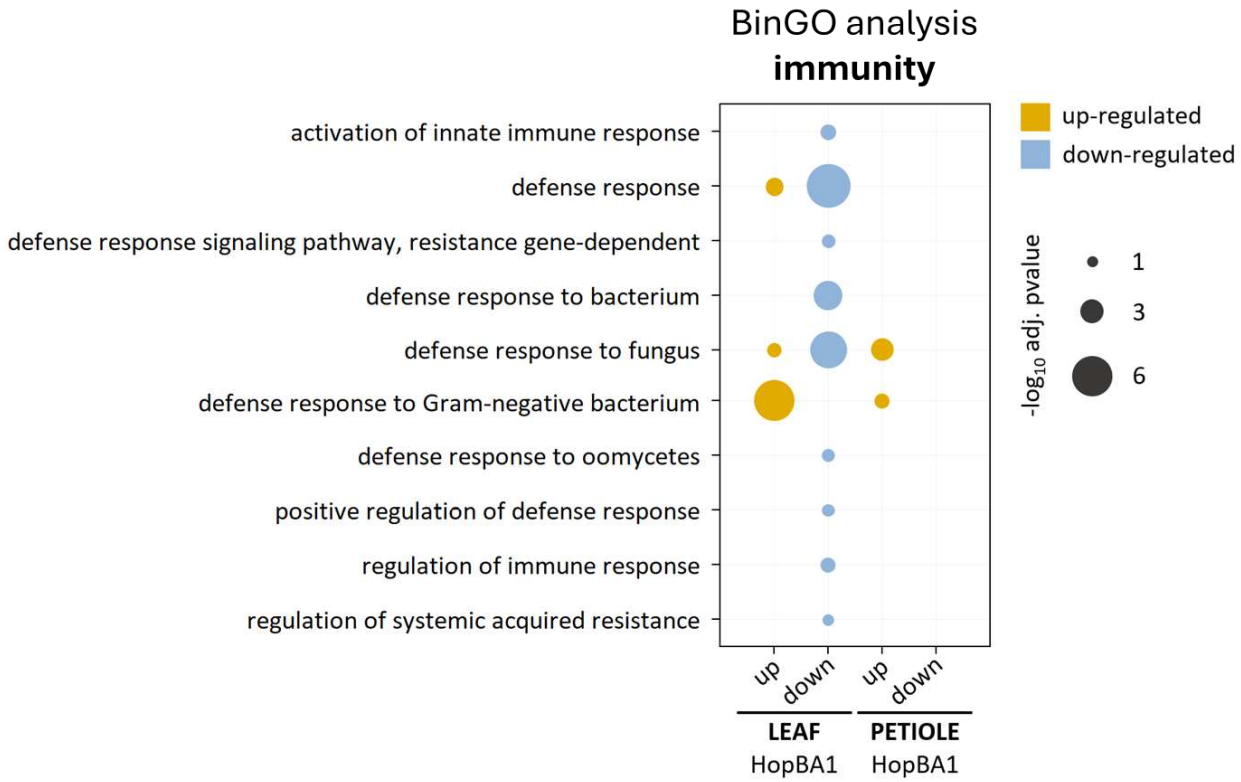

Figure 2.11-C. Enriched GO term analysis suggests the predominant effect of DC3000 Δ*hopQ* + *hopBA1* infiltration is suppression of immunity in leaves and a loss of suppression within petioles. Broadly, a wide range of immunity or defense related genes are down in leaves with infiltrated with DC3000 Δ*hopQ* + *hopBA1*. The major exception to this is defense response to Gram-negative bacterium, which is strongly (and uniquely) only up-regulated. This term is defined primarily by the involvement of UDP-D-glucuronate 4-epimerases (GAEs) and Plant invertase/pectin methylesterase inhibitors (PMEs and PMEIs).

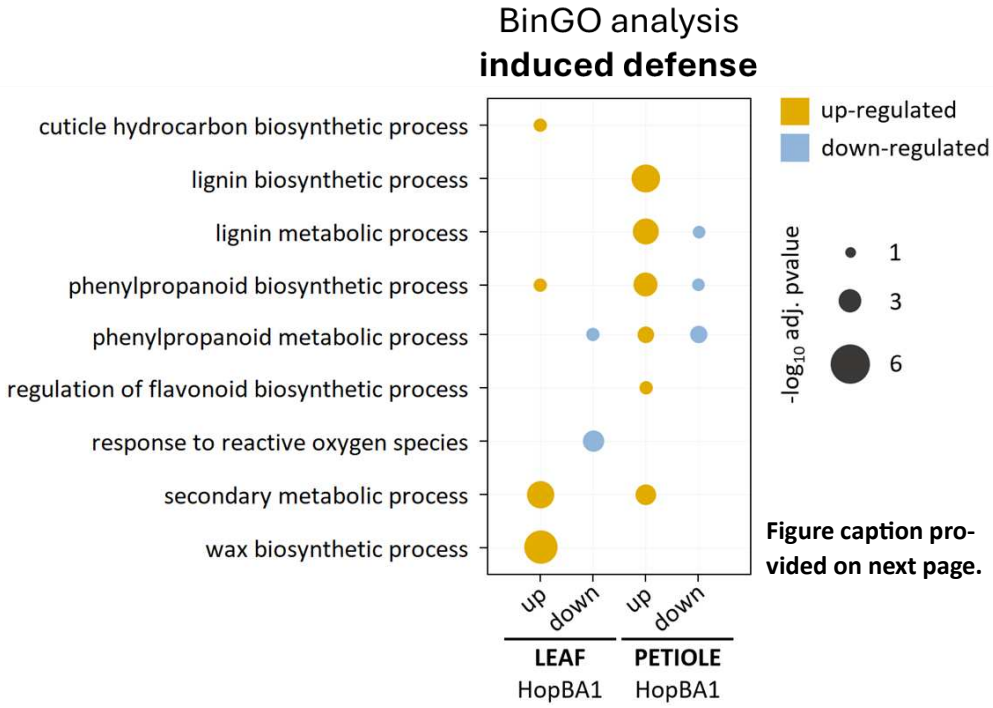

Figure caption provided on next page.

Figure 2.11-D. GO enriched terms with possible connection to induced defenses triggered by DC3000 Δ*hopQ* + *hopBA1* infiltration. Most processes are increased in petioles but are also downregulated to a lesser extent. The most notable up-regulated terms, which are unique to leaves, relate to cuticle and wax biosynthetic processes. Note that some of these terms could also relate to induced abiotic stress and the dramatic structural/morphological changes induced by DC3000 Δ*hopQ* + *hopBA1*.

Pst DC3000 Δ*hopQ* has an unrecognized role as an aggressive vascular pathogen of *N. benthamiana* and delivery of HopBA1 inhibits systemic infection

Next, we wondered if bacteria were present within the petioles of infiltrated leaves since hyponasty was a petiole-specific phenotype. To answer this question, we repeated whole leaf infiltrations, instead using a fluorescently labeled bacterial strain (DC3000 Δ*hopQ*::3xmCherry). Following infiltrations, fluorescence microscopy was used to assess the bacteria-associated signal within different parts of the petiole (at the distal petiole (DP), i.e., closest to the infiltrated leaf, and at the proximal petiole (PP), i.e., closest to the stem) and within the stem at different timepoints. Surprisingly, we found that by 9 – 12 dpi the fluorescent signal was not only strong within distant tissue (i.e., within the un-infiltrated petioles and stems), but was also localized to the vascular bundles of petioles for both strains, DC3000 Δ*hopQ*::3xmCherry + EV and Δ*hopQ*::3xmCherry + *hopBA1*, and within the stem of the plant for DC3000 Δ*hopQ*::3xmCherry + EV (Figure 2.12). This suggested that bacteria are primarily present within some component of the plant vascular system (i.e., xylem and/or phloem).

Interestingly, we found that DC3000 Δ*hopQ* is an aggressive colonizer of vasculature in *N. benthamiana*, and that HopBA1 apparently acts in a way that limits or inhibits the extent to which bacteria can colonize the plant vascular system, and thus, the ability to cause severe systemic disease symptoms (Figures 2.12, 2.13 A – C, and 2.15 C). In addition to the observation that DC3000 Δ*hopQ* + EV was present within the vasculature of petioles associated with infiltrated leaves and the stem, we found that the bacteria also spread significant distances (~8 cm away from the nearest infiltrated leaf), reaching distinct un-infiltrated organs, both above and below-ground (i.e.,

un-infiltrated leaves, as well as within the primary and secondary root system) by 12 dpi (Figure 2.13 A – C). Above-ground tissue colonized by bacteria was associated with vascular necrosis, as well as the typical chlorosis (Figures 2.13 A – B and 2.15 A), while roots never developed observable disease symptoms (Figure 2.13 C). Systemic disease caused by DC3000 Δ*hopQ* + EV is more severe than that caused by DC3000 Δ*hopQ* + *hopBA1* (Figures 2.15 A – C and S10 A). However, infection with DC3000 Δ*hopQ* + *hopBA1* still results in stunted plant growth and defects relating to maturation/flowering relative to the avirulent strain DC3000 Δ*hopQ* + *hopQ1* (Appendix B, Figure S10).

` Following these initial observations, we wanted to strengthen our confidence in these results and establish their reproducibility. Accordingly, we sought to quantify the bacteria that were present within a defined area of petioles and stems over an established time course of infection. To do this we developed a petiole and stem-based bacterial growth assay (based upon Thiergart *et al.*, 2020) to ensure the removal of epiphytic bacterial populations without the disruption of endophytic populations, which we previously demonstrated were primarily confined to the plant vasculature (Figure 2.12). In addition to the strains visualized with fluorescence microscopy, DC3000 Δ*hopQ* + EV and DC3000 Δ*hopQ* + *hopBA1*, DC3000 Δ*hopQ* + *hopQ1* was again included to help understand what bacterial growth for a "typical" avirulent strain would look like in this new sampling context (Figure 2.14).

The main finding from this assay was that DC3000 Δ*hopQ* + *hopBA1* grew at comparable levels to DC3000 Δ*hopQ* + EV at the distal petiole (DP), closest to the leaf, but was either growth limited or movement restricted when the sampling location was further away from the leaf (i.e., at the proximal petiole (PP) and the stem), growing at least 1 log less than DC3000 Δ*hopQ* + EV at all timepoints past 3 dpi, and at most, ~3 logs less at 9 dpi (Figure 2.14). These results seem

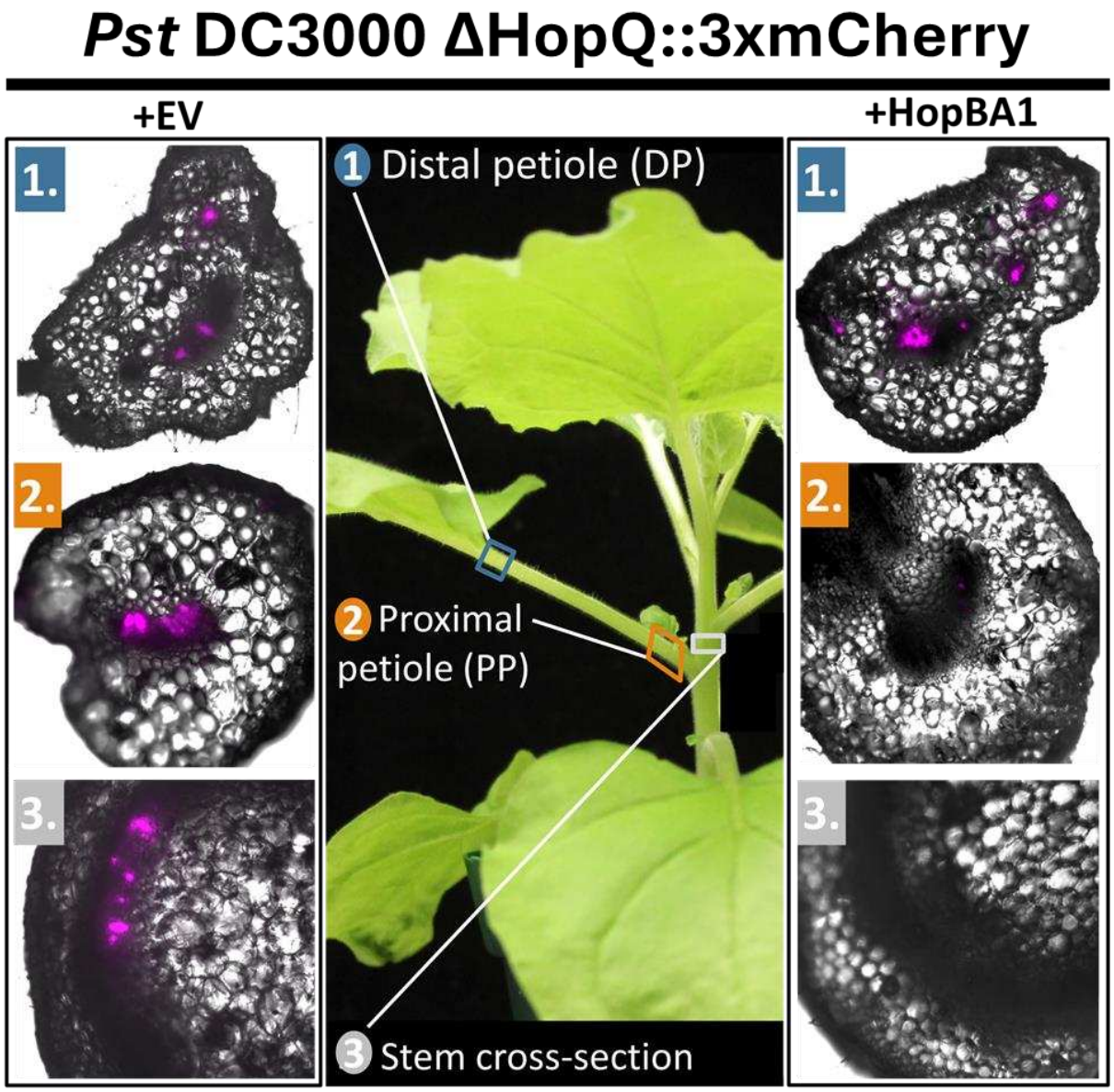

Figure 2.12. DC3000 Δ*hopQ* + EV readily colonizes the vascular system of *Nb* following whole leaf infiltration, while the addition of DC3000 Δ*hopQ* + *hopBA1* leads to the restriction of bacterial growth, entry, or movement. The strongest fluorescent signal (shown in magenta) is restricted to the vascular bundles of petioles and stems. DC3000 Δ*hopQ* + EV is present at all sampled points: distal petiole (closest to the infiltrated leaf) (DP), proximal petiole (petiole base next to the stem) (PP), and within the stem. DC3000 Δ*hopQ* + *hopBA1* is present in the DP, and is very faintly observable in the PP, but is absent from the stem. Strain: DC3000 Δ*hopQ*::3xmCherry. Representative images at 9 dpi in *Nb* WT.

harmonious with our fluorescence microscopy observations (Figure 2.12). Interestingly, DC3000 Δ*hopQ* + *hopBA1* and DC3000 Δ*hopQ* + *hopQ1* grew the same at the PP sampling location (except at 9 dpi), even though DC3000 Δ*hopQ* + *hopQ1* grew ~1.5 to ~2.5 logs less than DC3000 Δ*hopQ* + *hopBA1* when sampling the DP Figure 2.14). This comparison suggests that DC3000 Δ*hopQ* +

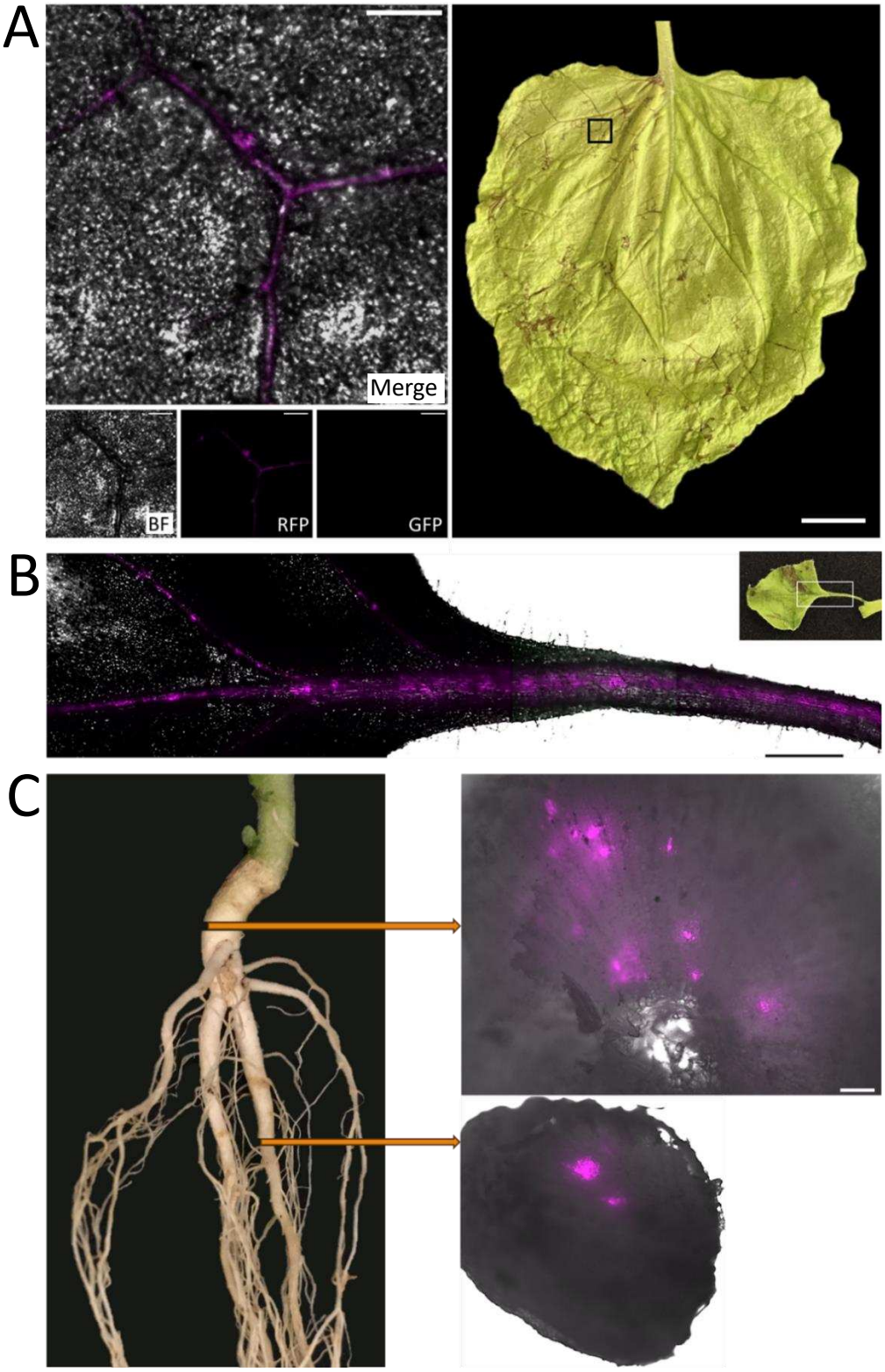

Figure 2.13. *Pst* DC3000 Δ*hopQ* + EV aggressively colonizes host vasculature (leaf, stem, and root) following whole leaf infiltration, leading to systemic disease symptoms (chlorosis and necrosis) in un-infiltrated aboveground tissue. (A) Bacteria (fluorescent signal) is confined to the vasculature of new vegetative growth (an expanded leaf closer to the apical meristem, relative to originally infiltrated leaves)

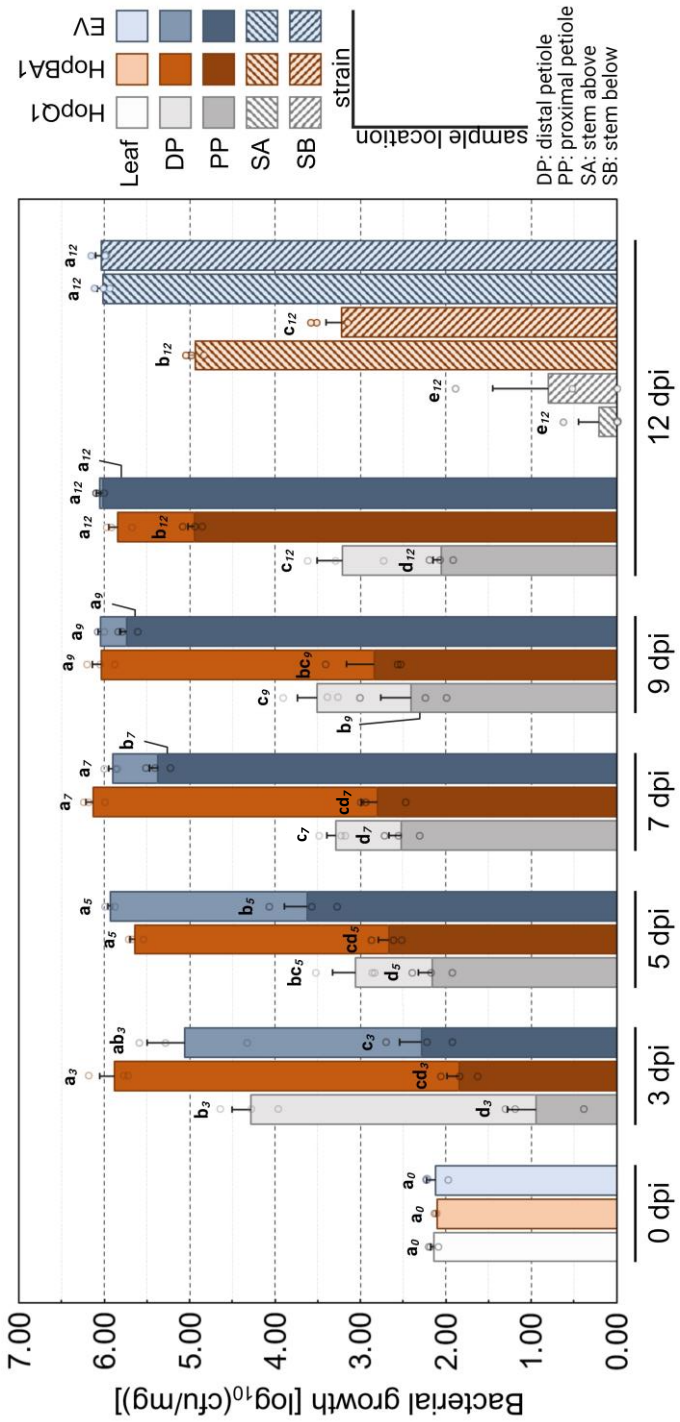

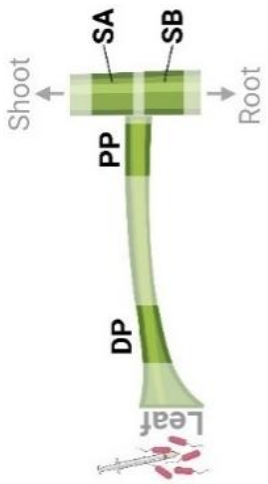

Figure 2.14. Petiole and stem bacterial growth curves for DC3000 Δ*hopQ* + EV, + *hopBA1*, and + *hopQ* in *Nb* WT. Results indicate that DC3000 ΔHopQ + HopBA1 growth is restricted, relative to + EV, further away from leaves (i.e., in proximal petioles and the stem), while DC3000 ΔHopQ + *hopQ1* growth is broadly restricted. 3 biological replicates. Significance groups are assigned within a given time point using one-way ANOVA and Tukey's HSD.

Figure 2.13 (Continued). and co-occurs with necrotic symptoms. BF: bright field. RFP: (red fluorescence filter). GFP: (green fluorescence filter, control for non-specific signal). Sampled at 12 dpi. Micro scale: 500µm, macro scale: 1cm. (B) Bacteria are present within the vasculature of basal axillary leaves. Image is BF + RFP + GFP (merge). Sampled at 12 dpi. Micro scale: 2mm. (C) Bacteria are present within the vasculature of the primary and secondary root, which was ~8cm away from the nearest infiltration site. Presented image is BF + RFP + GFP merge. Sampled at 15 dpi. Micro scale: 100µm. Bacteria are labeled with 3xmCherry.

hopBA1 transitions from a virulent strain within the leaf and an avirulent strain within the petiole, and perhaps more accurately, in a vascular-specific fashion. Bacterial growth results at 12 dpi, both for PP and stems, seem to demonstrate a "gap closing" between DC3000 Δ*hopQ* + EV and DC3000 Δ*hopQ* + *hopBA1* (Figure 2.14), however long-term plant and disease phenotypes suggest that DC3000 Δ*hopQ* + *hopBA1* likely fails to overcome systemic growth or movement restriction relative to DC3000 Δ*hopQ* + EV (Figure 2.15).

The realization that DC3000 Δ*hopQ* could extensively colonize the vasculature of *Nb* and that DC3000 Δ*hopQ* + EV bacterial growth was high in all sampled locations (e.g., petioles and stems) led us to wonder if a similar trend might occur in severely immunocompromised Arabidopsis. That is, we hypothesized that the plant immune system might be preventing *Pst* vascular entry and colonization in Arabidopsis, rather than *Pst* DC3000 lacking the necessary genetic adaptation to occupy such a niche within a host. To test this idea, we used an immunocompromised Arabidopsis mutant line, *deps rbohD* (Hillmer *et al.*, 2023), in combination with the previously tested DC3000 Δ*hopQ*::3xmCherry + EV and fluorescence microscopy. The selected Arabidopsis mutant line is a quintuple mutant, lacking *DDE2*, *EIN2*, *PAD4*, *SID2*, and *RBOHD*. Accordingly, the line is deficient in phytohormone signaling (jasmonic acid, ethylene, and salicylic acid), as well as camalexin synthesis, *Pathogenesis-Related 1* (*PR1*) expression, partial EDS1 function, and ROS production (Hillmer *et al.*, 2023). To our surprise, the ability of DC3000 Δ*hopQ*::3xmCherry + EV to colonize host vasculature in Arabidopsis *deps rbohD* largely resembled our observations from *Nb* plants and resulted in vascular-associated, systemic necrosis and chlorosis at later timepoints (Appendix B, Figure S12 D – E and C). We observed bacteria within the vasculature of the infiltrated leaf, as well as outside of this area of the leaf, including within leaf hydathodes (Appendix B, Figure S12 D – E). These results were observed within 12 – 15 dpi in Arabidopsis *deps rbohD*

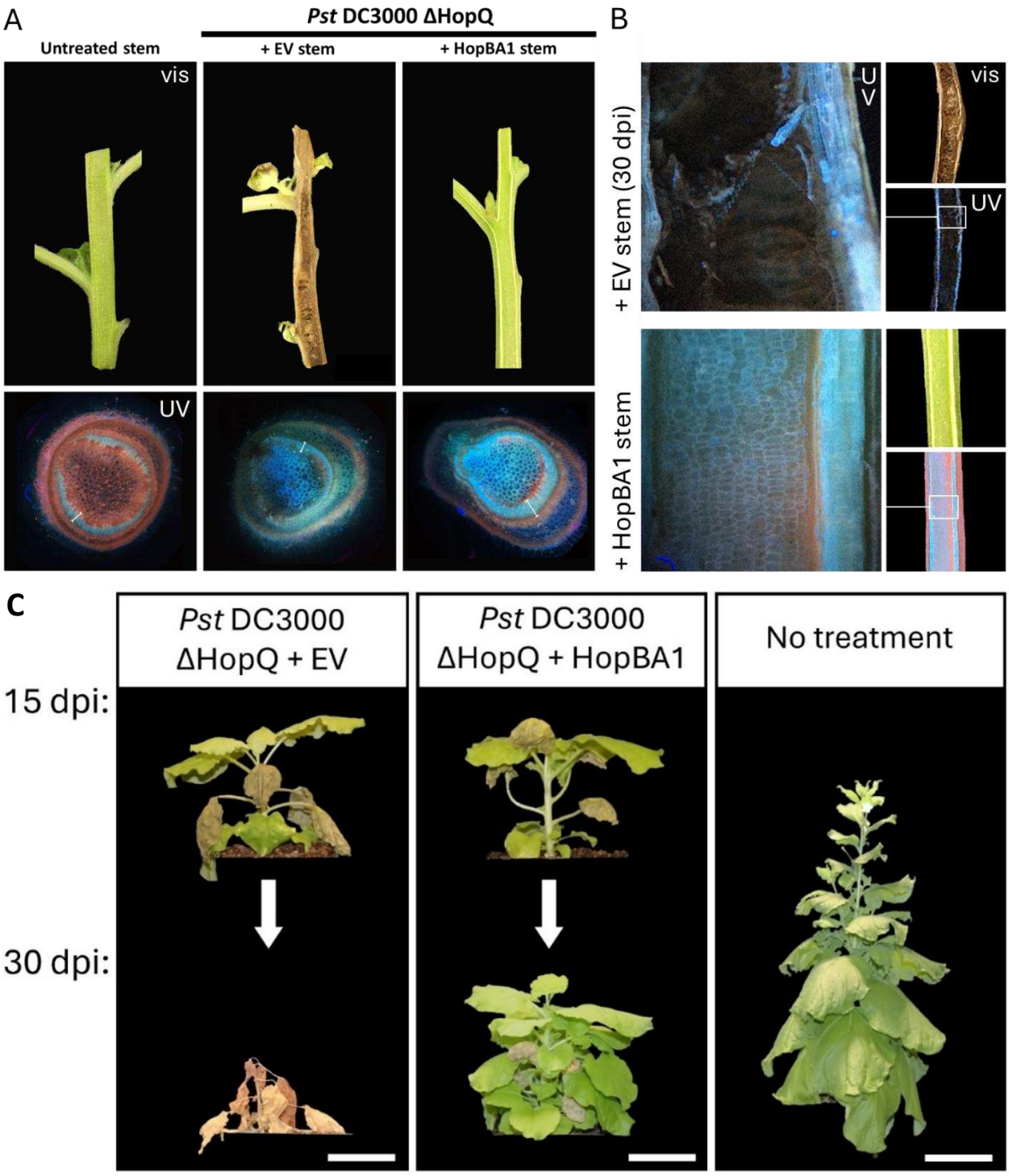

Figure 2.15. Infiltration with DC3000 Δ*hopQ* + EV and + *hopBA1* increase aromatic compound composition in stems; DC3000 Δ*hopQ* + EV overcomes induced defenses, ultimately leading to host mortality. (A) Low abundance of aromatic compounds is present in the stems of untreated plants (left; exclusive to xylem, seen as blue-gray under UV light). Infiltration with DC3000 Δ*hopQ* + EV leads to increased aromatic compound deposition in the stem, but also significant necrosis (middle). Infiltration with DC3000 Δ*hopQ* + *hopBA1* appears to increase deposition of aromatic compounds, thicken 1° or increase 2° growth, perhaps through additional lignification (right). Plants shown ~21 dpi. (B) By 30 dpi the stem interior (pith)

but did not occur at any point within Arabidopsis WT plants, even within the infiltrated leaf tissue (Appendix B, Figure S12 D – E and B).

Hyponasty appears to be a function of HopBA1's virulence activity, rather than host immune recognition

Since DC3000 Δ*hopQ* + *hopBA1* is either growth-restricted or movement-limited in petioles, but not leaves, and hyponasty is a petiole-specific phenotype, we sought to determine if petiole-specific effector triggered immunity (ETI) might be involved in this process. To test this idea, we repeated bacterial infiltrations and petiole angle measurements in a suite of existing *N. benthamiana* immune mutants with defects in ETI. Given the role of Arabidopsis ZAR1 in HopBA1 recognition (Laflamme *et al.*, 2020), we tested *Nb zar1* plants for loss of HopBA1-induced hyponasty. Similarly, we tested *Nb eds1* plants as HopBA1 activates the TIR-only RBA1 in Arabidopsis, and any TIR-mediated immunity in *Nb* is predicted to require EDS1 (Nishimura *et al.*, 2017; Lapin *et al.*, 2020). Given increasing evidence that RNLs or helper NLRs (i.e., ADR1s and NRG1s) may have EDS1-independent functions in immunity (Jacob *et al.*, 2023) and specifically may mediate local acquired resistance (LAR), preventing pathogen spread and systemic movement (Jacob *et al.*, 2023; Wang *et al.*, 2024), we also tested *Nb adr1/nrg1* plants for loss in hyponasty. Finally, *Nb nrc2,3,4* triple mutant was tested for their critical role in Solanaceous immune signaling, where the combination of NRCs enables the immune activity of at least seven NLRs and confer resistance against a broad range of pathogens (Wei *et al.*, 2017). In all tested immune mutants (which also

Figure 2.15 (Continued). is often entirely necrosed or hollowed out after infiltration with DC3000 ΔhopQ + EV (top). Plants infiltrated with DC3000 ΔhopQ + hopBA1 appear approximately the same as in (A) (bottom). Aromatic compounds fluoresce blue under UV. Vis: visible light. UV: ultraviolet light. (C) Long-term outcomes for DC3000 ΔhopQ + EV vs. + hopBA1 infiltrations relative to an unchallenged plant. Necrosis and host mortality associated with + EV largely occur between 15 – 30 dpi (left). Addition of HopBA1 dramatically shifts this trajectory, suggesting systemic restriction or suppression of the strain (middle). Plants are stunted, have an inhibited flowering rate, and show enhanced axillary, but not apical vegetative growth when compared to unchallenged plants (right). See also Figure S10 for the phenotype associated with a traditionally avirulent strain (DC3000 ΔhopQ + hopQ1). Scale = 6 cm.

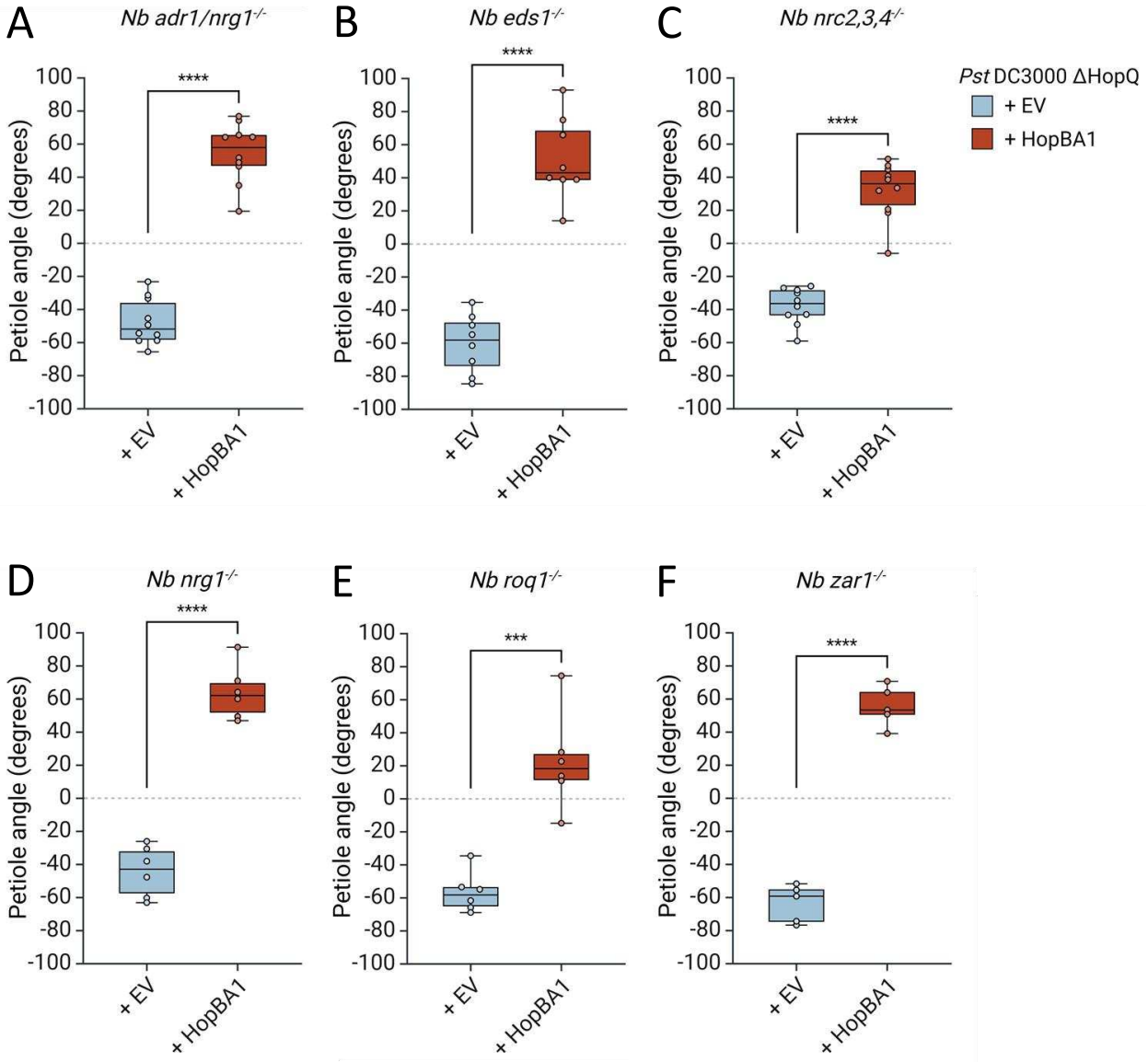

Figure 2.16. HopBA1-induced hyponasty was not lost in a suite of existing *Nb* immune receptor mutants. (A) Petiole angle results in *Nb adr1/nrg1* double mutant. (B) Petiole angle results in *Nb eds1* mutant. (C) *Nb ncr2,3,4* triple mutant. (D) Petiole angle results in *Nb nrg1* mutant. (E) Petiole angle results in *Nb roq1* mutant. (F) Petiole angle results in *Nb zar1* mutant. DC3000 Δ*hopQ* + *hopBA1*-induced hyponasty is conserved in all tested lines. **** $P < 0.0001$, *** $P = 0.000121$ (Student's T-test).

included *Nb nrg1* and *Nb roq1*, in addition to those mentioned above), DC3000 Δ*hopQ* + *hopBA1*still induced hyponasty (i.e., resulted in positive mean petiole angles comparable to those observed in *Nb* WT plants) and significantly greater petiole angles than in DC3000 Δ*hopQ* + EV (Figure 2.16 A – F).

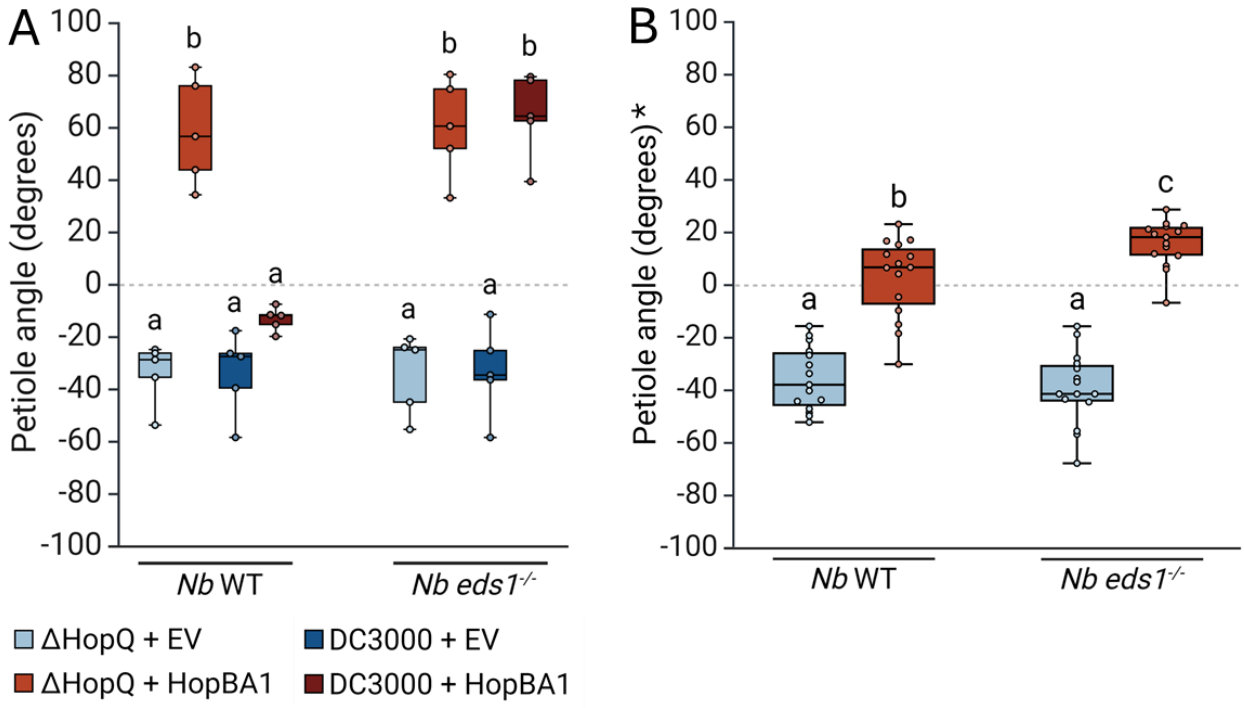

Figure 2.17. Effector triggered immunity blocks HopBA1-induced hyponasty, while the rate of hyponasty is accelerated in *Nb eds1*. (A) Measured petiole angles for DC3000 (WT) + EV, DC3000 (WT) + *hopBA1* in *Nb* WT vs. *Nb eds1*, as well as controls DC3000 Δ*hopQ* + EV and DC3000 Δ*hopQ* + *hopBA1*. The presence of HopQ (DC3000 WT) results in suppression of HopBA1-induced hyponasty in *Nb* WT plants (petiole angle is equal to any strain + EV). The suppressive effect is lost in *Nb eds1* where the petiole angle of DC3000 + *hopBA1* is equal to DC3000 Δ*hopQ* + *hopBA1*. Five biological replicates (plants) were used, and petiole angles were measured at 6 dpi. Two-way ANOVA and Tukey's HSD were used to assign significance groups. (B) Early petiole timepoint measurements (3 dpi, rather than 6 dpi) reveal that a greater proportion of petioles associated with DC3000 Δ*hopQ* + *hopBA1* leaf infiltration have started the transition into hyponasty (14/15, if using a petiole angle > 0 degrees as the metric) in *Nb eds1* vs. *Nb* WT plants (10/15). The measured petiole angle for + *hopBA1* in *Nb eds1* plants is significantly higher than in *Nb* WT plants at 3 dpi. Petiole angles for + *hopBA1* are significantly greater than + EV in all plant genotypes. Eight biological replicates (plants) were used, and petiole angles were measured at 3 dpi. "*" denotes the non-standard use of a 3 dpi timing for petiole angle measurement. Two-way ANOVA and Tukey's HSD were used to assign significance groups.

Following these results, we were interested in testing whether the opposite relationship might be true in *Nb*: whether the presence of an effector known to cause ETI could suppress or block HopBA1-induced hyponasty. To test this question, DC3000 (WT) was used to deliver HopBA1, since HopQ1 was present and would be recognized in wildtype *Nb* (Wei *et al.*, 2007). In a side-by-side experiment, we measured petiole angles in *Nb* WT and *Nb eds1* mutant plants after infiltration with DC3000 + *hopBA1* or DC3000 Δ*hopQ* + *hopBA1* (Figure 2.17 A). We found that

ETI significantly reduced the observed petiole angles in *Nb* WT leaves infiltrated with DC3000 + *hopBA1*, which were equal to both tested EV strains, but not DC3000 Δ*hopQ* + *hopBA1* (Figure 2.17 A). This suppression of petiole angle did not occur in *Nb eds1* mutant plants (lacking HopQ1 recognition) where DC3000 + *hopBA1* and DC3000 Δ*hopQ* + *hopBA1* both induced hyponasty (Figure 2.17 A). Since the *Nb* TNL immune receptor ROQ1 specifically recognizes HopQ1 (Schultink *et al.*, 2017), a more direct inquiry was also conducted in *Nb roq1* mutant plants, which yielded similar results (Supplemental Table 1).

During these assays, we observed that the petioles in *Nb eds1* plants appeared to become hyponastic at a slightly faster rate than in *Nb* WT plants following infiltration with DC3000 Δ*hopQ* + *hopBA1* (petiole curvature often became apparent at ~2 ¼ to 2 ½ dpi, rather than ~3 dpi). However, this early, rate-based difference was not apparent at the typical 6 dpi timepoint as both plant genotypes had equivalent petiole angles at this terminal point (Figure 2.17 A). To capture the early difference between *Nb* WT and *Nb eds1* hyponasty, we measured petiole angle at 3 dpi and found that *Nb eds1* plants had a significantly higher mean petiole angle (~15.8°) than *Nb* WT plants (~2.9°) at 3 dpi (Figure 2.17 B).

Bacterial growth restriction and/or inhibition of vascular entry caused by HopBA1 is EDS1-dependent (and vascular specific)

The observation that the rate of hyponasty was slightly increased in *Nb eds1* mutant plants relative to *Nb* WT plants, combined with the finding that ETI could block HopBA1-induced hyponasty, led us to hypothesize that EDS1 was involved in the recognition (or restriction) of DC3000 Δ*hopQ* + *hopBA1* and that hyponasty likely was an immune-independent phenotype relating to HopBA1's virulence activity instead. To test the first portion of this hypothesis (i.e.,

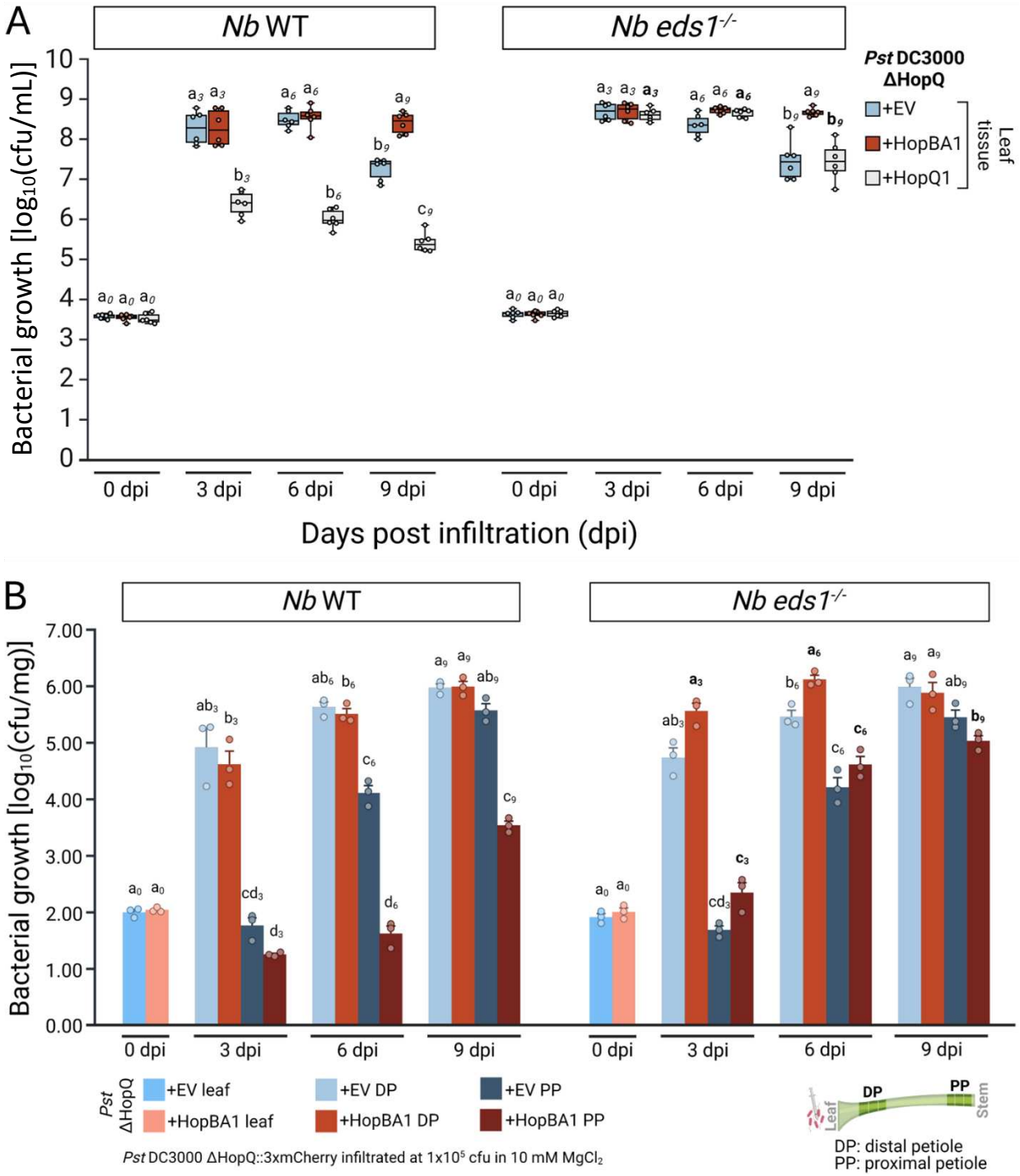

Figure 2.18. *Nb* EDS1 is required for HopBA1-dependent vascular/petiole-specific bacterial growth restriction. (A) Leaf bacterial growth curve comparing DC3000 Δ*hopQ* + EV, + *hopBA1*, and + HopQ in *Nb* WT vs. *Nb eds1*. DC3000 Δ*hopQ* + *hopBA1* growth does not change between plant genotypes. DC3000 Δ*hopQ* + EV does not change between genotypes. DC3000 Δ*hopQ* + HopQ growth is enhanced in *eds1* and is statistically equivalent to + EV at all timepoints. DC3000 Δ*hopQ* + *hopBA1* still demonstrates significantly greater growth than all other strains at 9 dpi. Statistically significant changes to bacterial growth between WT and *eds1* are noted by bold typeface for groupings in *eds1*. 6 biological replicates. Significance groups are assigned within a given time point using one-way ANOVA and Tukey's HSD. (B) Petiole

EDS1-dependent vascular growth restriction of DC3000 Δ*hopQ* + *hopBA1*), we repeated both leaf and petiole bacterial growth assays in *Nb* WT and *Nb* eds1 plants.

Our previous leaf-based growth curves in *Nb* WT (Figure 2.14) strongly suggested that DC3000 Δ*hopQ* + *hopBA1* was not growth restricted. This finding was further supported here and further we found that the HopBA1-specific enhancement of bacterial persistence at later timepoints was maintained in *Nb eds1* plants as well (Figure 2.18 A). Additionally, no growth benefit is conferred to either DC3000 Δ*hopQ* + EV nor DC3000 Δ*hopQ* + *hopBA1*, as both grow equally as well in *Nb* WT and *eds1* leaf tissue (Figure 2.18 A). The loss of growth restriction of DC3000 Δ*hopQ* + *hopQ1* in *eds1* plants is readily apparent at all timepoints (i.e., growth is statistically greater than in WT plants post-0 dpi) and the bacterial population decline at 9 dpi (which is equivalent to that observed in DC3000 Δ*hopQ* + EV, both in WT and *eds1*) relative to DC3000 Δ*hopQ* + *hopBA1* further supports that this is unique to HopBA1 expression (Figure 2.18 A).

In a separate side-by-side experiment, bacterial growth was compared between *Nb* WT and *Nb eds1* plants within petioles associated with either DC3000 Δ*hopQ* + EV or DC3000 Δ*hopQ* + *hopBA1* (Figure 2.18 B). The primary finding in this experiment was that at any non-0 dpi timepoint, DC3000 Δ*hopQ* + *hopBA1* bacterial growth within proximal petiole (PP) tissue was statistically equal to DC3000 Δ*hopQ* + EV in *Nb eds1* plants (also statistically equal to bacterial growth for DC3000 Δ*hopQ* + EV in *Nb* WT) (Figure 2.18 B). Further, the amount of bacterial growth for DC3000 Δ*hopQ* + *hopBA1* in *Nb eds1* PP tissue is significantly greater than DC3000

Figure 2.18 (Continued). bacterial growth curves (distal petiole (DP) and proximal petiole (PP)). DC3000 ΔhopQ + hopBA1 growth is enhanced at all timepoints and sampled tissue in Nb eds1 and is statistically equal to DC3000 ΔhopQ + EV, which doesn't change between Nb WT and Nb eds1. Statistically significant changes to bacterial growth between WT and eds1 are noted by bold typeface for groupings in eds1. 3 biological replicates. Significance groups are assigned within a given time point using one-way ANOVA and Tukey's HSD.

Δ*hopQ* + *hopBA1* in *Nb* WT plants at all non-0 dpi timepoints and we observed a significant increase in DC3000 Δ*hopQ* + *hopBA1* bacterial growth within *Nb eds1* distal petiole (DP) tissue at 3 and 6 dpi relative to its growth in WT (Figure 2.18 B). This suggests that EDS1 is responsible for HopBA1 growth restriction within the petioles or vasculature, however long-term plant phenotypes in *Nb eds1* plants infiltrated with DC3000 Δ*hopQ* + *hopBA1* seem to confound this result (Appendix B, Figure S13).

2.2 Discussion

The initiating goal of this research was to explore the use of *N. benthamiana* as a novel host to discover the presumed virulence function of HopBA1. Prior to this work, HopBA1 had primarily been studied in Arabidopsis and in transient assays in *N. benthamiana* in the context of RBA1 TIR-only cell death. These previous assays had focused on the host's effector-triggered immune responses to HopBA1 and revealed little about its evolved function to promote pathogen success. By moving HopBA1 into the DC3000 Δ*hopQ*-*N. benthamiana* pathosystem, we have revealed a virulence phenotype where HopBA1 promotes bacterial persistence in leaves. In the course of these assays, we also found that HopBA1 also promoted petiole hyponasty, a novel phenotype for a *Pseudomonas syringae* effector. Finally, these experiments led to a reconsideration of the lifestyle of DC3000, which has traditionally been considered as a foliar pathogen that thrives in the apoplastic spaces of leaves.

Despite structural similarity to several types of bacterial proteins, the biochemical function of HopBA1 inside host cells remains obscure. There are also no verified host target proteins for HopBA1, although recognition by ZRK2/ZAR1 presents the RLCK VII family of cytoplasmic kinases as compelling hypothetical virulence targets. Despite these uncertainties, our results demonstrate that HopBA1 suppresses host defense responses in leaves when delivered by DC3000,

a virulent pathogen on *N. benthamiana* in the absence of HopQ/Roq1 effector-triggered immunity. We find that HopBA1 promotes persistence in leaves, while at the same time reducing transcriptional markers for immune responses.

Previously, HopBA1 has been shown to promote virulence in the context of the wheat pathogen *P. syringae* SM-R (Dudnik and Dudler, 2014). This virulence effect was only seen in the context of an effector polymutant (Dudnik and Dudler, 2014). Here we have found a strong virulence effect solely dependent on HopBA1. Interestingly, in surveys of *P. syringae* isolated from monocot hosts, HopBA1 appears to be distributed as a core effector and is highly conserved at the amino acid level (Sultanov *et al.*, 2016). It will be interesting to understand if HopBA1 virulence targets are conserved across Arabidopsis and *N. benthamiana*, and then the further phylogenetic distance into monocots. Despite unclear targets, plant genomes have evolved multiple mechanisms to detect HopBA1, so it is clearly relevant in terms of the plant/pathogen arms race.

At this point, it is unclear how genetic requirements for HopBA1 effector-triggered immunity might be related to the requirements for its virulence function. In this work, I found that previously described HopBA1 mutants that lose RBA1 cell death also lose the ability to trigger hyponasty. These mutants were originally tested based on structural similarities between HopBA1 and EreA/ChaN, their mechanistic role in HopBA1 is unclear. The simultaneous loss of both RBA1 activation and hyponasty is perhaps most parsimonious with a "guard hypothesis" model wherein RBA1 recognizes HopBA1 indirectly through modification of its virulence targets. However, a detailed model for how HopBA1 triggers virulence and avirulence phenotypes requires a clearer mechanistic understanding of its biochemical function.

Why HopBA1 induces hyponasty is unclear. Given that hyponasty is a developmental change, it seemed likely that hyponasty could be a reflection of HopBA1's virulence effect.

However, as HopBA1 appears to trigger EDS1-dependent vascular immunity, it was also possible that this bending is a consequence of tissue-specific cell death/immunity. To test this, we assayed a variety of host immune mutants to attempt to dissect immune activation from petiole bending. For the *eds1* mutant which is defective in TIR-based immunity, we found that HopBA1 vascular immunity was lost, but petiole bending was retained. This result is most consistent with the hypothesis that petiole bending is not a consequence of TIR-based immunity, but instead a consequence of HopBA1's unknown virulence function. It is important to note that petiole bending itself need not provide an adaptive benefit to *P. syringae*, it may merely be the outcome of HopBA1's "intended" virulence function and crosstalk with hormonal/developmental pathways in this particular genotype of plant. Alternatively, petiole bending may actually be a generalized adaptive mechanism that has yet to be observed in other systems. The fact that we did not observe hyponasty induced by two strains of *Pseudomonas syringae* (*Ptt* and *Pja*) that natively contain HopBA1 is potentially explained by immune activation triggered by other effectors present in their genomes (similar to hyponasty inhibition by HopQ/Roq1 ETI with WT DC3000). Putative immune activators could include *Ptt* and *Pja* effectors that are not present in DC3000, such as HopZ and HopBC, or any effectors that are not sequence-identical, such as HopAZ. HopAG, HopBF, and HopC (Baltrus *et al.*, 2011). Similarly, *Pja* and *Ptt* both have additional toxins, syringopeptin, syringomycin, and syringolin, while also lacking virulence genes for coronatine production, and auxin inactivation (*iaaL*) (Baltrus *et al.*, 2011). Alternatively, there may be an unknown DC3000-specific contribution to HopBA1-dependent hyponasty.

Overall, the RNA-Seq and GO-term analysis suggest that HopBA1 effectively suppresses defense responses in leaves, with the exception of a few defense genes (e.g., GAEs and PMEIs) (Bethke *et al.*, 2014; Bethke *et al.*, 2016). Potentially, these induced defense-related genes could

relate to HopBA1's transition from functioning as a virulence factor in general leaf tissue, to functioning as an avirulence factor in leaf vasculature. GO term analysis also reveals that any potential suppression of defense is lost within petiole tissue and is accompanied by several terms relating to inducible defenses (e.g., phenylpropanoid, lignin, and anthocyanins synthesis). However, considering a non-trivial amount of cell wall remodeling and rapid morphological changes are induced in petioles associated with HopBA1 infiltration, it is not without possibility that these genes are being induced due to substantial abiotic stress. Another point that may be relevant is that GO terms associated with transport are largely downregulated by HopBA1within leaves. This could be a reflection of leaf vasculature (and later the vascular system within petioles) being the primary point of bacterial restriction, or alternatively physical blockage associated with the rapid structural changes that HopBA1 induces. This is also accompanied by water stress and osmotic stress, which might similarly suggest either structural changes that impact transport and cause drought stress or it might relate to induced biotic defense responses caused by HopBA1's activity in the plant.

Vascular pathogens are often considered relatively specialized microbes that require specialized genomes and virulence mechanisms. While some strains of *Pseudomonas*, such as *P. syringae* pv. *aesculi* have been reported as vascular pathogens (de Keijzer *et al.*, 2012), DC3000 is classically considered to grow primarily either on, or in leaves. The only previous report of DC3000 growing as a vascular pathogen was in a system that required toothpick wounding (Misas-Villamil *et al.*, 2011). In that system, DC3000 *hopQ* was observed to spread locally in leaf xylem, traveling no more than 10 mm from the site of injury. Using the same genotypes of pathogen and plant, but a different inoculation technique, we find that DC3000 is an aggressive vascular pathogen, growing to extremely high titers, travelling systemically to shoot and root, and eventually killing the plant. This result tells us that DC3000 has all the genetic tools required to be a successful

plant pathogen, but that it is typically blocked from entry to the vasculature by the immune system. Our preliminary results are consistent with DC3000 being localized to the xylem, but this will need to be confirmed with SEM. Where and how DC3000 enters and exits the vasculature is unknown. The fact that different in-lab inoculation techniques can have an impact on disease outcome is not unappreciated (e.g., injections bypass stomatal immunity), however the magnitude of the final phenotypic difference between toothpick inoculation and whole leaf infiltration (local symptoms vs plant death) is remarkable. It will be interesting to revisit vascular spread of DC3000 in Arabidopsis, especially in the context of immunocompromised mutants.

It is still unclear if vascular movement is necessary for DC3000 HopBA1-induced petiole movement. We attempted to test this hypothesis by generating non-motile bacteria, however the DC3000 Δ*hopQ* Δ*fliC* Δ*pilA* mutant could still trigger HopBA1-dependent hyponasty. Preliminary observation of fluorescence microscopy suggested that bacteria did in fact enter into the leaf vasculature in a way that was comparable to DC3000 Δ*hopQ*, leaving an open question regarding whether passive vs. active movement by the bacteria is required or not, or alternatively whether this triple mutant is actually motility-deficient. Similarly, *Agrobacterium* doesn't spread systemically in published transient assays, but we have not tested if it can spread in the whole-leaf infiltration assays used to trigger hyponasty. It remains an open question, but it seems likely that both hyponasty and vascular-specific HopBA1/EDS1-dependent ETI are triggered locally in leaf vasculature or within the petiole by bacteria that have descended through the petiole. If ETI is truly occurring in vascular-specific tissues, it would seem most likely that phloem (via its companion cells), rather than xylem is the target of HopBA1 activity.

The plant immune system must actively defend against pathogens with diverse lifestyles. This work suggests that there may be many "non-vascular" pathogens that are non-vascular

primarily due to effective host immunity, rather than a lack of specialized pathogen virulence strategies necessary to thrive in a vascular environment. If this is the case, then a better understanding of vascular immunity may emerge from study of immune-limited vascular pathogens such as DC3000. Understanding how DC3000 Δ*hopQ* manages to enter leaf vasculature, traverse long distances, and colonize distant tissues should provide novel insights into how plants can be engineered for increased resistance to vascular pathogens.

2.3 Methods

Plant materials and growth conditions

Nicotiana benthamiana and *Nicotiana tabacum* were grown in a Conviron ATC60 under a 15-hour photoperiod at 75 μE, 25°C, and 70% RH, following seedling transplant. Individual plants were grown in 4-inch pots with Pro-Mix HP+ potting mix amended with Osmocote Plus (15-9-12). Plants were additionally fertilized using Miracle-Gro (24-8-16) water soluble all-purpose plant food 3 – 5 times during their lifespan. Plants used for most assays were between 5 – 7 weeks old. Older plants (8 – 12 weeks old) were specifically used as noted to assess developmental phenotypes and age-related survivorship differences. *Arabidopsis thaliana* was grown in a Conviron GEN1000 (3 shelf configuration) under a 9-hour photoperiod at 100 μE, 22°C/18°C (day/night), and 75 % RH, following seedling transplant. 16 to 22 plants were grown in 21-inch X 10-inch flats with Pro-Mix HP+ potting mix amended with Osmocote Plus (15-9-12). Plants were 6 – 8 weeks of age at the time of infiltration.

All *Pseudomonas syringae* strains were grown in/on King's B media (KB), liquid culture or agar plates, with antibiotic selection at 28°C in an Annova 42 incubator shaker. Liquid cultures were allowed to grow ~24 hours and were shaken at 250 rpm. *Pst* strains used in all assays were grown on KB plates for ~24 hours prior to a given experiment, rather than using liquid cultures

directly for cell suspension and infiltration. *Agrobacterium tumefaciens* GV3101 and *Pseudomonas fluorescens* (Pf0-1 EtHAn) were grown at 28°C in/on Luria-Bertani (LB) and KB, respectively (Thomas *et al.*, 2009).

Bacterial growth assays

Bacterial growth curves were conducted as previously described (Morel & Dangl, 1999). Briefly, bacterial cell suspensions in 10 mM $MgCl_2$ were abaxially infiltrated into the apoplast of leaves via needleless syringe. Experiments utilized whole leaf infiltration and consisted of four to five leaves per plant. To minimize variation and the impact of systemic bacterial movement within plants, individual plants were only infiltrated with one experimental strain. Leaf tissue was cored from the infiltrated area, taking care to avoid higher order vasculature and sampling from leaf mesophyll. Cores were taken from leaves using a #4 cork borer (~9mm in diameter) and each sample consisted of six cores from three biological replicates (i.e., plants). Three technical replicates consisting of six unique cores from the three biological replicates were used in serial dilutions for each experimental strain following tissue homogenization. Plant tissue was homogenized using a Qiagen Tissuelyser II. Colony forming units (cfu) were then counted one and a half days after plating serial dilutions on KB agar plates with appropriate antibiotic selection. Bacterial growth was assessed at 0, 3, 6, 9, and 12 days post infiltration (dpi). Optical density for the initial cell suspension was measured using a Jenway 7205 UV/Visible spectrophotometer and an OD_{600} of 0.0002 was utilized for all growth curves.

Petiole and stem growth curves

At present, there is no standard method for *Pst* growth curves utilizing petiole and stem tissue. Accordingly, a new method was devised to quantify bacterial growth in these distant tissue types, which was partially based upon bacterial growth curves from root tissue described by

Thiergart *et al.*, 2020. Briefly, petioles were excised from infiltrated leaves. Petioles were divided into the sub-regions of distal petiole (DP) and proximal petiole (PP), which consisted of tissue that was closest to the infiltrated leaf and stem, respectively. Petiole tissue was allowed to seal/dry after being cut from the plant using a sterile razor blade. Petiole tissue was then surface sterilized utilizing two washes of 1X TE (2 min. each), one wash of 70% EtOH (1 min.), one wash of 3% bleach (1 min.), and five washes of ddH_2O (~1 min. each).

Following surface sterilization, tissue from each sub-region was divided into three equal parts and a corresponding segment from each of three biological replicates was combined into a single sample. Three technical replicates were utilized for each strain and for each petiole sub-region. All samples were weight adjusted to account for the variable dimensions of petioles and stems. Plant tissue homogenization, serial dilution, and cfu estimates were conducted the same as in the previous section. Stem growth curves were carried out in essentially the same way, except that tissue was divided into sub-regions from above and below the petiole/leaf that was infiltrated with bacteria. Bacterial growth was assessed at 3, 6, 9, and 12 dpi for petioles and at 12 dpi for stems. See Appendix B, Figure S9 for a visual representation of the full process.

Relative ion leakage assay

To quantify cell death associated with *Pst* disease symptoms, electrolyte or ion leakage was measured from spot infiltrated leaf tissue, as previously described (Aguilar *et al.*, 2019; Sun *et al.*, 2022). Briefly, 5 to 7-week-old plants were abaxially spot infiltrated (~3 cm in diameter) with *Pst* DC3000 Δ*hopQ* ($1x10^5$ cfu in 10 mM $MgCl_2$) or 10 mM $MgCl_2$ ("mock") by needleless syringe. At the relevant time point (0, 1, 3, and 6 dpi), cores were taken from the infiltrated area using a #4 corer (~9mm in diameter). Each measured sample consisted of 6 cores from 3 plants (biological replicates). This was replicated 6 times as technical replicates, each of which consisted of unique

cores from the 3 plants. Leaf cores were briefly and individually washed in deionized H_2O (submerged 2X, flipped, and submerged 2X using a wetted Q-tip) to remove soil or other unwanted impurities. Leaves were then placed into glass scintillation vials with polypropylene (or urea) caps with 10 mL of deionized H_2O.

Samples were then shaken at room temperature (~19 – 22°C) at 100 rpm using an Annova 42 incubator shaker for 3 – 4 hours. After this period, an initial conductivity measurement (reading 1 in µS/cm) was taken using an Orion Star A112 conductivity meter. Reading 1 is treated as representing free ion count that could readily be removed from or leached out of dead or compromised leaf tissue (i.e., ion leakage associated with cell death or disease symptoms like necrosis). After all initial readings were taken, samples were boiled (15 minutes at ≥ 100°C) before taking a final reading. Sample vials were labeled and secured onto a stainless-steel steam pan filled with ~1in. of water covered with aluminum foil. The steam pan was then heated on a VWR heat plate/stirrer at 75% of the max heat setting. Sample vials were removed and allowed to cool (≤ 35°C) prior to taking the final conductivity measurement (reading 2 also in µS/cm). Reading 2 is treated as encompassing all potential ions contained within and associated with the sampled tissue (i.e., all the ions previously measured in reading 1, plus all the remaining ions that are released during the destructive process of prolonged boiling). Using the two conductivity measurements (reading 1 and reading 2), relative conductivity is calculated as follows: [(reading 1 in µS/cm) / (reading 2 in µS/cm)]. This provides a proportional value (0.0 – 1.0) for the initial ion leakage associated with the phenotype of interest (i.e., disease symptoms, cell death, or lack thereof) relative to the total possible ion leakage associated with the sampled leaf tissue. See Appendix B, Figure S1 for a visual representation of the full process.

Hyponasty/petiole curvature assay and angle measurements

Evaluation of petiole hyponasty was based upon a terminal measurement of petiole angle, which took place most commonly at 6 days post infiltration (dpi), but up to 9 dpi in some instances (unless otherwise specified as part of the experiment). Hyponasty, as well as petiole angle more generally, has been measured in numerous different ways over time (Reid *et al.*, 1981; Edelman and Jones, 2014). Because of the prominent arc-based curvature or bending associated with HopBA1-induced hyponasty in *Nicotiana benthamiana* (often generating a sigmoidal curve, rather than just an acute angle), a slightly different – but easily reproducible – approach was taken. In short, all treated petioles, as well as a segment of the adjacent stem, were excised from plants. The entirety of the leaf was then excised so that only the petiole and stem segment were visible prior to photographing. Following this, lines were added to the petioles using drawing software. An initial line set to 0 degrees was drawn along the adaxial surface of the petiole base (i.e., immediately adjacent to the junction with the stem). A second line was then drawn along the adaxial surface of the petiole-leaf junction. Annotated petiole images were then imported into ImageJ (vers. 1.53t, Java 1.8.0_322) and the angle tool was used to establish petiole angle. The resulting angle of the two lines' intersection is defined as petiole angle for this work. As it applies to this work, a petiole angle greater than 0° was considered as displaying hyponasty, while a petiole angle less than 0° was considered non-hyponastic or normal. See Appendix B, Figure S3 for additional details, as well as a visual representation of this approach.

Phytohormone panel (UPLC-MS/MS)

Leaves of *N. benthamiana* (at ~6 weeks old) were infiltrated with either DC3000 Δ*hopQ* + EV or DC3000 Δ*hopQ* + *hopBA1* in 10 mM $MgCl_2$ via needleless syringe at an OD_{600} of 0.0002 (1×10^5 cfu) from the abaxial leaf surface. 3 days after whole-leaf infiltration, leaf and petiole

tissue were excised from plants by surface sterilized razor blade. Leaves and petioles were collected separately by plant in 50 mL conical tubes. Samples were immediately frozen in liquid nitrogen and were stored at -80°C until further processing was possible (~2 weeks). 6 plants or biological replicates were used. Each replicate consisted of 4 leaves or petioles from a single plant. See Appendix B, Figure S6 for a visual summary of experimental design and sample collection.

Frozen samples were lyophilized for 2 days and dried tissue was then homogenized with stainless-steel balls in a Bullet Blender for 2 minutes. Dried, ground tissue was then weighed (each sample was 30 mg +/- 5 mg, when possible) and transferred to 2 mL glass vials. 1 mL of chilled, 80% methanol was added to each sample, along with 40 µL of the phytohormone internal standard mix (20 ng/mL of each standard in 50% methanol). The internal standards of abscisic acid-D6 (ABA-D6), indole-2,4,5,6,7-d5-3-acetic acid (IAA-D5), jasmonic acid-d5 (JA-D5), and salicylic acid-D4 (SA-D4) were utilized to determine relative peak values for samples. Samples were then shaken in a cold cabinet for 30 min., sonicated for 15 min., and shaken again for 30 min. before centrifugation at 15,000 g at 4°C for 15 min. Recovered supernatant was collected in glass vials with inserts and were then dried down. 20 µL of all samples were pooled for quality control samples (n = 5). The dried extracts were resuspended in 100 µL of 50% methanol and were kept at -80°C until analysis.

UPLC-MS/MS analysis was conducted by Colorado State University (CSU) Analytical Resources Core Bioanalysis and Omics (arc.BIO) facility and was conducted utilizing an ACQUITY Classic UPLC paired with Xevo TQ-S triple quadrupole mass spectrometer (Waters) (Trapp *et al.*, 2014). Raw data was processed using Skyline (MacLean *et al.*, 2010). Relative quantification was accomplished by normalizing raw peak data against the internal standards, which

were stable isotope labeled. Normalized peak area was further adjusted by sample weight in all cases.

RNA-Seq and transcriptomic analysis

Plants were infiltrated with either DC3000 Δ*hopQ* + EV or DC3000 Δ*hopQ* + *hopBA1* in 10 mM $MgCl_2$ via needleless syringe at an OD600 of 0.0002 (1 x 10^5 cfu). 3 days following whole leaf infiltration (4 – 5 leaves / plant), leaf and petiole tissues were separately collected from 3 biological replicates. Fresh tissue was then combined with liquid nitrogen and ground using a mortar and pestle. Homogenized tissue in liquid nitrogen was decanted into microfuge tubes and total RNA was extracted using a RNeasy Plant Mini Kit (Qiagen).

Paired-end sequencing libraries were generated by the CU Anschutz Genomics Core with a Tecan Universal Plus kit and sequenced with the NovaSeq platform. Reads were aligned to the v1.0.3 assembly of the *Nicotiana benthamiana* genome, NbLab360 (Ranawaka *et al.*, 2023). Analysis of differential gene expression was performed with DESeq2 (1.38.3) in R (v4.2.3) and was split by tissue type (i.e., leaf and petiole). An FDR of 0.05 was used with a shrunken LFC and log_2 of 1. EggNOG-Mapper was further utilized for functional annotations (Huerta-Cepas *et al.*, 2017).

Principal Component Analysis (PCA) was conducted with the "prcomp" function in R using the log transformed expression values (CPM, counts per million) of the top 500 genes with the highest variance among samples. Gene Ontology (GO) enrichment analysis was performed utilizing the BiNGO tool for Cytoscape (Maere *et al.*, 2005). EggNOG (Cantalapiedra *et al.*, 2021) was used for GO annotations using the NbLAB360 proteome. Annotation files were then generated according to BiNGO recommendations. A hypergeometric test combined with a Benjamin and Hochberg FDR correction with a cutoff of 0.05 was applied.

Fluorescence and general microscopy

A Leica CTR 5500 DM-5500B was utilized to view fluorescently labeled bacterial cells (DC3000 Δ*hopQ*::3xmCherry) within sampled plant tissues (leaf, petiole, stem, and root). Images were taken in brightfield and with fluorescence light filter (red and green fluorescence filter cubes). LASX imaging software was used for image processing. In some instances, artificial color was applied to grayscale images using ImageJ (vers. 1.53t, Java 1.8.0_322). A Leica (Leica S9i) dissecting microscope with UV lights was used for qualitative assessment of petiole and stem aromatic compound composition.

Time-lapse imaging of *Nicotiana benthamiana*

Nicotiana benthamiana plants were moved to 24-hour light at ~115 μE, room temperature (~22°C), and ~16% RH following growth in previously described chamber conditions until ~6 weeks of age. Plants were photographed at 20-minute intervals following infiltration with either DC3000 Δ*hopQ* + EV or DC3000 Δ*hopQ* + *hopBA1* for 7 days using a Canon EOS Rebel T6. A 60-inch tripod was utilized for stabilization and an intervalometer was used for timed collection of images. A DC coupler (DR-E10, Canon) and compact power adapter (CA-PS700, Canon) were also used to ensure that no movement of the camera from the tripod or disruption of image collection was necessary.

Statistical analysis

RStudio was used for all two-way ANOVA calculations with Tukey's HSD post-hoc analysis for bacterial growth assays and petiole angle measurements. Microsoft Excel was used for one-way ANOVA calculation with Tukey's HSD. All t-tests were conducted using Microsoft Excel and/or BioRender Graph (beta version). Analysis of differential gene expression was performed using DESeq2 (1.38.3) in R (v4.2.3) with an FDR of 0.05, shrunken LFC, and $\log_2$FC of 1. Gene

Ontology (GO) enrichment analysis was conducted using the BiNGO tool in Cytoscape (vers. 3.9.1) using a hypergeometric test combined with a Benjamin and Hochberg FDR correction with a 0.05 cutoff.

2.4 Acknowledgments

Sincere thanks to Dr. Marc Nishimura for his work and time with RNA-Seq data analysis and Caio Mendes (Dr. Paulo Teixeira Lab) for assistance with downstream RNA-Seq data analysis provided in this chapter (e.g., PCA, GO enrichment analysis, and summary figures). We would also like to thank Dr. Erin Osborne-Nishimura for RNA-Seq support (computing/server access and online data hosting), Dr. Brian Kvitko for fluorescently labeled bacterial cells and related tools, Dr. Cris Argueso Lab for sharing phytohormones and other chemicals, and CSU arc.BIO core facilities. Thank you to Dr. Jeff Dangl and Dr. El Kasmi Labs for feedback during lab meetings with special thanks to Dr. Nak Hyun for the initial experimental suggestion that ultimately led to such an interesting finding.

Regarding Appendix A: sincere thanks to Dr. Alex Schultink and Dr. Adam Steinbrenner (collectively, the Staskawicz Lab) for providing *Nb zar1* plants, the original VIGS constructs, which were used to generate the experiment's *Nb* RLCK VII-specific hpRNAi vectors, and for sequence and phylogenic data/assistance. We would like to thank Dr. Paulo Teixeira for providing the hpRNAi vector used here. Thank you to Dr. Farid El Kasmi for sharing the Cas9 shuttle vectors (on behalf of the Stuttmann Lab), which were used to generate *Nb* RLCK VII polymutants.

2.5 References

Aguilar E, Del Toro FJ, Brosseau C, Moffett P, Canto T, Tenllado F. 2019. Cell death triggered by the P25 protein in Potato virus X-associated synergisms results from endoplasmic reticulum stress in *Nicotiana benthamiana*. *Mol Plant Pathol.* **20**, 194—210.

Almeida-Trapp M, Souza GD, Rodrigues-Filho E, Boland W, Mithöfer A. 2014. Validated method for phytohormone quantification in plants. *Front Plant Sci.* **5**, 1—11.

Bao Z, Stodghill PV, Myers CR, Lam H, Wei HL, Chakravarthy S, Kvitko BH, Collmer A, Cartinhour SW, Schweitzer P, Swingle B. 2014. Genomic plasticity enables phenotypic variation of *Pseudomonas syringae* pv. *tomato* DC3000. *PLoS One*. **9**, e86628.

Baltrus DA, Nishimura MT, Romanchuk A, Chang JH, Mukhtar MS, Cherkis K, Roach J, Grant SR, Jones CD, Dangl JL. 2011. Dynamic evolution of pathogenicity revealed by sequencing and comparative genomics of 19 Pseudomonas syringae isolates. *PloS Pathog*. **7**, e1002132.

Bartsch M, Gobbato E, Bednarek P, Debey S, Schultze JL, Bautor J, Parker E. 2006. Salicylic Acid–Independent ENHANCED DISEASE SUSCEPTIBILITY1 Signaling in Arabidopsis immunity and cell death is regulated by the Monooxygenase FMO1 and the Nudix Hydrolase NUDT7. *Plant Cell.* **18**, 1038—1051.

Berens ML, Berry HM, Mine A, Argueso CT, Tsuda K. 2017. Evolution of Hormone Signaling Networks in Plant Defense. *Annu Rev Phytopathol.* **55**, 401—425.

Bethke G, Thao A, Xiong G, Li B, Soltis NE, Hatsugai N, Hillmer RA, Katagiri F, Kliebenstein DJ, Pauly M, Glazebrook J. 2016. Pectin Biosynthesis Is Critical for Cell Wall Integrity and Immunity in Arabidopsis thaliana. *Plant Cell.* **28**, 537—56.

Bethke G, Grundman RE, Sreekanta S, Truman W, Katagiri F, Glazebrook J. 2014. Arabidopsis PECTIN METHYLESTERASEs contribute to immunity against *Pseudomonas syringae*. *Plant Physiol.* **164**, 1093—107.

Cantalapiedra CP, Hernández-Plaza A, Letunic I, Bork P, Huerta-Cepas J. 2021. Eggnog-mapper v2: Functional Annotation, Orthology Assignments, and Domain Prediction at the Metagenomic Scale. *Mol Biol Evol.* **38**, 5825—5829.

De Keijzer J, van den Broek LAM, T. Ketelaar, van Lammeren AAM. 2012. Histological examination of horse chestnut infection by *Pseudomonas syringae* pv. Eggnog and non-destructive heat treatment to stop disease progression. *PloS ONE.* **7**, e39604.

Donati I, Cellini A, Sangiorgio D, Vanneste JL, Scortichini M, Balestra GM, Spinelli F. 2020. *Pseudomonas syringae* pv. *actinidiae*: ecology, infection dynamics and disease epidemiology. *Microb Ecol.* **80**, 81—102.

Edelman NF, Jones ML. 2014. Evaluating ethylene sensitivity within the family *Solanaceae* at different developmental stages. *Hort Science.* **49**, 628—636.

Freeman BC, Beattie GA. 2009. Bacterial growth restriction during host resistance to *Pseudomonas syringae* is associated with leaf water loss and localized cessation of vascular activity in *Arabidopsis thaliana*. *Mol Plant Microbe Interact.* **22**, 857–867.

Gallego-Giraldo L, Escamilla-Trevino L, Jackson LA, Dixon RA. 2011. Salicylic acid mediates the reduced growth of lignin down-regulated plants. *Proc Natl Acad Sci USA.* **108**, 20814—20819.

Geng X, Jin L, Shimada M, Kim MG, Mackey D. 2014. The phytotoxin coronatine is a multifunctional component of the virulence armament of *Pseudomonas syringae*. *Planta.* **240**,1149—1165.

Hillmer RA, Igarashi D, Stoddard T, Lu Y, Liu X, Tsuda K, Katagiri F. 2023. The Kinetics and Basal Levels of the Transcriptome Response During Effector-Triggered Immunity in Arabidopsis are mainly controlled by Four Immune Signaling Sectors. *Journal of Bioinformatics and Systems Biology*. **6**, 347—363.

Hoffmann N, Benske A, Betz H, Schuetz M, Samuels AL. 2020. Laccases and peroxidases co-localize in lignified secondary cell walls throughout stem development. *Plant Physiol*. **184**, 806—822.

Huerta-Cepas J, Forslund K, Coelho LP, Szklarczyk D, Jensen LJ, von Mering C, Bork P. 2017. Fast genome-wide functional annotation through orthology assignment by Eggnog-Mapper. *Mol Biol Evol*. **34**, 2115—2122.

Jacob P, Hige J, Song L, Bayless A, Russa D, Bonardi V, El Kasmi F, Wünsch L, Yang Y, Fitzpatrick CR, McKinney BJ, Nishimura MT, Grant MR, Dangl JL. 2023. Broader functions of TIR domains in Arabidopsis immunity. *Proc Natl Acad Sci USA.* **120**, 1—22.

Jacob P, Hige J, Dangl JL. 2023. Is localized acquired resistance the mechanism for effector-triggered disease resistance in plants? *Nat Plants.* **9**, 1184-1190.

Klement Z, Rozsnyay DS. 1984. The effect of cold on development of bacterial canker in apricot trees infected with *Pseudomonas syringae* pv. *syringae*. *Physiological Plant Pathology*. **24**, 237—246.

Kupers JJ, Snoek BL, Oskam L, Pantazopoulou CK, Matton SEA, Reinen E, Liao CY, Eggermont EDC, Weekamp H, Biddanda-Devaiah M, Kohlen W, Weijers D, Pierik R. 2023. Local light signaling at the leaf tip drives remote differential petiole growth through auxin-gibberellin dynamics. *Curr Biol.* **33**, 75—85.

Lang J, Genot B, Bigeard J, Colcombet J. 2022. MPK3 and MPK6 control salicylic acid signaling by up-regulating NLR receptors during pattern- and effector-triggered immunity. *J Exp Bot.* **73**, 2190—2205.

Lapin D, Bhandari DD, Parker JE. 2020. Origins and Immunity Networking Functions of EDS1 Family Proteins. *Annu Rev Phytopathol.* **58**, 253—276.

Lee MH, Jeon HS, Kim SH, Chung JH, Roppolo D, Lee HJ, Cho HJ, Tobimatsu Y, Ralph J, Park OK. 2019. Lignin-based barrier restricts pathogens to the infection site and confers resistance in plants. *EMBO J.* **38**, e101948.

Lin H, Wang M, Chen Y, Nomura K, Hui S, Gui J, Zhang X, Wu Y, Liu J, Li Q, Deng Y, Li L, Yuan M, Wang S, He SY, He Z. 2022. An MKP-MAPK protein phosphorylation cascade controls vascular immunity in plants. *Sci Adv*. **8**, 1—13.

Ma, S.W., Morris, V.L. and Cuppels, D.A. (1991) Characterization of a DNA region required for production of the phytotoxin coronatine by *Pseudomonas syringae* pv. *tomato*. *Mol Plant Microbe Interact.* **4**, 69–74.

MacLean B, Tomazela DM, Shulman N, Chambers M, Finney GL, Frewen B, Kern R, Tabb DL, Liebler DC, MacCoss MJ. 2010. Skyline: an open source document editor for creating and analyzing targeted proteomics experiments. *Bioinform.* **26**, 966—968.

Maere S, Heymans K, Kuiper M. 2005. BiNGO: a Cytoscape plugin to assess overrepresentation of Gene Ontology categories in Biological Networks. *Bioinform.* **21**, 3448—3449.

Misas-Villamil JC, Kolodziejek I, van der Hoorn RA. 2011. Pseudomonas syringae colonizes distant tissues in *Nicotiana benthamiana* through xylem vessels. *Plant J.* **67**, 774—782.

Morel JB, Dangl JL. 1999. Suppressors of the Arabidopsis lsd5 cell death mutation identify genes involved in regulating disease resistance responses. *Genetics.* **151**, 305—319.

Nishimura MT, Anderson RG, Cherkis KA, Law TF, Liu QL, Machius M, Nimchuk ZL, Yang L, Chung E, El Kasmi F, Hyunh M, Nishimura EO, Sondek JE, Dangl JL. 2017. TIR-only protein RBA1 recognizes a pathogen effector to regulate cell death in *Arabidopsis*. *Proc Natl Acad Sci USA.* **114**, 2053—2062.

Paauw M, van Hulten M, Chatterjee S, Berg JA, Taks NW, Giesbers M, Richard MMS, van den Burg HA. 2023. Hydathode immunity protects the Arabidopsis leaf vasculature against colonization by bacterial pathogens. *Curr Biol.* **33**, 697—710.

Pérez-Mendoza D, Felipe A, Ferreiro MD, Sanjuán J, Gallegos MT. 2019. AmrZ and FleQ Co-regulate Cellulose Production in *Pseudomonas syringae* pv. Tomato DC3000. *Front Microbiol.* **10**, 746.

Pruitt RN, Locci F, Wanke F, Zhang L, Saile SC, Joe A, Karelina D , Hua C, Fröhlich K, Wan WL, Hu M, Rao S, Stolze SC, Harzen A, Gust AA, Harter K, Joosten MHAJ, Thomma BPHJ, Zhou JM, Dangl JL, Weigel D, Nakagami H, Oecking C, El Kasmi F, Parker JE, Nürnberger T. 2021. The EDS1–PAD4–ADR1 node mediates *Arabidopsis* pattern-triggered immunity. *Nature.* **598**, 1—23.

Ranawaka B, An J, Lorenc MT, Jung H, Sulli M, Aprea G, Roden S, Llaca V, Hayashi S, Asadyar L, LeBlanc Z, Ahmed Z, Naim F, Bolzan de Campos S, Cooper T, de Felippes FF, Dong P, Zhong S, Garcia-Carpintero V, Orzaez D, Dudley KJ, Bombarely A, Bally J, Winefield C, Giuliano G, Waterhouse PM. 2023. A multi-omic *Nicotiana benthamiana* resource for fundamental research and biotechnology. *Nature Plants.* **10**, 1—27.

Reid MS, Mor Y, Kofranek AM. 1981. Epinasty of Poinsettias-the Role of Auxin and Ethylene. *Plant Physiol*. **67**, 950—952.

Schultink A, Qi T, Lee A, Steinbrenner AD, Staskawicz B. 2017. Roq1 mediates recognition of the *Xanthomonas* and *Pseudomonas* effector proteins XopQ and HopQ1. *Plant J*. **92**, 787—795.

Sultanov RI, Arapidi GP, Vinogradova SV, Govorun VM, Luster DG, Ignatov AN. 2016. Comprehensive analysis of draft genomes of two closely related pseudomonas syringae phylogroup 2b strains infecting mono- and dicotyledon host plants. *BMC Genomics*. Doi: 10.1186/s12864-016-3358-y.

Sun Y, Wang Y, Zhang X, Chen Z, Xia Y, Wang L, Sun Y, Zhang M, Xiao Y, Han Z, Wang Y, Chai J. 2022. Plant receptor-like protein activation by a microbial glycoside hydrolase. *Nature.* **610**, 335—342

Thiergart T, Durán P, Ellis T, Vannier N, Garrido-Oter R, Kemen E, Roux F, Alonso-Blanco C, Ågren J, Schulze-Lefert P, Hacquard S. 2020. Root microbiota assembly and adaptive differentiation among European Arabidopsis populations. *Nat Ecol Evol*. **4**, 122—131.

Thomas WJ, Thireault CA, Kimbrel JA, Chang JH. 2009. Recombineering and stable integration of the *Pseudomonas syringae* pv. *syringae* 61 hrp/hrc cluster into the genome of the soil bacterium *Pseudomonas fluorescens Pf0-1*. *Plant J.* **60**, 919—928.

Wang H, Song S, Gao S, Yu Q, Zhang H, Cui X, Fan J, Xin X, Liu Y, Staskawicz B, Qi T. 2024. The NLR immune receptor ADR1 and lipase-like proteins EDS1 and PAD4 mediate stomatal immunity in Nicotiana benthamiana and Arabidopsis. *Plant Cell.* **36**, 427-446.

Wasendorf C, Schultz DL, Schmitz-Esser S, Peters NT. 2022. Genome sequences of soft rot-causing *Pseudomonas* isolates from spinach. *Microbiol Resour Announc.* **11**, 1—3.

Wei CF, Kvitko BH, Shimizu R, Crabill E, Alfano JR, Lin NC, Martin GB, Huang HC, Collmer A. 2007. A *Pseudomonas syringae* pv. tomato DC3000 mutant lacking the type III effector HopQ1-1 is able to cause disease in the model plant *Nicotiana benthamiana*. *Plant J*. **51**, 32—46.

Wei HL, Chakravarthy S, Mathieu J, Swingle B, Martin GB, Collmer A. 2015. Pseudomonas syringae pv. tomato DC3000 Type III secretion effector polymutants reveal an interplay between HopAD1 and AvrPtoB. *Cell Host Microbe.* **17**, 752—762.

Wei HL, Zhang W, Collmer A. 2018. Modular Study of the Type III Effector Repertoire in *Pseudomonas syringae* pv. *tomato* DC3000 Reveals a Matrix of Effector Interplay in Pathogenesis. *Cell Rep.* **23**, 1630—1638.

Wu CH, Abd-El-Haliem A, Bozkurta TO, Belhaj K, Terauchid R, Vossen JH, Kamoun S. 2017. NLR network mediates immunity to diverse plant pathogens. *Proc Natl Acad Sci USA.* **114**, 8113—8113.

Ye L, Li L, Wang L, Wang S, Li S, Du J, Zhang S, Shou H. 2015. MPK3/MPK6 are involved in iron deficiency-induced ethylene production in Arabidopsis. *Front Plant Sci.* **6**, 1—10.

Zhang G, Kong G, Li Y. 2021. Long-distance communication through systemic macromolecular signaling mediates stress defense responses in plants. *Physiol Plant.* **173**, 1926—1934.

Zhao Y, Thilmony R, Bender CL, Schaller A, He SY, Howe GA. 2003. Virulence systems of Pseudomonas syringae pv. tomato promote bacterial speck disease in tomato by targeting the jasmonate signaling pathway. *Plant J.* **36**, 485—99.

3 Chapter 3: Conclusion

3.1 Future directions

The approaches described below in A – C (SEM, staining, and BEP-5 probe) are feasible to complete (and are planned to be) in the near future (1 – 3 months). All necessary materials were obtained and substantial planning, if not action, has been put toward their completion. The material components for the approaches described in D and E (new labeled bacterial strains, *Nb* est::HopBA1, and transcriptional reporters) are present in the lab, but further development and/or implementation requires significant additional time (likely greater than 6 months for high quality deliverables). F and G (forward genetics and scRNA-Seq) represent distinct future projects that could flow from the data that was generated in this work. They require extensive future work and development (grant writing, funding, and likely 1+ years of experimental development). Finally, H (*Nb* RLCK VII polymutants) represents a portion of the existing project with substantial progress/completion, but that requires extensive further development for completion (at least 6 months to a 1+ years, depending on the required order of mutants; maximum would be a 13x mutant).

A. Scanning Electron Microscopy

Scanning electron microscopy (SEM) has a long history of use in biology and for imaging of anatomical structures at high resolution. In this case, SEM will be utilized to resolve bacterial placement within plant vasculature with greater accuracy/certainty than with fluorescent microscopy alone. We hypothesize that bacteria are present within the xylem of infected plants given previous reports (Misas-Villamil *et al.*, 2011), however vascular bundles are tightly grouped, and fluorescent signal can further obscure precise placement of bacteria. It is also feasible that the

bacteria are colonizing the entirety of the vasculature given the associated disease symptoms at advanced time points (Figure 2.15).

As planned, distal petiole (DP), proximal petiole (PP), and stem cross sections will be sampled at 9 or 12 dpi following infiltration with *Pst* DC3000 Δ*hopQ* + *hopBA1*, + EV, or 10 mM $MgCl_2$ (mock). Briefly, cross sections of petioles associated with infiltrated leaves will be fixed and dehydrated using a critical point drier. Samples will be coated with gold or platinum using a sputter coater. Colorado State University (CSU) core analytical facility will be utilized for SEM examination and imaging. A JEOL JSM-6500 Field Emission Scanning Electron Microscope will be used. Another, more intriguing and modern approach to SEM that might be utilized is that described by Caldwell *et al.*, 2019.

B. Histochemical and other staining approaches

Figure 2.15 A and B provides a cursory inquiry into possible differences in lignification based on HopBA1 recognition or possibly activity. Since UV light causes any aromatic compound to fluoresce, a more specific or diagnostic stain would be better. Minimally, phloroglucinol-HCl can be used to definitively stain lignin and can be combined with additional stains to distinguish cellulose (Mitra and Loqué, 2014). Additional stains are available to distinguish between the three lignols that crosslink to form the lignin polymer, if understanding composition was warranted at some point. Further cell wall components that might be worth staining for their relevance in induced defense would be pectin and callose.

3,3′-diaminodbenzidine (DAB) staining can be used to qualitatively assess reactive oxygen species (ROS) content in leaves, as previously described (Torres *et al.*, 2002). This method could be used to support or provide additional information about the observed differences in leaf tissue following infiltration with DC3000 Δ*hopQ* + EV and + *hopBA1* that lead up to the overt outcome

of cell death/necrosis with DC3000 Δ*hopQ* + EV. Additionally, we are interested in seeing if DAB could be utilized to stain ROS in the vasculature, which may or may not be feasible (i.e., there is no established method for this).

C. BEP-5 small molecule probe for ethylene production and/or GC-MS/MS

BEP-5 is a fluorescent small-molecule that interacts with ethylene and potentially can be used as a probe to quantify local (i.e., leaf tissue and petiole tissue) differences in ethylene production. This probe is generally used in combination with fluorescent microscopy, however, we are interested in developing a plate reader-based assay to measure excitation of the compound after reaction with tissue from leaves vs. petioles for the strains used in this project DC3000 Δ*hopQ* + EV, and DC3000 Δ*hopQ* + *hopBA1*. In addition to this (or perhaps first, to determine if this experiment is a viable approach), a signal-to-noise comparison should be made using plant tissue treated with $AgNO_3$ or 1-Methylcyclopropene (1-MCP) (ethylene inhibitors) and 1-aminocyclopropane-1-carboxylate (ACC) (ethylene precursor and induces of ethylene responses). Ideally, in either case, a time course would be utilized to establish the most appropriate timepoint or time frame for data acquisition.

D. Vascular presence and HopBA1 sufficiency to induce hyponasty

It's possible that the deciding factor for the absence of HopBA1-induced hyponasty when delivered both by *Pf0-1* + TTSS and *Agrobacterium* (GV3101) is due to an inability of both strains to access host vasculature, though this has not yet been established. A simple qualitative experiment to establish whether this is the case would be to insert a fluorescent label into these strains and assess presence/absence via microscopy with following tripaerental mating with EV and HopBA1 plasmids. Preferably this would be a 3X fluorescent label (e.g., 3xmCherry as was previously used in this work). This can be accomplished with a Tn7 insertion site in *Pf0-1* (a previous

attempt with a sub-optimal Clover (GFP) miniTn7 vector confirmed viability). GV3101 lacks a Tn7 insertion site, but other groups have reported adding one to enable Tn7 insertions (Figueroa-Cuilan *et al.*, 2016). Another reasonable approach, if a functional leader sequence for translocation can be established, would be to use a virulent strain of an established vascular pathogen (e.g., *Xanthomonas* or *Ralstonia*) to deliver HopBA1 in *N. benthamiana*.

The best experiment to test whether hyponasty is a bona fide consequence of HopBA1 function alone would be to generate a transgenic *N. benthamiana* line that inducibly expresses HopBA1 (i.e., *Nb* est::HopBA1 or DEX::HopBA1). This would allow an assessment in a bacteria-free system and would definitively remove all other possible contributions to the phenotype borne of pathogen delivery (non-HopBA1 derived ETI or ETS, PTI, phytotoxin activity, plant structural barriers, etc.). To further dissect the mechanism of HopBA1 function in petioles, an inducible HopBA1 system could be expressed in specific cell types under tissue-specific promoters. These transgenic approaches likely require much more time to accomplish than the bacterial approaches mentioned.

E. Transcriptional reporters

Transgenic transcriptional reporter plants would improve the data collected so far. The Khakhar Lab kindly provided segregating T1 seed reporter lines for both auxin (IAA) and gibberellic acid (GA) (Khakhar *et al.*, 2018). Among the two lines, the dual (Venus-Luciferase) reporter line for IAA would be the most useful to understand how DC3000 Δ*hopQ* + *hopBA1* infiltration may be altering the distribution of IAA in leaves and petioles. Another less developed resource that we have available is several *Agrobacterium* strains that could be used to transform *Nb* and generate ethylene report lines (Fernandez-Moreno and Stepanova, 2020; unpublished).

F. Spatial transcriptomics – scRNA-Seq

Single-cell RNA-Seq (scRNA-Seq) is an increasingly popular and feasible (but still cost-prohibitive) method to characterize cell-specific transcriptional patterns. This has already been put to great use in understanding/characterizing spatial expression patterns as they related to plant immunity (NLRs and markers for disease responses) (Zhu *et al.*, 2023; Tang *et al.*, 2023). The present project is an incredibly interesting subject model for this approach, as defense processes are layered alongside developmental processes, which suggests a very nuanced and fine-tuned flow of events. Being able to observe, with single cell resolution, expression patterns across the leaf (as well as within a sub-set of leaf tissue, namely vascular tissue), as well as within the associated petiole where significant structural remodeling is an extremely attractive prospect. Further, and with broader impact, since DC3000 has not been investigated as a vascular pathogen causing systemic infection this would be a very critical addition of information to understanding non-fungi based vascular pathogenesis and immunity at the same time (i.e., by testing both DC3000 Δ*hopQ* + EV and DC3000 Δ*hopQ* + *hopBA1*).

G. EMS mutagenesis – screen for hyponasty negative mutants

An ambitious, but intriguing follow-up project to understand the genetic underpinning of HopBA1-induced hyponasty on the plant side could be a forward genetics screen using ethyl methanesulfonate (EMS), which has been shown as feasible in *N. benthamiana* (Schultink *et al.*, 2019). HopBA1 can induce hyponasty in plants as young as three weeks in age (younger plants were not screened, so it is possible that the phenotype could be assessed at an earlier time point). However, it is worth noting that this would be an extremely laborious screen since multiple individual leaves would need to be infiltrated to screen in thousands of mutants. It's possible that vacuum infiltration could be utilized to reduce time and effort.

H. *Nb* RLCK VII polymutants

The partially completed goal of the experiments detailed in Appendix A is the generation of an *Nb* RLCK VII polymutant. These mutants would allow us to test whether clade 5 and/or clade 6 are in fact genetically required for the reconstructed immune response (cell death) that was demonstrated by transient co-expression of HopBA1 and *At* ZRK2 (through endogenous ZAR1 and rescued by *At* ZAR1 in *Nb zar1* plants) (Appendix A, Figure A1 A and B). Subsequent results (Appendix A, Figures A3 and A4) indicated that *Nb* RLCK VII clade 5 and clade 6 were co-required for perception of HopBA1, as specific silencing of either clade resulted in a loss of cell death. Presently, a clade 5 triple mutant has been generated (as well as two additional segregating T2 triple mutant lines). Additional multi-guide Cas9 vectors (Stuttmann *et al.*, 2021) were generated to target the four remaining genes in clade 5. Another Cas9 vector set was generated to target six genes within clade 6. Presently, these vectors have been used in *Agrobacterium*-mediated transformation of tissue, as previously described (Huang *et al.*, 2023), but transgenic plantlets have yet to be obtained.

3.2 References

Alassimone J, Fujita S, Doblas VG, van Dop M, Barberon M, Kalmbach L, Vermeer JE, Rojas-Murcia N, Santuari L, Hardtke CS, Geldner N. 2016. Polarly localized kinase SGN1 is required for Casparian strip integrity and positioning. *Nat Plants.* **25**, 16113.

Caldwell D, Iyer-Pascuzzi AS. 2019. A Scanning Electron Microscopy Technique for Viewing Plant-Microbe Interactions at Tissue and Cell-Type Resolution. *Phytopathology*. **109**, 1302—1311.

Fernandez-Moreno JP, Stepanova AN. 2020. Monitoring ethylene in plants: genetically encoded reporters and biosensors. *Small Methods* **4**, 1—13.

Figueroa-Cuilan W, Daniel JJ, Howell M, Sulaiman A, Brown PJ. 2016. Mini-Tn7 Insertion in an Artificial attTn7 Site Enables Depletion of the Essential Master Regulator CtrA in the Phytopathogen Agrobacterium tumefaciens. *Appl Environ Microbiol.* **82**, 5015—5025.

Fujita S, De Bellis D, Edel KH, Köster P, Andersen TG, Schmid-Siegert E, Tendon VD, Pfister A, Marhavý P, Ursache R, Doblas VG, Barberon M, Daraspe J, Creff A, Ingram G, Kudla J, Geldner N. 2020. SCHENGEN receptor module drives localized ROS production and lignification in plant roots. *EMBO J.* **39**, e103894.

Huang WRH, Braam C, Kretschmer C, Liu H, Ferik F, van der Burgh AM, Pluis M, Hagan AO, Villanueva SL, Wu J, van Loosbroek A, Wang Y, Seidl MF, Stuttmann J, Joosten MHAJ. 2023. Receptor-like cytoplasmic kinases belonging to different subfamilies mediate immune responses downstream of the Cf-4 resistance protein in *Nicotiana benthamiana*. *bioRxiv*. https://doi.org/10.1101/2023.04.25.538242

Khakhar A, Leydon AR, Lemmex AC, Klavins E, Nemhauser JL. 2018. Synthetic hormone-responsive transcription factors can monitor and re-program plant development. *Elife.* **7**, e34702.

Lozano-Duràn R, Zipfel C. 2015. Trade-off between growth and immunity: role of brassinosteroids. *Trends Plant Sci.* **20**, 12—19.

Luo X, Wu W, Liang Y, Xu N, Wang Z, Zou H, Liu J. 2020. Tyrosine phosphorylation of the lectin receptor-like kinase LORE regulates plant immunity. *EMBO J.* **39**, 1—16.

Misas-Villamil JC, Kolodziejek I, van der Hoorn RA. 2011. Pseudomonas syringae colonizes distant tissues in Nicotiana benthamiana through xylem vessels. *Plant J.* **67**, 774—782.

Mitra PP, Loqué D. 2014. Histochemical staining of *Arabidopsis thaliana* secondary cell wall elements. *JOVE.* **87**, 1—11.

Schultink A, Qi T, Bally J, Staskawicz B. 2019. Using forward genetics in *Nicotiana benthamiana* to uncover the immune signaling pathway mediating recognition of the *Xanthomonas perforans* effector XopJ4. *New Phytol*. **221**, 1001—1009.

Singh P, Mishra V, Tripathi DK, Corpas FJ, Singh VP. 2022. RIPK: a crucial ROS signaling component in plants. *Trends Plant Sci*. **27**, 214—216.

Stuttmann J, Barthel K, Martin P, Ordon J, Erickson JL, Herr R, Ferik F, Kretschmer C, Berner T, Keilwagen J, Marillonnet S, Bonas U. 2021. Highly efficient multiplex editing: one-shot generation of 8× Nicotiana benthamiana and 12× Arabidopsis mutants. *Plant J*. **106**, 8—22.

Tang B, Feng L, Hulin MT, Ding P, Ma W. 2023. Cell-type-specific responses to fungal infection in plants revealed by single-cell transcriptomics. *Cell Host Microbe*. **10**, 1732—1747.

Torres MA, Dangl JL, Jones JD. 2002. Arabidopsis gp91phox homologues AtrbohD and AtrbohF are required for accumulation of reactive oxygen intermediates in the plant defense response. *Proc Natl Acad Sci USA*. **99**, 517—22.

Wang W, Hu C, Li X, Zhu Y, Tao L, Cui Y, Deng D, Fan X, Zhang H, Li J, Gou X, Yi J. 2022. Receptor-like cytoplasmic kinases PBL34/35/36 are required for CLE peptide-mediated signaling to maintain shoot apical meristem and root apical meristem homeostasis in Arabidopsis. *Plant Cell.*. **34**, 1289—1307.

Yang DL, Yao J, Mei CS, Tong XH, Zeng LJ, Lia Q, Xiao LT, Sun T, Li J, Deng XW, Lee CM, Thomashow MF, Yang Y, He Z, He SY. 2012. Plant hormone jasmonate prioritizes defense over growth by interfering with gibberellin signaling cascade. *Proc Natl Acad Sci USA.* **109**, 1192—1200.

Zhu J, Lolle S, Tang A, Guel B, Kvitko B, Cole B, Coaker G. 2023. Single-cell profiling of *Arabidopsis* leaves to *Pseudomonas syringae* infection. *Cell Reports.* **42**, 1—21.

4 Appendix A: Preliminary works

The transient reconstruction of a plant immune pathway & the impact of silencing *Nb* RLCK VIIs

This appendix provides additional background information for preliminary works that were done immediately leading up to the materials and experiments of Chapter 2.

Summary

The present work establishes that the functional ZAR1-ZRK2-based (HopZ-activated resistance 1 and ZED1 related kinase 2) immune pathway from *Arabidopsis thaliana* (*At*) can be transiently reconstructed in *Nicotiana benthamiana* (*Nb*) using *Agrobacterium tumefaciens* (GV3101) to trigger a localized immune response to the bacterial effector HopBA1, which is not otherwise recognized by the plant within leaf tissue. Co-expression of the proteins *At* ZRK and HopBA1 trigger programmed cell death or a hypersensitive response within the infiltrated tissue, suggesting that HopBA1 modifies a protein in *Nb* and this activity is not endogenously recognized due to an insufficient interaction with or perception by *Nb* RLCK XIIs (receptor-like cytoplasmic kinase, subfamily XII). Utilizing *Nb zar*⁻ mutant plants, it is further demonstrated that *Nb* ZAR1 is required for the transient recognition of HopBA1. Following these results, hairpinRNA-interference (hpRNAi) was used to silence a subfamily of *Nb* proteins, specifically receptor-like cytoplasmic kinases subfamily VII (*Nb* RLCK VIIs), which are hypothesized to be HopBA1 modification targets based upon ZAR1 recognition. HpRNAi silencing results suggest that HopBA1 recognition is based on the co-required function of proteins from two independent clades of *Nb* RLCK VIIs, clade 5 and clade 6. This information was used to inform the generation of *Nb* RLCK VII polymutants via Cas9, which is presently ongoing.

Transient expression of HopBA1 does not illicit an immune response in *N. benthamiana*, but co-expression with *Arabidopsis* ZRK2 activates ZAR1-dependent immune recognition

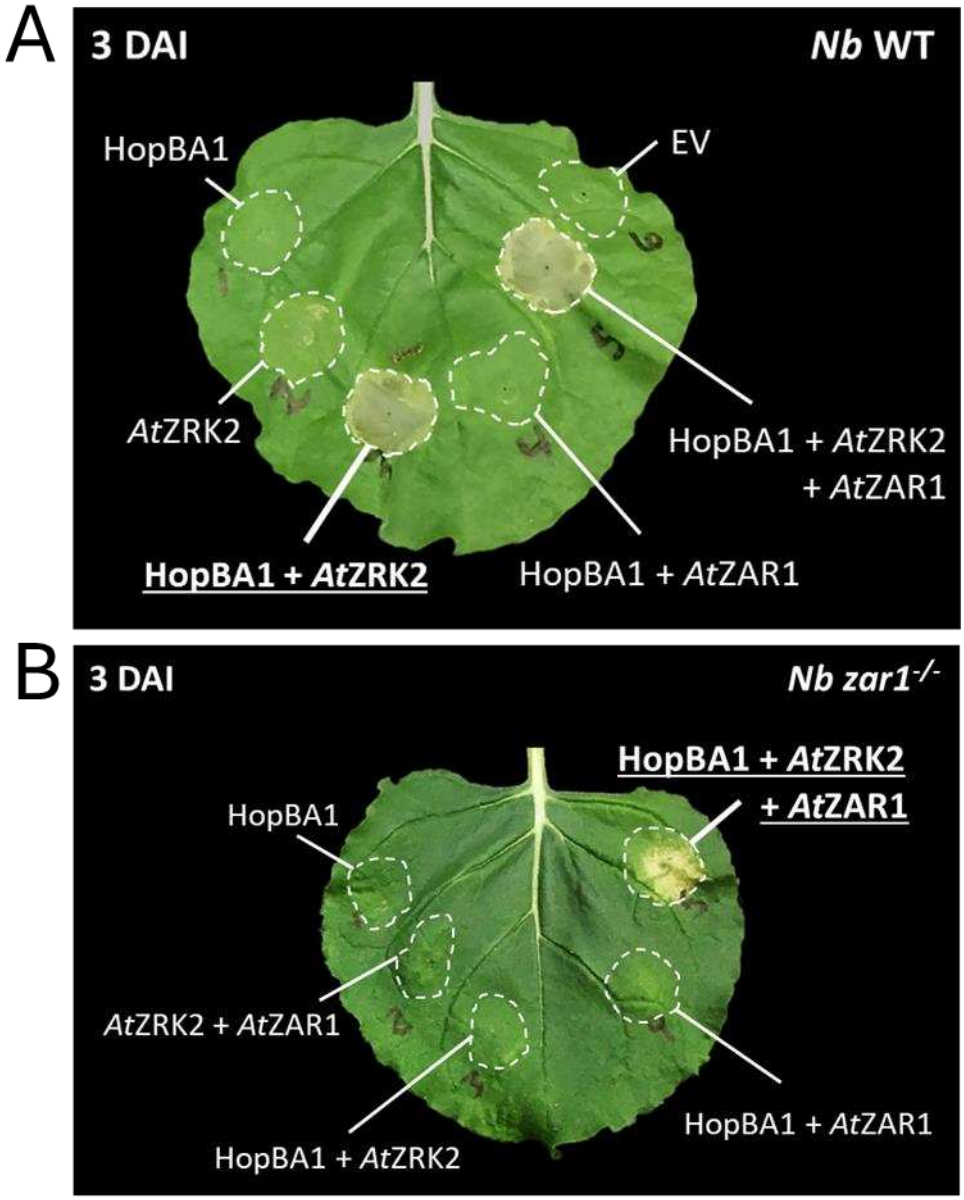

Figure A1. *Agrobacterium* transient co-expression of HopBA1 and *At* ZRK2 activates ZAR1-dependent immunity in *N. benthamiana*. (A) Transient expression of HopBA1 by *Agrobacterium* is insufficient to trigger immunity (i.e., cell death or hypersensitive response). Cell death occurs only when HopBA1 is co-expressed with the *Arabidopsis* pseudokinase adapter, ZRK2. (B) Cell death is no longer triggered by transient co-expression of HopBA1 and *At* ZRK2 in the *Nb zar1* background, further indicating that reconstructed immunity requires *Nb* ZAR1. Host recognition of HopBA1 can be rescued by co-expression with *At* ZKR2 and *At* ZAR1. Leaves pictured at 3 days after infiltration. Bacteria were delivered by needleless syringe at a total optical density (OD_{600}) of 0.6. Experiments were replicated multiple times on 2 – 3 plants (3 leaves per plant) on each occasion.

Silencing of *Nb* RLCK VIIs suggests a cross-clade co-requirement for the reconstruction of HopBA1 recognition

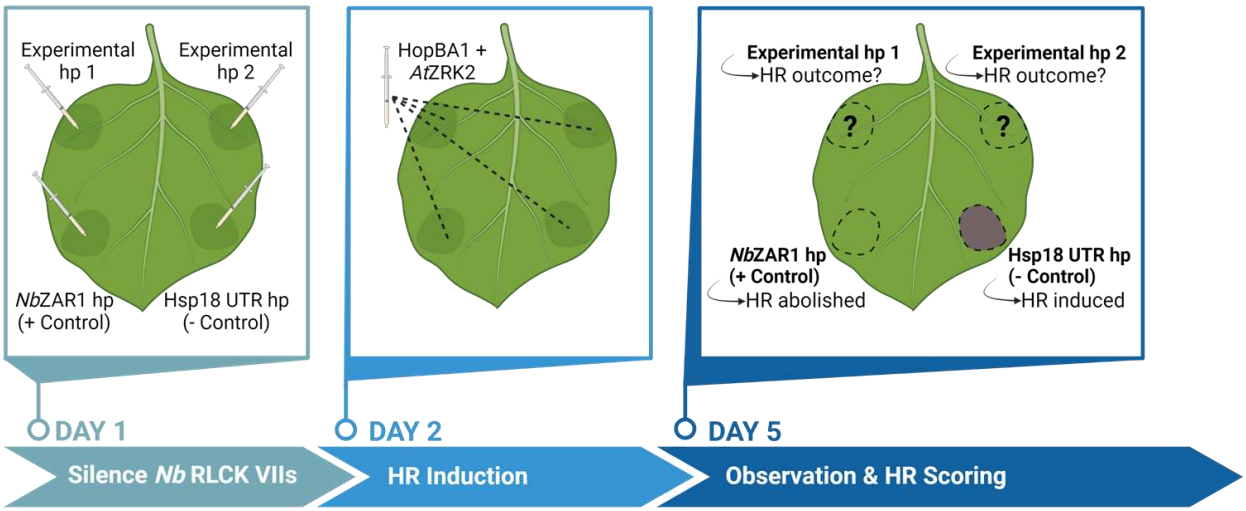

Figure A2. Overview of the hpRNAi screening process utilized to identify potential *Nb* RLCK VIIs targeted by HopBA1. Conceptually, if *At* ZRK2 facilitates *Nb* ZAR1 recognition of RLCK VII modification by HopBA1, a knockdown of HopBA1's target would result in a loss of cell death. Agrobacterium was used to deliver silencing constructs 18 – 24hrs. prior to re-infiltration with the cell death-inducing (i.e., HopBA1 + *At* ZRK2) component of the screen. Cell death or hypersensitive response (HR) was then evaluated 3 days later. *Nb* ZAR1 was silenced as a positive control and an empty vector silencing construct served as a negative control for the screen.

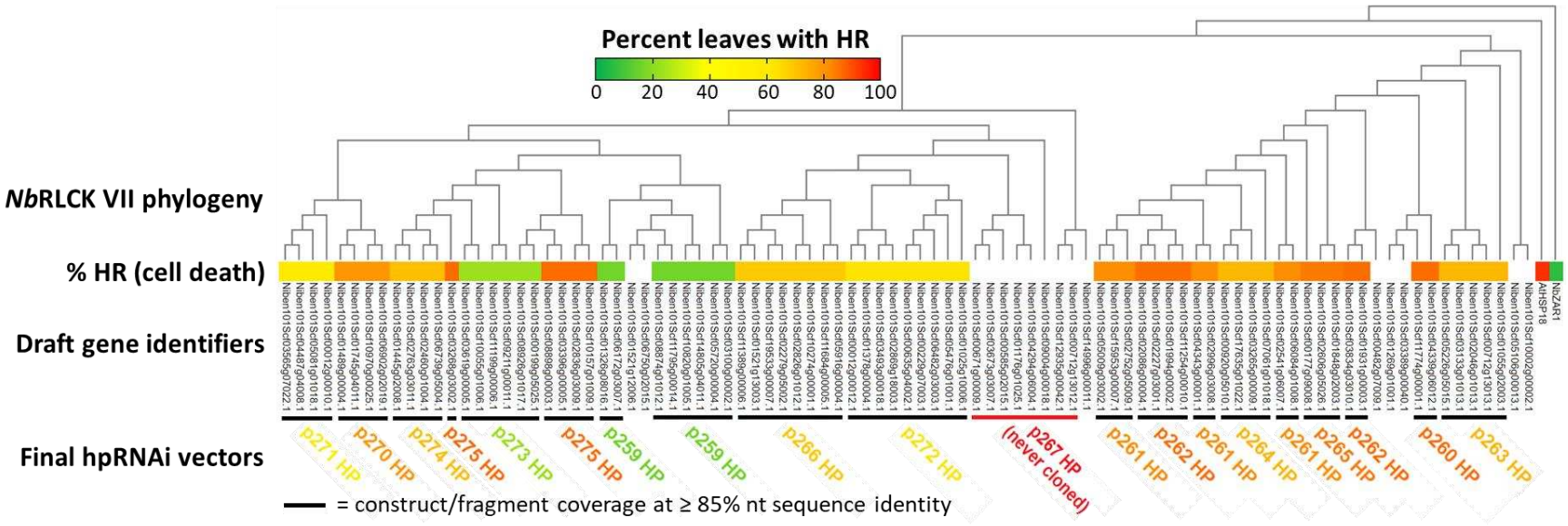

Figure A3. The draft *Nb* RLCK VII phylogeny based on homology to the published subfamily phylogeny in Arabidopsis with silencing constructs overlaid based on fragment coverage of the listed genes. The observed % cell death is given by color, ranging from 0% cell death (green) to 100% cell death (red). The silencing construct "p267 HP" was never cloned and therefore was not tested in the RNAi screen. The positive control (ZAR1) and the negative control (Hsp18 3' UTR) hairpin/silencing constructs are also provided for reference. "p259 HP" (clade 5) and "p273 HP" (clade 6) were identified as promising HopBA1 targets as their silencing resulted in the greatest reduction in % cell death. See A5 – A7 for additional details.

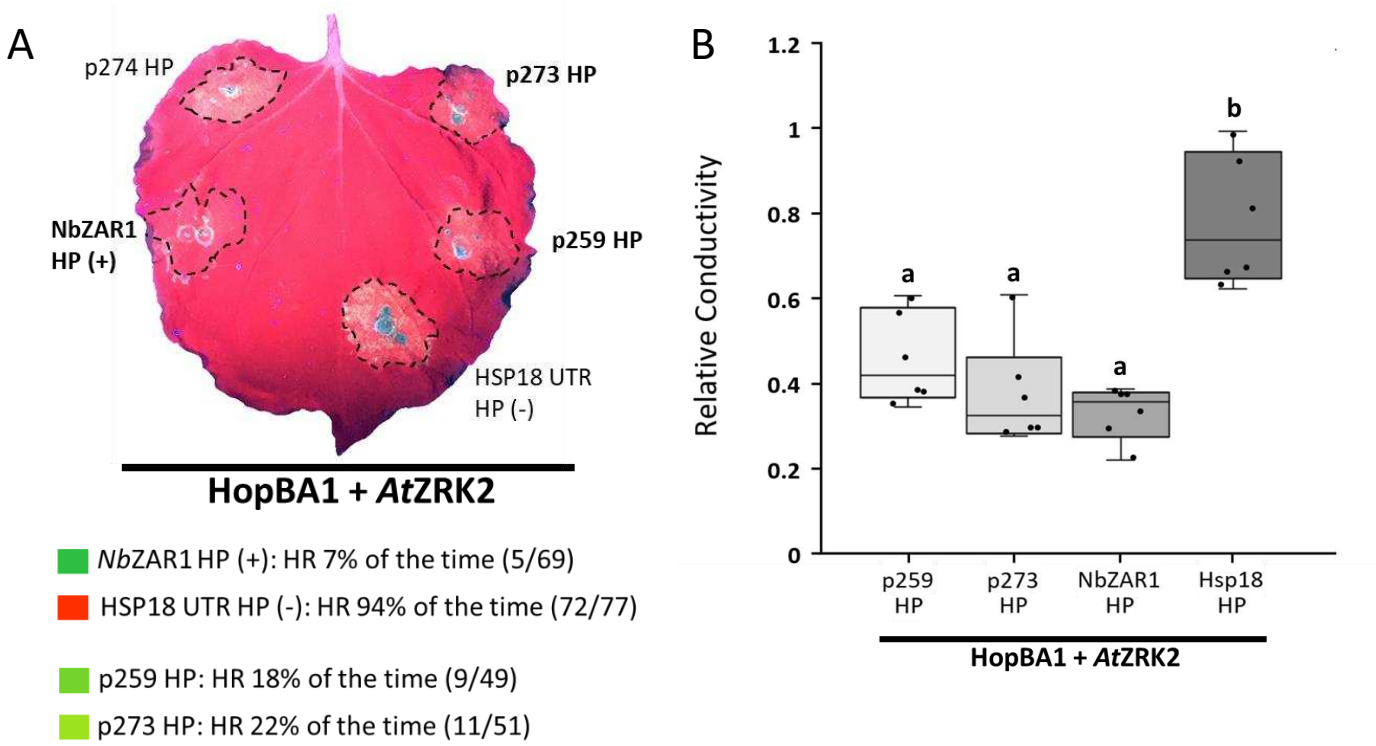

Figure A4. Percent (%) cell death results from the RNAi/silencing screen given as a representative leaf image (A) and quantitative values (both the scored proportion (A) and as relative conductivity (B)). (A) The two most promising "hits" from the silencing screen (p259 HP, 18% and p273 HP, 22%) showed a reduction in cell death ("HR" or hypersensitive response) relative to the negative control (HSP18 UTR HP, 94%), but a greater % than the positive control (NbZAR1 HP, 7%). (B) In terms of relative conductivity, a proxy for cell death, the two silencing "hits" were equal to ZAR1 silencing for conductivity and had significantly lower conductivity than HSP16 UTR silencing. One-way ANOVA and Tukey HSD. 6 biological replicates were used and the assay was repeated multiple times with equivalent results.

Generation of Cas9 editing vectors and *Nb rlck vii* polymutants via Agrobacterium-mediated transformation of tissue culture

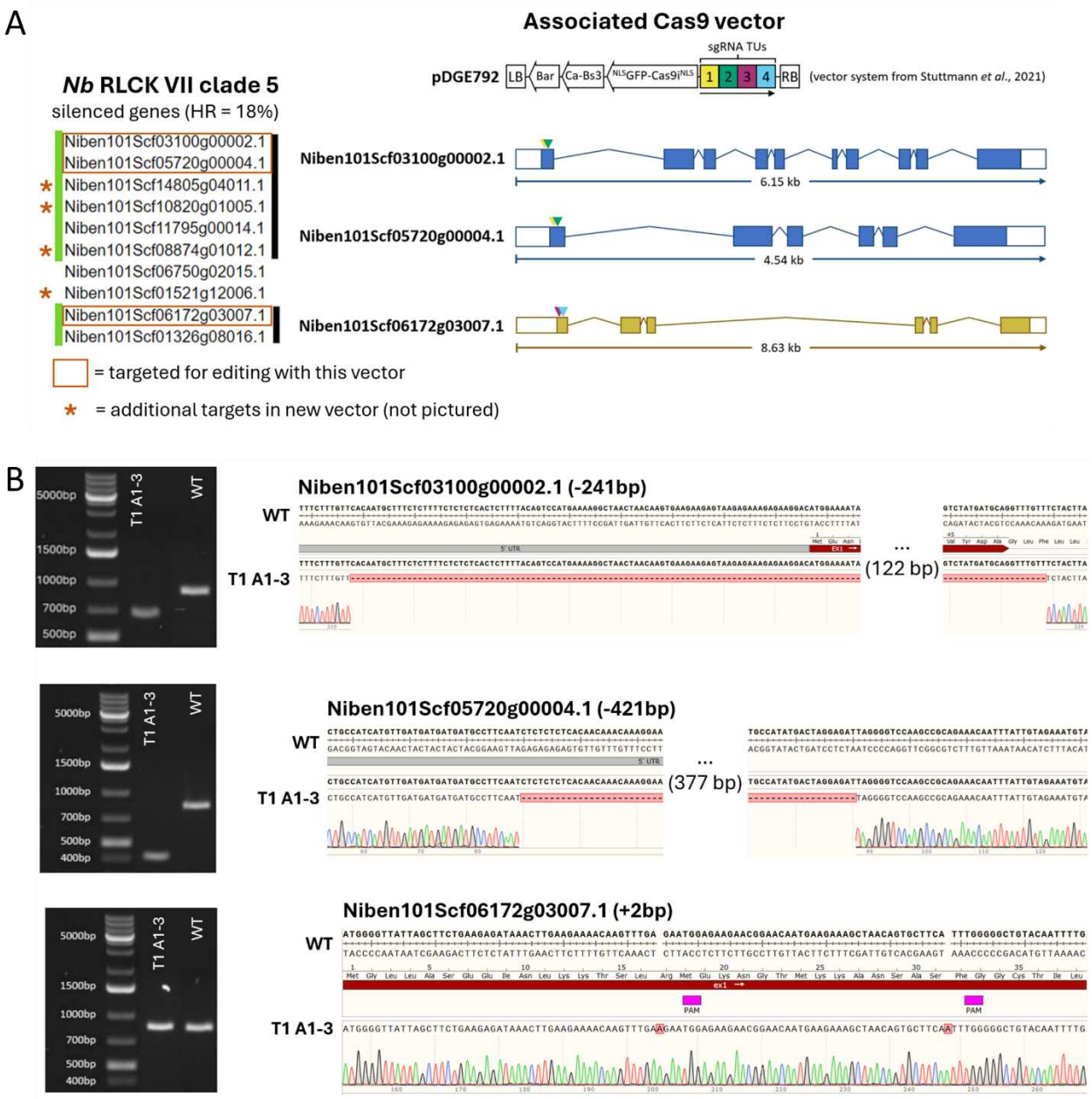

Figure A5. Multi-guide cas9 vectors and target *Nb* RLCK VII genes from clade 5; gel results and Sanger sequencing for a T1 mutant line. (A) The first multi-guide Cas9 vector only targets 3 genes from clade 5 (boxed in red) that resulted in reduced % cell death in the RNAi screen. A second vector was designed to target 4 additional genes within this clade. The progeny of T1 A1-3 will be assessed for loss of cell death; pending results, the T2 line will be transformed with the additional cas9 vector. (B) PCR amplicons run on a gel for the 3 targeted genes for editing. Both the bands and Sanger sequencing support homozygous mutations within the T1 line. 2 additional T1 lines have independent mutations (not pictured) in the three genes and were either homozygous or segregating.

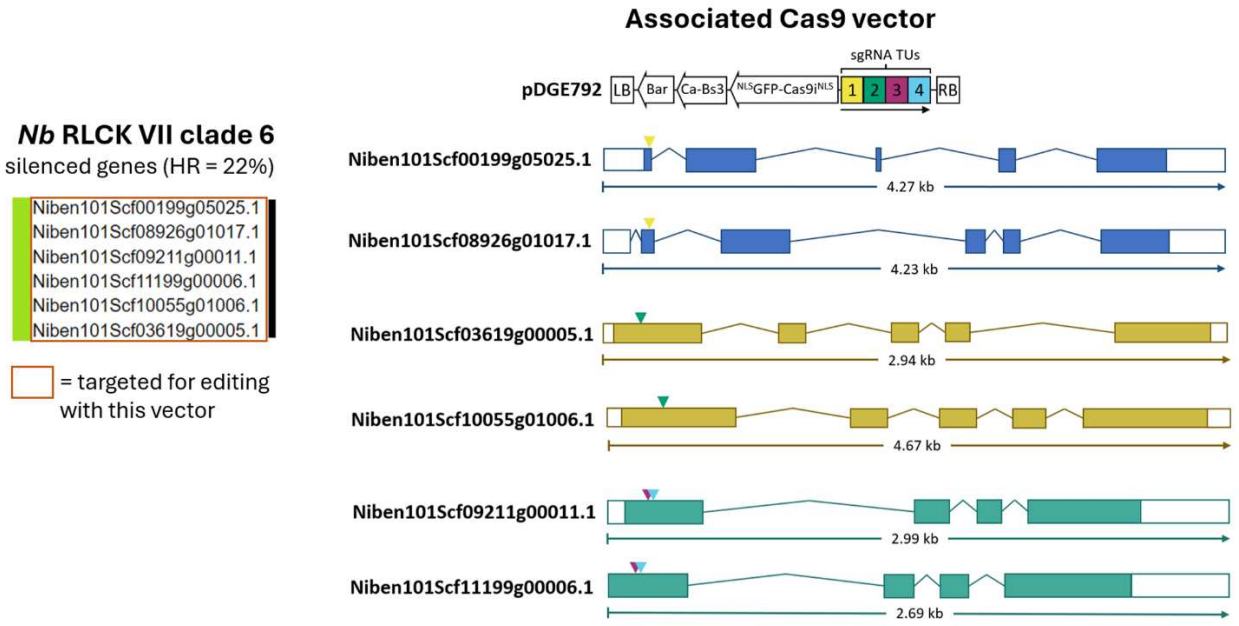

Figure A6. Multi-guide cas9 vectors and target *Nb* RLCK VII genes from clade 6. All 6 genes that resulted in reduced % cell death in the RNAi screen are effectively targeted for Cas9 editing. To date, no transformed plantlets for this clade have been successfully obtained from tissue culture/callus.

5 Appendix B: Supplemental data

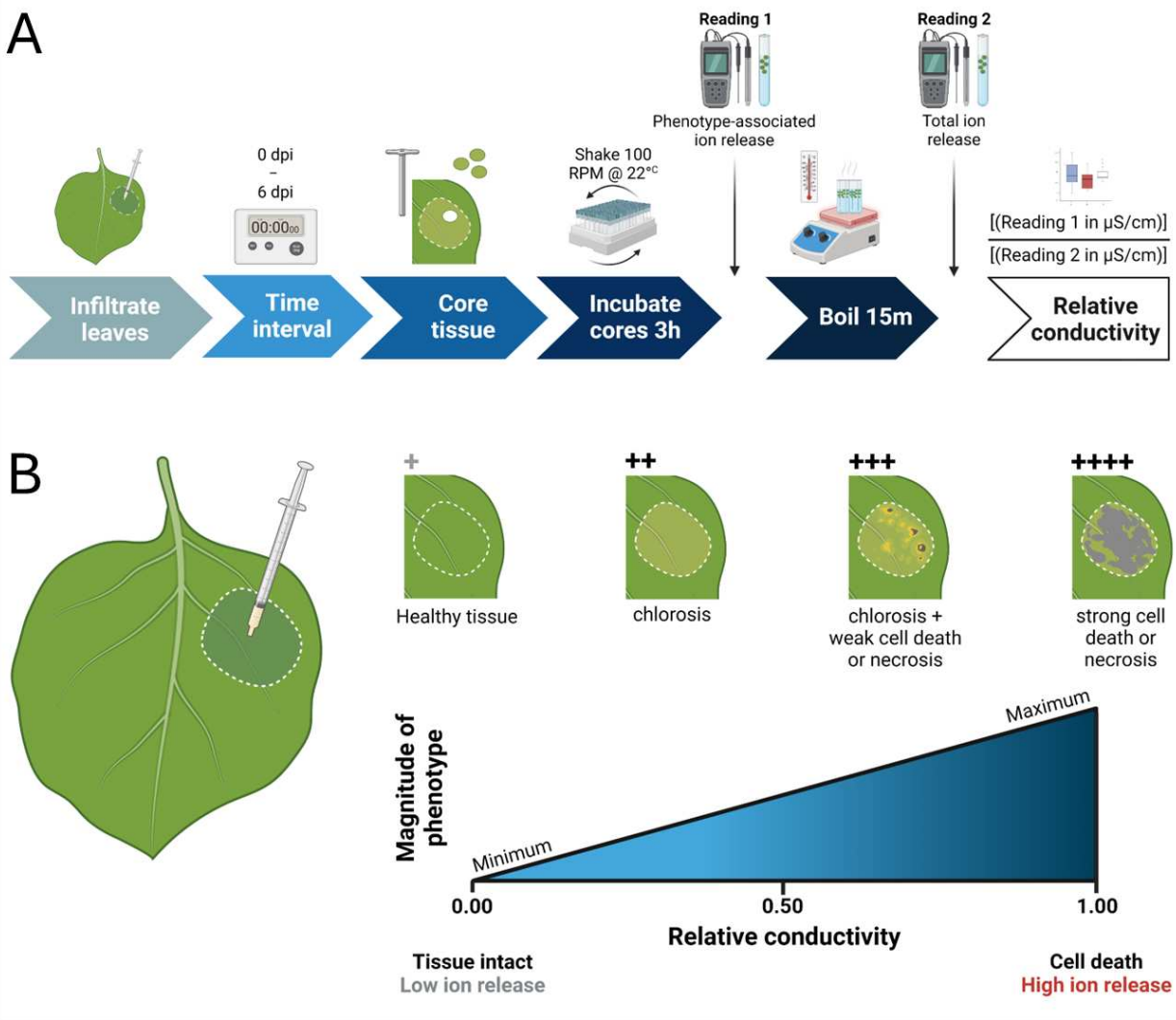

Figure S1. Procedural overview of the relative conductivity assay utilized to quantify cell death and/or necrosis following spot infiltration of leaves. (A) Timeline of the major steps of the assay. (B) Relationship between the observed phenotype and relative conductivity measurements.

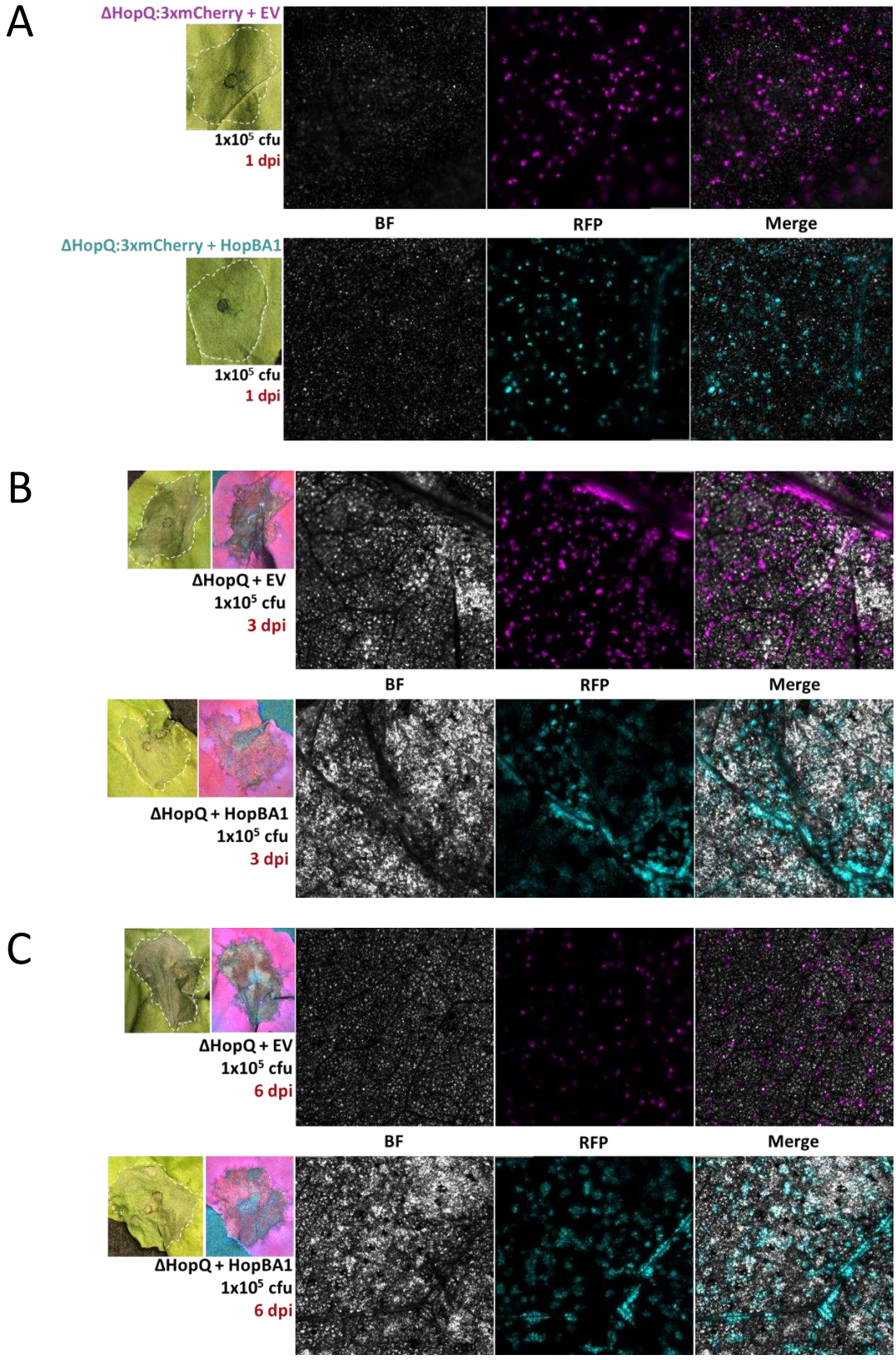

Figure S2. Qualitative comparison of relative abundance of bacteria within spot infiltrations at (A) 1, (B) 3, and (C) 6 dpi. DC3000 Δ*hopQ* + EV (magenta false color) and DC3000 Δ*hopQ* + *hopBA1* (cyan false color).

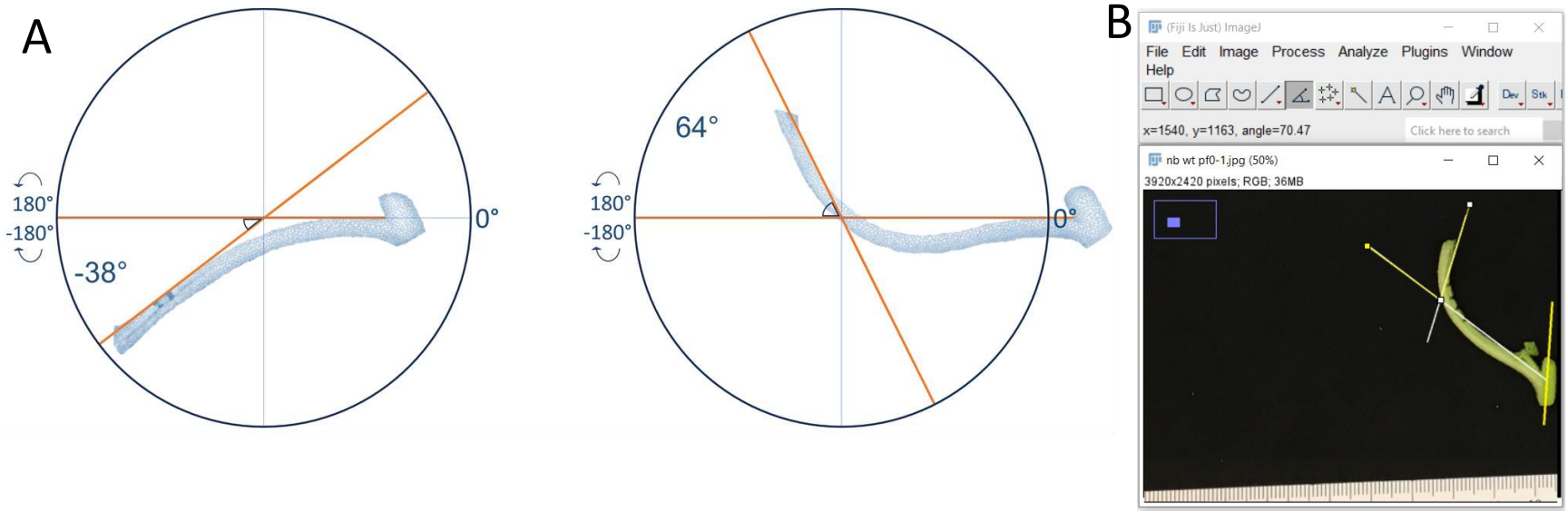

Figure S3. Approach utilized to measure and assign petiole angle. (A) Petioles from treated leaves with a portion of the stem attached and leaf removed. Circles added to help illustrate degree positions and assignment. An initial line is drawn at the petiole base (adaxial surface nearest to the stem), which is set to 0°. A second line is drawn at the opposite end of the petiole terminus (i.e., petiole-leaf junction). The angle that results from the intersection of these two lines is the assigned petiole angle (in degrees). If the petiole is hyponastic (bent upward) the angle will be positive (right example) and if the petiole is epinastic (bent downward) the angle will be negative (left example). (B) An example of the assay in practice. At 6 dpi (unless otherwise noted), petioles are excised, leaves are removed, lines are drawn (as described in A) with software, and petiole angles are measured using imageJ. The petiole angle for this example is 70.47°.

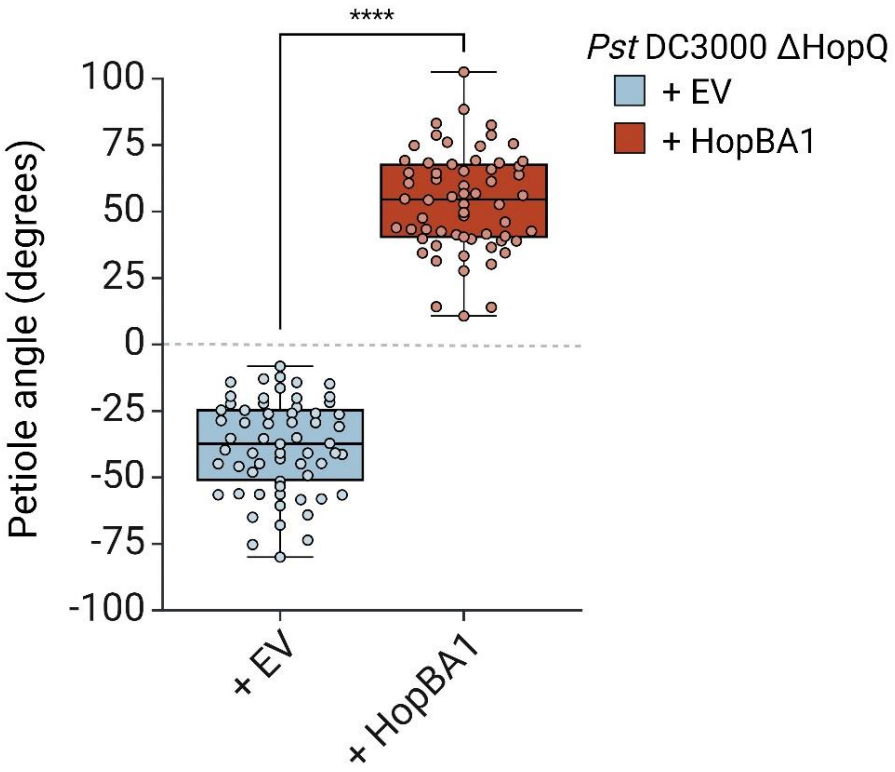

Figure S4. Cumulative petiole angle measurements from all experiments in *Nb* WT for DC3000 ΔHopQ + EV and DC3000 ΔHopQ + HopBA1 further supports HopBA1-induced hyponasty and its characterization as a petiole angle > 0° (degrees). DC3000 ΔHopQ + HopBA1 has a compiled mean petiole angle of 54°, while DC3000 ΔHopQ + EV has a compiled mean petiole angle of -38°. N = 62. **** $P < 0.0001$ (Student's T-test).

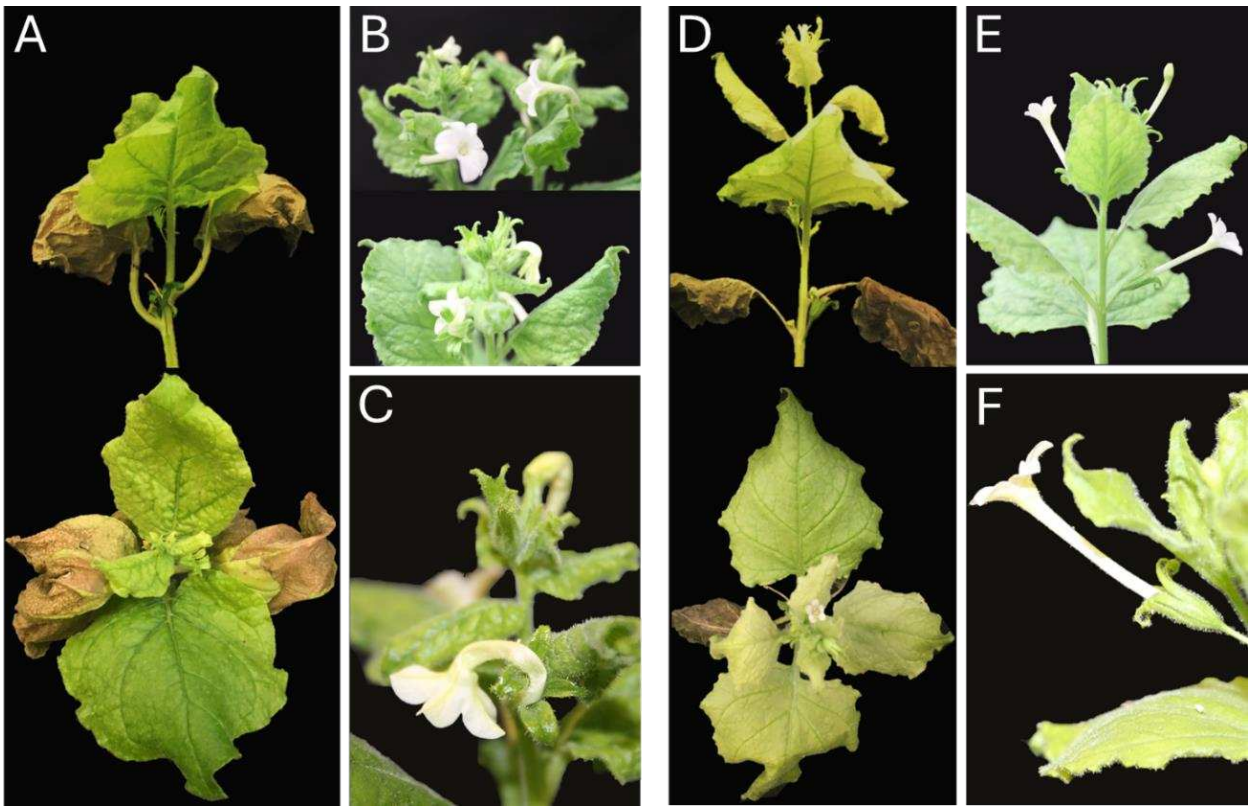

Figure S5. Long-term phenotype differences (whole plant and floral morphology) for *Pst* DC3000 Δ*hopQ* + *hopBA1* and + EV. (A – C) DC3000 Δ*hopQ* + *hopBA1* phenotypes. (A) In addition to induced hyponasty, infiltration with DC3000 Δ*hopQ* + *hopBA1* stunts vertical and apical plant development, while causing mild to moderate apical chlorosis in leaves, which are waxy and crinkled/bumpy. Plants were ~ 7 weeks old at the time of infiltration. (B) HopBA1 induces modified phyllotaxy and morphology of flowers. Petals of flowers formed after infiltration appear whirled, with petals encircling the stem in 360° or down-turned/wrapped around the flower's carpels. (C) A closeup of the floral phenotype shown in (B), note that in addition to being curved/curled, petals are also irregularly wavy or crinkled rather than cylindrical. Mature plants with two completely developed flowers and two additional buds in formation were infiltrated. Images taken 12 dpi. (D – F) DC3000 Δ*hopQ* + EV phenotypes. (D) Infiltration with DC3000 Δ*hopQ* + EV results in comparatively stronger and more homogenous chlorosis than + *hopBA1*, as well as greater vertical elongation and floral development. Plants were ~ 7 weeks old at the time of infiltration. (E) Infiltration of mature plants with DC3000 Δ*hopQ* + EV does not alter floral development/progression or morphology. Stem elongation is etiolated but continues normally relative to + *hopBA1*. (F) A closeup of the flower morphology shown in (E). Mature plants with two completely developed flowers and two additional buds in formation were infiltrated. Images taken 12 dpi.

Plant genotype	Bacterial strain	Hyponasty (y/n)	Mean petiole angle (°)	Empty vector [- control] (°)	HopBA1 [+ control] (°)	Sample size (n)
Nb WT	*Pst* DC3000 ΔHopQ + HopBA1	y	66.35	-35.32	--	10
	Pst DC3000 ΔHopQ + EV	n	-35.32	--	66.35	
	Pst DC3000 ΔHopQ + HopQ1	n	-23.94	-35.32		
Nb adr1$^{-/-}$ *nrg1*$^{-/-}$	*Pst* DC3000 ΔHopQ + HopBA1	y	54.66	-47.54	--	10
Nb eds1$^{-/-}$	*Pst* DC3000 + HopBA1	y*	64.88	-33.91	60.26	5
	Pst DC3000 ΔHopQ + HopBA1	y	60.26		--	
Nb roq1$^{-/-}$	*Pst* DC3000 + HopBA1	y*	22.18	-56.52	22.56	6
	Pst DC3000 ΔHopQ + HopBA1	y	22.56		--	
Nb nrc2$^{-/-}$ *nrc3*$^{-/-}$ *nrc4*$^{-/-}$	*Pst* DC3000 ΔHopQ + HopBA1	y	32.05	-37.81	--	10
Nb nrg1$^{-/-}$	*Pst* DC3000 ΔHopQ + HopBA1	y	63.84	-44.28	--	6
Nb zar1$^{-/-}$	*Pst* DC3000 ΔHopQ + HopBA1	y	55.60	-63.48	--	5
Nb WT	*Pst* DC3000 + HopBA1	n	-13.10	-33.68	58.87	5
Nb WT	*Pst* DC3000 D36E + HopBA1	y*^	31.11	-74.56	22.50	4
Nb WT	*Pst* DC3000 ΔHopQ + HopBA1 H56A	n	-25.78	-35.42	71.64	8
	Pst DC3000 ΔHopQ + HopBA1 Y158A	n	-25.87			
	Pst DC3000 ΔHopQ + HopBA1 Y158F	y**	21.62			
	Pst DC3000 ΔHopQ + HopBA1 R162A	n	-35.09			
	Pst DC3000 ΔHopQ + HopBA1 W122A	n	-36.13			
Nb WT	*Pst* DC3000 ΔHopQ ΔFliC ΔPilA + HopBA1	y*	41.23	-32.75	43.95	6
Nb roq1$^{-/-}$	*Pst* DC3118 (-Cor) + HopBA1	y*	24.06	-66.86	29.03	4
Nb eds1$^{-/-}$	*Pst* DC3118 (-Cor) + HopBA1	y*	32.89	-65.91	61.64	4
Nb WT	*Pja*	n	-20.66	-30.17	45.09	10
	Ptt	n	-15.77			
Nb WT	*Pf0-1* + HopBA1	n	-36.84	-52.40	39.59	4
Nb WT	*Agrobacterium* GV3101 + HopBA1	n	-27.36	-30.06	62.29	5
Nt eds1$^{-/-}$	*Pst* DC3000 ΔHopQ + HopBA1	n	-18.37	-24.05	--	6
Nt WT	*Pst* DC3000 ΔHopQ + HopBA1	n	not measured	not measured	not measured	6
At$_{Col-0}$ WT	*Pst* DC3000 ΔHopQ + HopBA1'	n				10
At$_{Col-0}$ *zar1*$^{-/-}$	*Pst* DC3000 ΔHopQ + HopBA1'	n				10
At$_{Ag-0}$ *rba1*$^{-/-}$ *zar1*$^{-/-}$	*Pst* DC3000 ΔHopQ + HopBA1	n				6
At$_{Col-0}$ *'helperless'*	*Pst* DC3000 ΔHopQ + HopBA1'	n				10
At$_{Col-0}$ *'deps' rbohD*	*Pst* DC3000 ΔHopQ + HopBA1'	n				6

** statistically greater petiole angle than the negative (-) control and within the same statistical group as the positive (+) control*

**^ statistically greater petiole angle than the negative (-) control and within the same statistical group as the positive (+) control when ' infiltrated at same optical density (OD_{600} = 0.1)*

*** statistically greater petiole angle than the negative (-) control; not within the same statistical group as the positive (+) control*

-- the presented strain is the same as the control

' Pst DC3000 + HopBA1 was also tested

Rationale for testing

- Initial experiment / observation
- Plant genotype / genetic contribution (ETI/loss of ETI)
- DC3000 effector contribution (ETI/ETS)
- HopBA1 functional contribution
- Bacterial motility contribution
- Phytotoxin contribution
- Bacterial genus / species contribution
- Plant genus / species contribution

Supplemental Table 1. HopBA1-induced hyponasty summary table. Summary data for all bacterial strains and plant genotypes tested. Color-coding relates to the objective or classification of the experiment (detailed to right). Hyponasty results are reported as yes/no relative to the positive control (DC3000 ΔHopQ + HopBA1). Reported petiole angles were measured between 6 to 9 dpi.

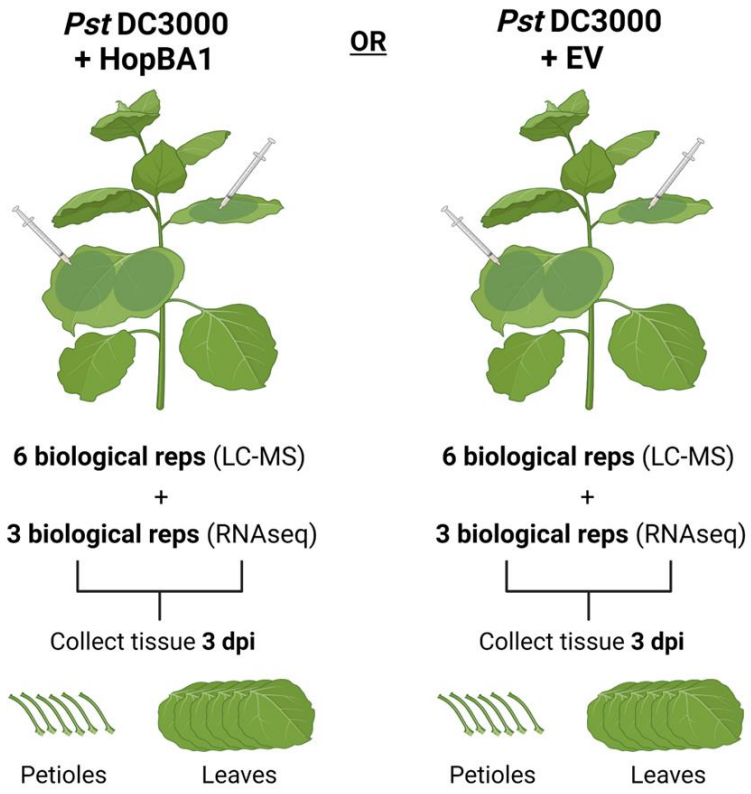

Figure S6. The sampling approaches used for LC-MS and RNA-Seq. Individual plants were infiltrated with either DC3000 ΔHopQ + EV or DC3000 ΔHopQ + HopBA1 at low OD (1×10^5 cfu). 4 – 5 leaves and associated petioles were sampled per plant. Tissue was collected at 3 dpi; leaves and petioles were processed separately. 6 biological replicates (i.e., plants) were used in LC-MS and 3 were used in RNA-Seq.

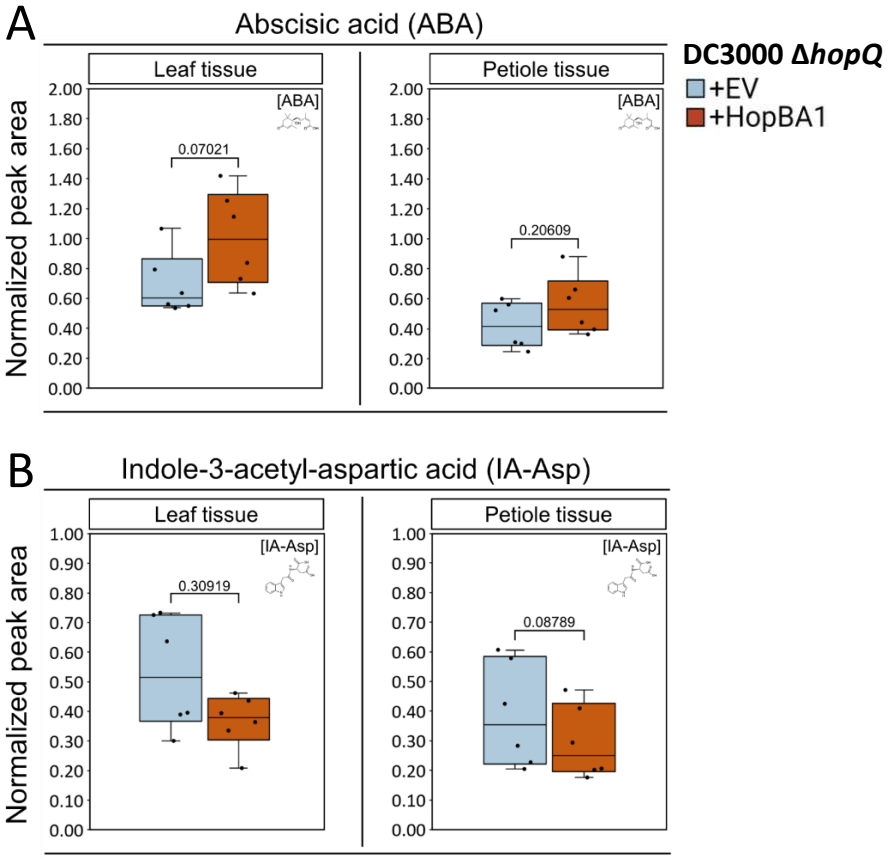

Figure S7. Non-significant results for phytohormone abundance (normalized peak area) in leaf and petiole tissue for DC3000 ΔHopQ + EV and DC3000 ΔHopQ + HopBA1 infiltrations. (A) **ABA**-related results. Leaf + EV ~0.693, leaf + HopBA1 ~1.004 ($P \approx 0.070$). Petiole + EV ~0.425, petiole + HopBA1 ~0.562 ($P \approx 0.206$). (B) **IA-Asp**-related results. Leaf + EV ~0.529, leaf + HopBA1 ~0.367 ($P \approx 0.309$). Petiole + EV ~0.387, petiole + HopBA1 ~0.294 ($P \approx 0.088$). Tissue sampled at 3 dpi. 6 biological replicates. Strain used: DC3000 ΔHopQ + EV (blue) or + HopBA1 (orange). One-way ANOVA.

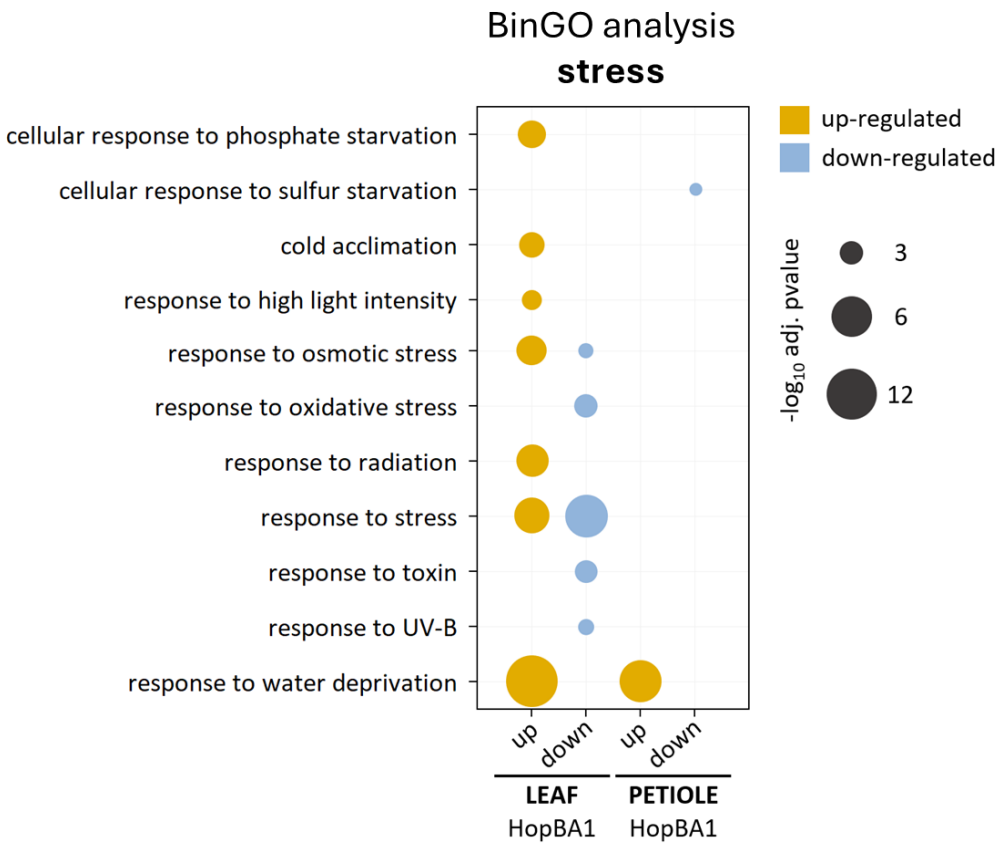

Figure S8-A. HopBA1 enriched GO terms directly qualified as stress responses and those that likely contribute biological stress. Up-regulation Overall, leaves infiltrated with DC3000 Δ*hopQ* + *hopBA1* appear to undergo elevated stress relative to DC3000 Δ*hopQ* + EV at 3 dpi. Increased stress and stress-related terms are based on resource deprivation/starvation (water and phosphate), osmotic stress (likely related to water deprivation), temperature, and light intensity (presumably due to the vertical reorientation of leaves and interception of less diffuse light). Surprisingly, petioles undergo less (reduction in sulfate starvation) or comparable levels of stress as DC3000 Δ*hopQ* + EV with the notable exception of response to water deprivation, which is enriched for both leaves and petioles infiltrated with DC3000 Δ*hopQ* + *hopBA1*. Notably leaves infiltrated with DC3000 Δ*hopQ* + *hopBA1* seem less responsive to oxidative stress, toxins, and UV-B.

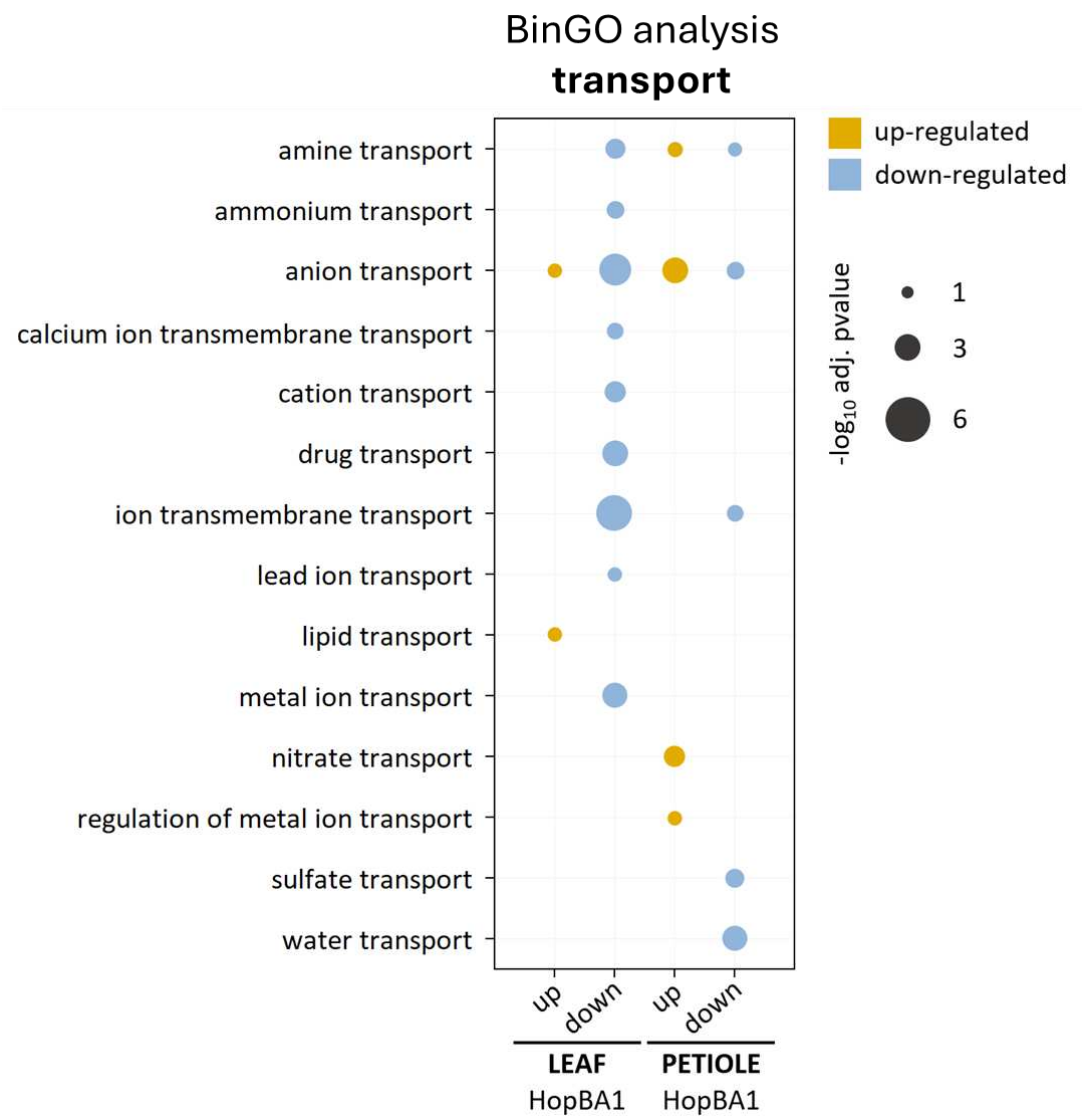

Figure S8-B. HopBA1 enriched GO terms relating to transport in leaves and petioles. The predominant observation was that transport was downregulated within leaves following DC3000 Δ*hopQ* + *hopBA1* infiltration. Lipid transport was distinctly upregulated within leaves following DC3000 Δ*hopQ* + *hopBA1* infiltration. Petioles were distinct in upregulation of nitrate transport and regulation of metal ion transport, as well as by the downregulation of sulfate and water transport.

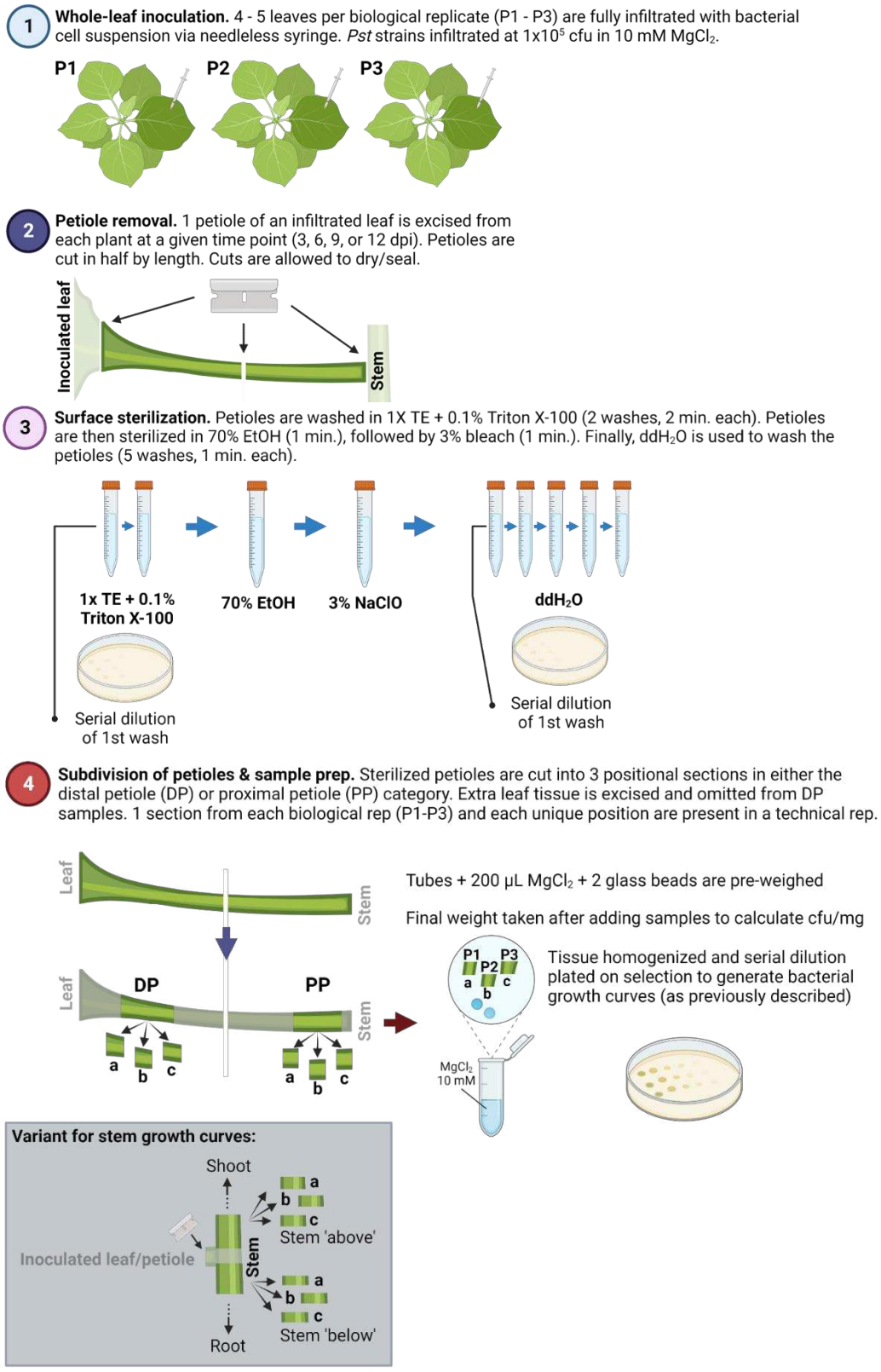

Figure S9. A visual summary of the approach taken for petiole and stem bacterial growth curves with additional written details.

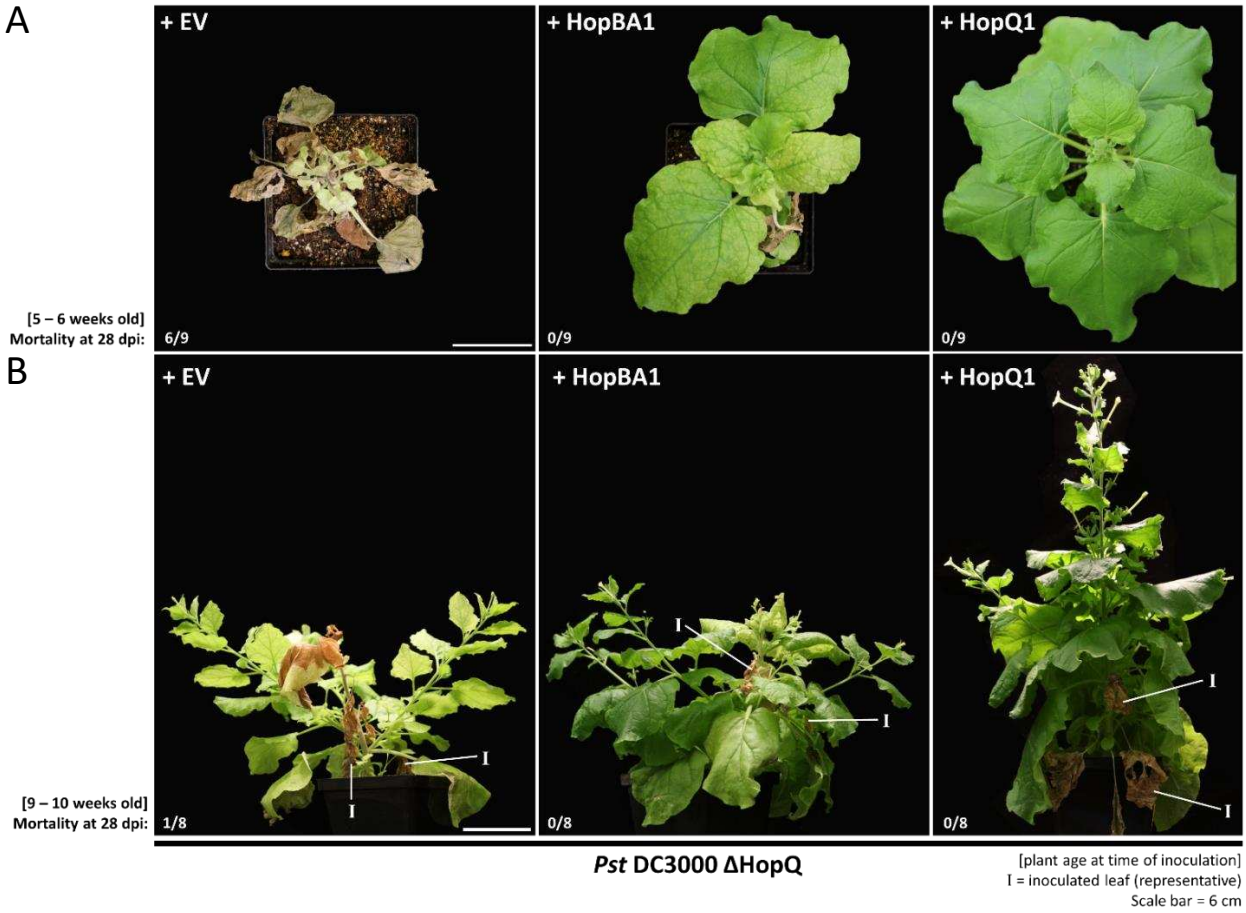

Figure S10. Long-term phenotypes and plant survivorship following DC3000 Δ*hopQ* + EV, + *hopBA1*, and + *hopQ1* in young and mature *Nb* plants. (A) Infiltration with DC3000 Δ*hopQ* + EV results in a high proportion of mortality (~67%) in plants of the typical experimental age (5 – 6 weeks old), while infiltrations of DC3000 Δ*hopQ* + *hopBA1* and + *hopQ1* do not lead to host mortality. DC3000 Δ*hopQ* + *hopBA1* stunts plant growth and results in systemic chlorosis. DC3000 Δ*hopQ* + *hopQ1* causes no observable plantwide disease symptoms. (B) DC3000 Δ*hopQ* + EV-associated mortality is substantially reduced (~13%) in plants infiltrated at 9 – 10 weeks old, resulting in apical and stem necrosis, while lateral branching appears to facilitate enhanced survivorship at 28 dpi. No mortality occurs following infiltration with DC3000 Δ*hopQ* + *hopBA1* and + *hopQ1*. Older plants infiltrated with DC3000 Δ*hopQ* + *hopBA1* undergo similar branching patterns to + EV and maintain the chlorotic and stunted growth phenotypes observed in younger plants. DC3000 Δ*hopQ* + *hopQ1* causes no observable plantwide disease symptoms. Four leaves were infiltrated per plant and with only one strain per plant. All images and mortality counts were taken at 28 dpi.

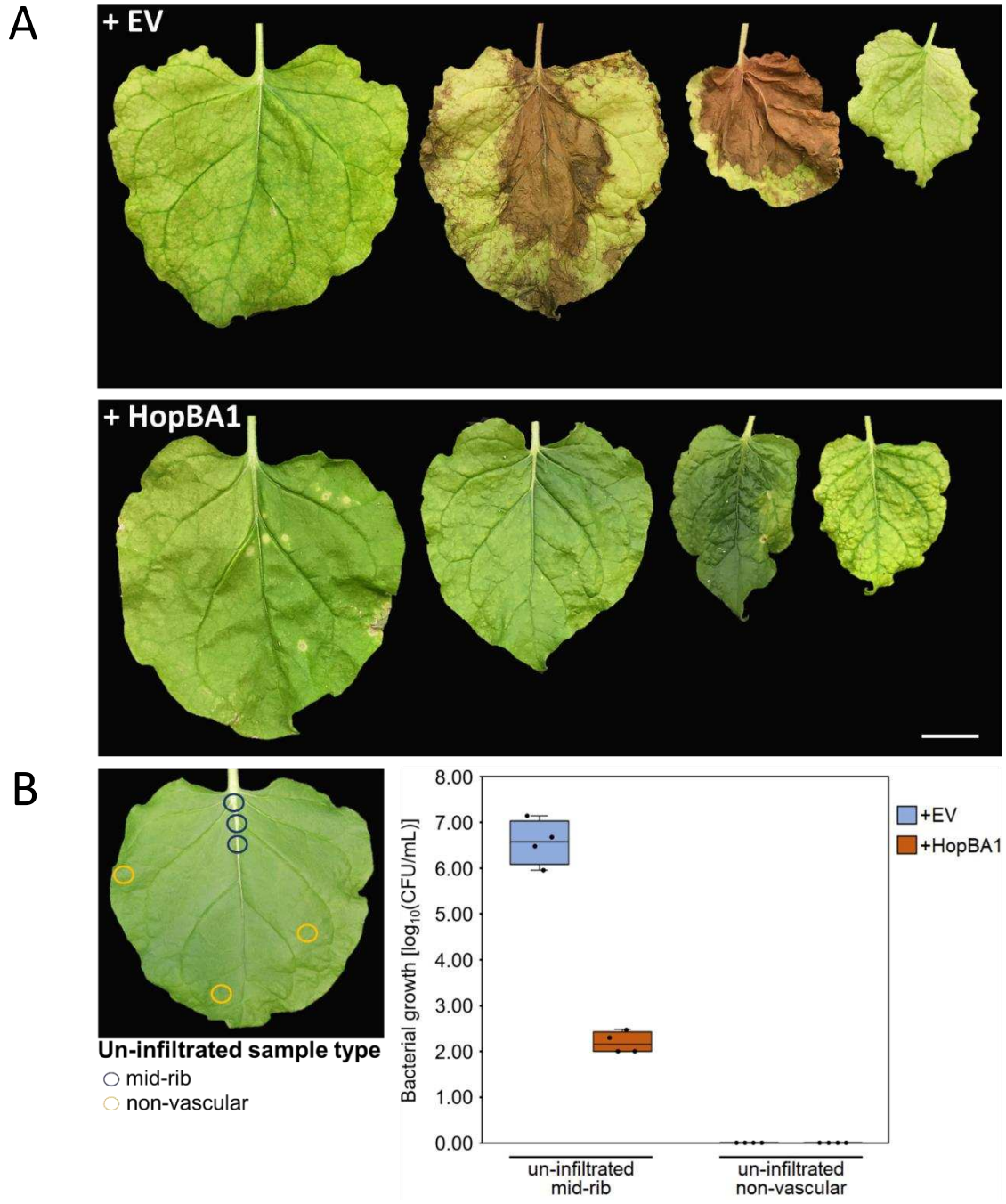

Figure S11. Survey of un-infiltrated symptomatic leaves associated with DC3000 Δ*hopQ* + EV and DC3000 Δ*hopQ* + *hopBA1* at ~21 dpi. (A) Representative leaf images showing differences in symptom development between DC3000 Δ*hopQ* + EV (top) and DC3000 Δ*hopQ* + *hopBA1* (bottom). (B) Bacterial growth curve from un-infiltrated symptomatic (but still living) leaf tissue. Samples were taken from vascular tissue (mid-rib, shown with blue circles) and general mesophyll/leaf tissue (shown with yellow circles). The presented leaf is a representative image for sampling location. DC3000 Δ*hopQ* + EV had ~5 logs more bacterial growth than DC3000 Δ*hopQ* + *hopBA1* in sampled mid-rib (vascular) tissue and there was no difference in growth between strains in non-vascular tissue.

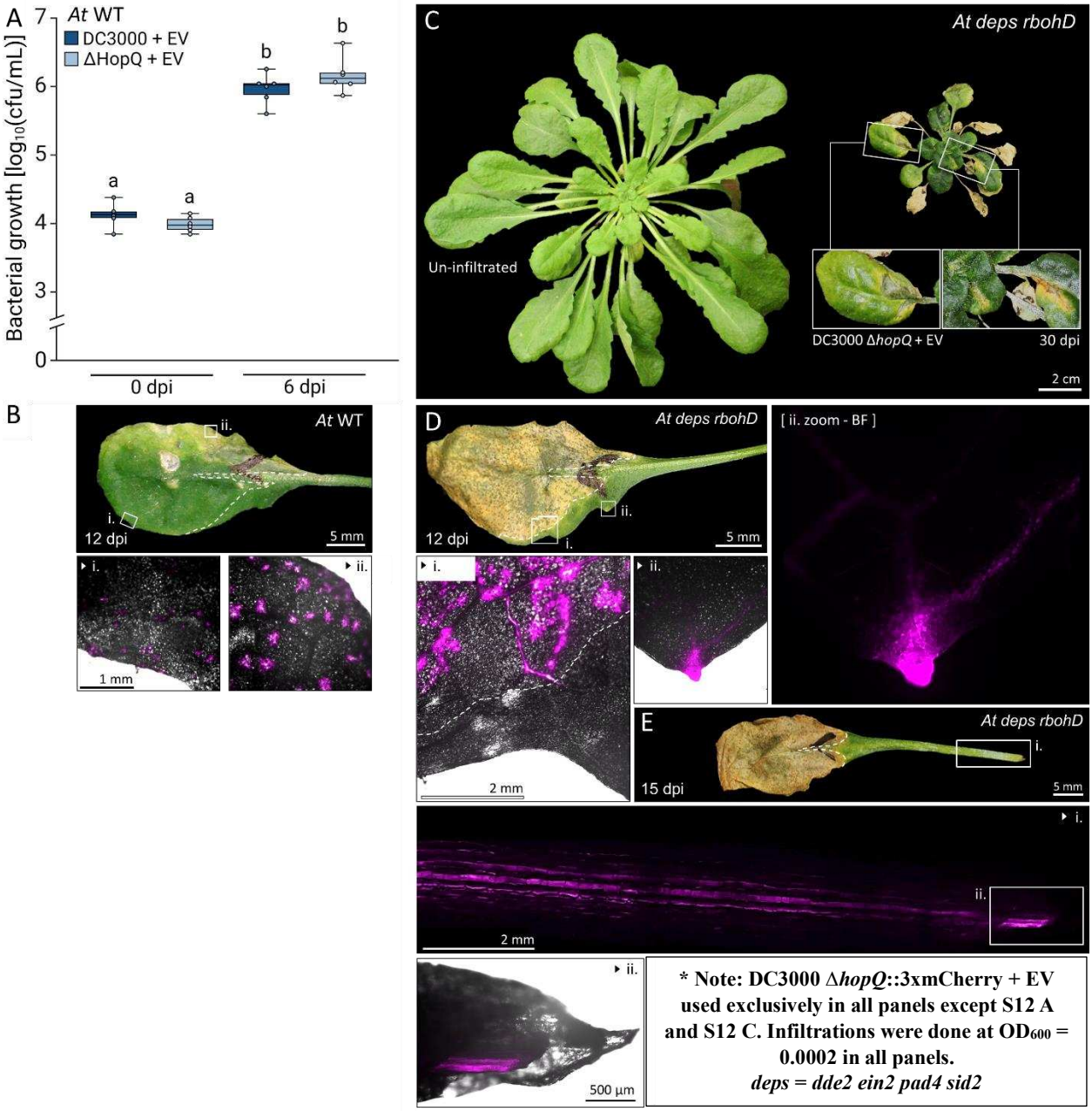

Figure S12. Relative to *Nb*, DC3000 Δ*hopQ* + EV infiltration results in a similar pattern of vascular colonization in *Arabidopsis deps rbohD* mutants, but not in WT. (A) A bacterial growth curve confirming neither a loss or gain in virulence for DC3000 + EV vs. DC3000 Δ*hopQ* + EV in WT Arabidopsis at 6 dpi. No statistical difference is observed between the bacterial strains. Two-way ANOVA and Tukey's HSD with 6 biological replicates. Assay repeated 3 times with similar results. (B) Representative leaf phenotype for At WT plants infiltrated with DC3000 ΔhopQ::3xmCherry + EV at 12 dpi. Infiltrated leaves have relatively weak disease symptoms. Fluorescence microscopy (i and ii) reveal a non-vascular bias or bacterial absence from leaf vasculature in WT plants, as well as the association between bacterial fluorescence signal and disease symptoms. (C) At deps rbohD plants, un-infiltrated (left) and DC3000 ΔhopQ::3xmCherry + EV infiltrated (right) at 30 dpi. In addition to stunted growth, infiltrated plants show systemic disease symptoms (chlorosis and necrosis) which lie predominantly along the vasculature of un-infiltrated leaves (i and ii). (D) At deps rbohD infiltrated leaf phenotype (12 dpi,

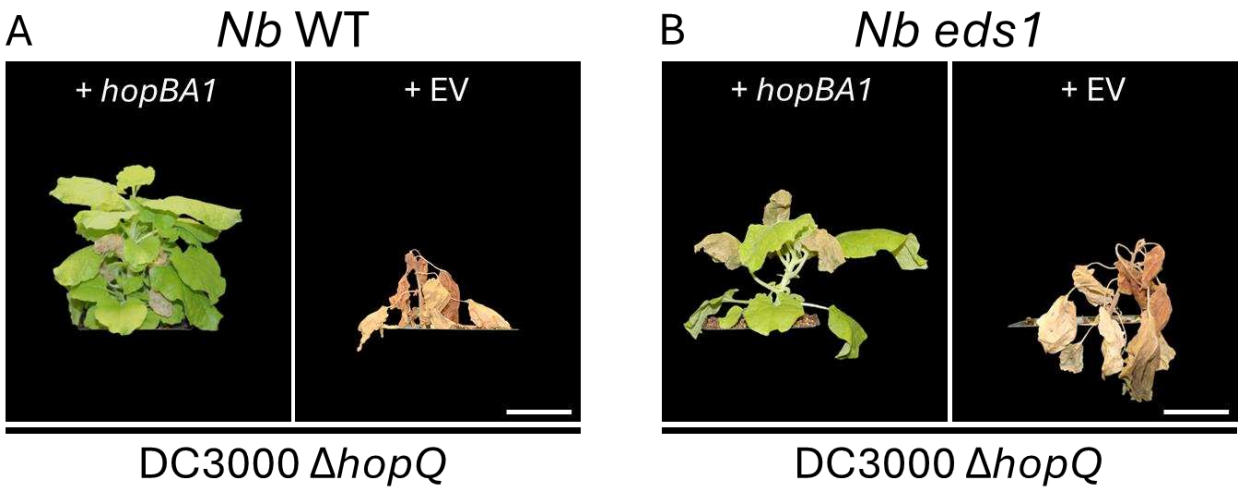

Figure S13. Comparison of long-term phenotypes and survivorship in *Nb* WT vs. *Nb eds1* following infiltration with DC3000 Δ*hopQ* + EV or DC3000 Δ*hopQ* + *hopBA1*. (A) Infiltration of WT plants with DC3000 Δ*hopQ* + EV leads to host mortality, while DC3000 Δ*hopQ* + *hopBA1* stunts vertical growth and inhibits sexual maturation but does not kill the host. (B) Infiltration of *eds1* mutant plants with DC3000 Δ*hopQ* + EV leads to host mortality, while DC3000 Δ*hopQ* + *hopBA1* has increased symptoms relative to WT, but still does not kill the host like + EV. This suggests EDS1 alone does not account for HopBA1-recogniution and plantwide phenotype differences between + EV and + *hopBA1*. Images are representative, but results were observed in 12+ plants over multiple experiments. Images at 30 dpi. Scale bar = 6 cm.

Figure S12 (Continued). DC3000 Δ*hopQ*::3xmCherry + EV). Leaves are strongly chlorotic and feature spotted pockets of cell death within the infiltrated area (denoted by the white dotted line). Fluorescence microscopy further reveals that the bacterial signal within infiltrated tissue is present within both the apoplast and the vasculature (i), unlike WT plants. Further, we observed strong signal at hydathodes outside of the infiltrated area, suggesting a gained route of vascular entry or migration in *At deps rbohD* undergoing *Pst* infection (ii and ii zoom – BF (far right)). (E) *At deps rbohD* infiltrated leaf phenotype (15 dpi, DC3000 Δ*hopQ*::3xmCherry + EV) and evidence of vascular entry/movement beyond the primary site of infection. Bacterial signal can be observed through host tissue, visually indicating that bacteria are located within the interior core of the petiole (most likely within the vascular bundle) (i). The strongest fluorescence is observed at the cross-sectional laceration of the petiole (proximally located) where the interior vascular bundle is exposed (i and ii).